

ACKNOWLEDGEMENTS

The author wishes to express his gratitude and deep appreciation to his research directors, Dr. D.N. Hawkins and Dr. H.J. McQueen. In addition, the author is grateful to Dr. J.J. Jonas for providing continued guidance throughout the investigation. He also thanks Sidbec-Dosco Steel Company for providing the experimental materials.

TABLE OF CONTENTS

iii

Page

ABSTRACT	i
ACKNOWLEDGMENTS	ii
LIST OF FIGURES	vi
LIST OF TABLES	x
NOMENCLATURE	xi
CHAPTER 1. INTRODUCTION	1
CHAPTER 2. DEVELOPMENT OF HSLA STEELS	3
2.1 LOW CARBON STEELS	3
2.1.1 Weldability	4
2.1.2 Grain Refined Steels	9
2.2 HIGH STRENGTH LOW ALLOY STEELS (HSLA)	12
CHAPTER 3. HOT WORKING CHARACTERISTICS OF STEELS	20
3.1 INTRODUCTION	20
3.2 RESTORATION PROCESSES ON HOT WORKING	20
3.3 DYNAMIC RECOVERY	22
3.3.1 Mechanism of Dynamic Recovery	22
3.4 DYNAMIC RECRYSTALLIZATION	24
3.4.1 Mechanism of Dynamic Recrystallization	26
3.5 INTERRELATIONSHIPS BETWEEN FLOW STRESS, STRAIN RATE, TEMPERATURE AND GRAIN SIZE	27
3.6 STATIC RECOVERY	28
3.6.1 Effect of Experimental Variables on the Rate of Static Recovery	28
3.7 STATIC RECRYSTALLIZATION	30
3.7.1 Experimental Variables Affecting Recrystallization	30
3.8 METADYNAMIC RECRYSTALLIZATION	32
3.9 MULTIPLE DEFORMATION	33

	<u>Page</u>
3.9.1 Interrupted Tests	33
3.10 CONTROLLED ROLLING	38
3.10.1 Problems in Controlled Rolling	38
3.11 METALLURGY OF STEELS ON HOT ROLLING CHARACTERISTICS	44
3.11.1 Strength and Ductility of Mild Steel	44
3.11.2 Restoration Processes During Plate Rolling of Mild Steel	45
3.11.3 Effects of Nb on Hot Rolling	46
CHAPTER 4. EXPERIMENTAL PROCEDURE	48
4.1 TORSION TESTING	48
4.2 TORSION TESTING SYSTEM AND PROCEDURE	49
4.3 TEST MATERIALS AND TEST PROCEDURES	53
4.3.1 Test Materials and Its Preparation	53
4.3.2 Test Procedures	56
CHAPTER 5. EXPERIMENTAL RESULTS	59
5.1 CONTINUOUS DEFORMATION	59
5.2 INTERRUPTED DEFORMATION	63
CHAPTER 6. DISCUSSION	83
6.1 BEHAVIOUR DURING CONTINUOUS DEFORMATION	83
6.2 BEHAVIOUR DURING INTERRUPTED DEFORMATION	86
6.2.1 Softening Mechanisms of Low Carbon and Nb-Bearing Steel During Low Strain Rate Interrupted Deformation	91
6.2.2 Softening Mechanisms of Low Carbon and Nb-Bearing Steel During High Strain Rate Interrupted Deformation	92
6.3 EFFECT OF STARTING GRAIN SIZE AND PRE-HOLDING TIME ON THE INITIAL FLOW CURVE	93
6.4 STATIC RESTORATION STUDY OF PREVIOUS WORKERS ON LOW CARBON AND Nb-BEARING STEEL	94

CHAPTER 7. CONCLUSIONS
REFERENCES

Page

100

102

LIST OF FIGURES

	<u>Page</u>
FIGURE 2.1 Factors Contributing to the Strength of C-Mn Steel (After Irvine, Ref. 2)	5
FIGURE 2.2 Factors Contributing to the Strength of C-Mn Steel (After Irvine, Ref. 2)	6
FIGURE 2.3 Solid-Solution Strengthening of Ferrite (After Pickering, Ref. 3)	7
FIGURE 2.4 The Effect of Carbon and hence the Pearlite Content on Impact-Transition Temperature Curves of Ferrite-Pearlite Steels (After Pickering, Ref. 3)	8
FIGURE 2.5 Grain Size Dependence of the Yield Strength of a 0.1%C - 1.5% Mn Steel (After Irvine, Ref. 2)	11
FIGURES 2.6 AND 2.7 The Effect of Al and N on Impact Properties (After Irvine, Ref. 2)	13
FIGURE 2.8 The Effect of Rolling Variables on the Strength-Grain Size Relationship of Nb Steel (After Irvine, Ref. 2)	15
FIGURE 2.9 The Effect of Base Composition on the Strength-Grain Size Relationship of V Steel (After Irvine, Ref. 2)	16
FIGURE 2.10 Variation of Yield Strength of X65 Steels as a Function of Finish Rolling Temperature (After Morrison et al., Ref. 9)	18
FIGURE 3.1 Schematic Representation of the Flow Curve of Metals that Recover Dynamically.	23
FIGURE 3.2 Schematic Representation of the Flow Curves for Dynamic Recrystallization at High and Low Strain Rates.	25
FIGURE 3.3 Relationship Between Subgrain Size(d) and Zener-Holloman Parameter (Z).	29
FIGURE 3.4 Log-Log Plot of Flow Stress Against Subgrain Size in Extrusion and Creep, the Slope of Approximately -1 Indicates an Inverse Proportionality (After McQueen, Ref. 26).	29

FIGURE 3.5	The Progress of Isothermal Annealing After Cold Deformation.	31
FIGURE 3.6	Typical Schedule for Rolling 216 mm Slab to 2 mm Strip (Tinplate) (After Sellars et al., Ref. 58)	34
FIGURE 3.7	Effect of Increasing Delay Time on the Interrupted Flow Curve (After Petkovic, Ref. 21).	36
FIGURE 3.8	Effect of Interrupted Deformation by Incremental Surface Shear Strains of 1.38 Followed by Rests of 2 min. on the Torque-Revolution Curve for Al-5% Mg at 450°C and a Surface Shear Strain Rate of 3.93 s ⁻¹ (After Farag et al., Ref. 66).	37
FIGURE 3.9	The Effect of Niobium Addition on the Room Temperature Yield Strength and Impact Transition of a 0.04%C, 6.5%Mn Steel. The Improvement Resulting from a Lower Rolling Temperature is also Shown (After Jones et al., Ref. 70).	39
FIGURE 3.10	Schematic Diagram Contrasting Recrystallization Effects in the Two Schedules ('Continuous' and 'Rough-hold-finish') for C-Mn-Nb Steel (R = Recrystallized Structure) (After Duckworth et al., Ref. 1).	41
FIGURE 3.11	Schematic Representation of State of Recrystallization During Hot Rolling of C-Mn-Nb Steels (After Duckworth et al., Ref. 1).	42
FIGURE 3.12	Schematic Representation of Recrystallization During Rolling Schedules Involving a Cooling Delay (After Duckworth et al., Ref. 1).	43
FIGURE 4.1	Servo-Controlled Hydraulic Torsion Machine.	50
FIGURE 4.2	The Control System.	52
FIGURE 4.3	Test Piece Design.	55
FIGURE 4.4	Method of Data Analysis.	58
FIGURE 5.1	Equivalent Stress/Equivalent Strain Curves for a 0.14%C Steel on Hot Working at Strain Rates of (a) 0.1 s ⁻¹ (b) 1.0 s ⁻¹ .	60
FIGURE 5.2	Equivalent Stress/Equivalent Strain Curves for 0.12%C, 0.05%Nb Steel on Hot Working at Strain Rates of (a) 0.1 s ⁻¹ (b) 1.0 s ⁻¹ .	61

FIGURE 5.3	Effect of Temperature and Strain Rate on Equivalent Strain to the Peak.	62
FIGURE 5.4	The Stress Dependence of the Strain Rate for a 0.14%C Steel at Various Temperatures Plotted to Demonstrate the Power Law Relationship.	64
FIGURE 5.5	The Stress Dependence of the Strain Rate for a 0.12%C, 0.05%Nb Steel at Various Temperatures Plotted to Demonstrate the Power Law Relationship.	65
FIGURE 5.6	The Temperature Dependence of the Stress for a 0.14%C Steel at Various Strain Rates Plotted to Demonstrate an Arrhenius Law Relationship.	66
FIGURE 5.7	The Temperature Dependence of the Stress for a 0.12%C, 0.05%Nb Steel at Various Strain Rates Plotted to Demonstrate an Arrhenius Law Relationship.	67
FIGURE 5.8	Interrupted Flow Curves for a 0.14%C Steel at 900°C and 0.1 s ⁻¹ at Pass Strains of 0.2 and Interruption Times of 40, 20 and 10 s.	69
FIGURE 5.9	Interrupted Flow Curves for a 0.14%C Steel at 950°C and 0.1 s ⁻¹ at Pass Strains of 0.2 and Interruption Times of 40, 20 and 10 s.	70
FIGURE 5.10	Interrupted Flow Curves for a 0.14%C Steel at 1000°C and 0.1 s ⁻¹ at Pass Strains of 0.2 and Interruption Times of 40, 20 and 10 s.	71
FIGURE 5.11	Interrupted Flow Curves for a 0.12%C, 0.05%Nb Steel at 900°C and 0.1 s ⁻¹ at Pass Strains of 0.2 and Interruption Times of 40, 20 and 10 s.	72
FIGURE 5.12	Interrupted Flow Curves for a 0.12%C, 0.05%Nb Steel at 950°C and 0.1 s ⁻¹ at Pass Strains of 0.2 and Interruption Times of 40, 20 and 10 s.	73
FIGURE 5.13	Interrupted Flow Curves for a 0.12%C, 0.05%Nb Steel at 1000°C and 0.1 s ⁻¹ at Pass Strains of 0.2 and Interruption Times of 40, 20 and 10 s.	74
FIGURE 5.14	Interrupted Flow Curves for a 0.14%C Steel at 900°C and 1.0 s ⁻¹ at Pass Strains of 0.4 and Interruption Times of 40, 20 and 10 s.	75

FIGURE 5.15	Interrupted Flow Curves for a 0.14%C Steel at 950°C and 1.0 s ⁻¹ at Pass Strains of 0.4 and Interruption Times of 40, 20 and 10 s.	76
FIGURE 5.16	Interrupted Flow Curves for a 0.12%C, 0.05%Nb Steel at 900°C and 1.0 s ⁻¹ at Pass Strains of 0.4 and Interruption Times of 40, 20 and 10 s.	77
FIGURE 5.17	Interrupted Flow Curves for a 0.12%C, 0.05%Nb Steel at 950°C and 1.0 s ⁻¹ at Pass Strains of 0.4 and Interruption Times of 40, 20 and 10 s.	78
FIGURE 5.18	Variation of Fractional Softening with Temperature, Interruption Time and Accumulated Strain for a 0.14%C Steel at 0.1 s ⁻¹ .	79
FIGURE 5.19	Variation of Fractional Softening with Temperature, Interruption Time and Accumulated Strain for a 0.12%C, 0.05%Nb Steel at 0.1 s ⁻¹ .	80
FIGURE 5.20	Variation of Fractional Softening with Temperature, Interruption Time and Accumulated Strain for a 0.14%C Steel at 1.0 s ⁻¹ .	81
FIGURE 5.21	Variation of Fractional Softening with Temperature, Interruption Time and Accumulated Strain for a 0.12%C, 0.05%Nb Steel at 1.0 s ⁻¹ .	82
FIGURE 5.22	Recrystallization - Temperature - Time Diagram for a 0.17%C - 0.04%Nb Steel (After Le Bon et al., Ref. 74).	95
FIGURE 5.23	Precipitation - Temperature - Time Diagram for a 0.05%C-0.035%Nb Steel (After Weiss et al., Ref. 76).	96
FIGURE 5.24	Correlation of the Static Softening Observed in the First Interruption of the Present Study with that of Petkovic (Ref. 65) for Low Carbon Steels.	98
FIGURE 5.25	Correlation of the Static Softening Observed in the First Interruption of the Present Study with Previous Workers for Nb-Bearing Steels.	99

LIST OF TABLES

	<u>Page</u>
TABLE 3.1 High Temperature Softening Processes	21
TABLE 4.1 Chemical Composition in wt% of the Materials Tested	54
TABLE 6.1 Comparative Values of n and Activation Energy	85
TABLE 6.2 Softening, s , During Interruption, t_i and Relation of Interrupted to Continuous Curve	89

NOMENCLATURE

xi

A	constant
D	diameter; mm
d	grain size; mm
K	constant; $^{\circ}\text{C} \cdot \text{mm}^2$
K_y	the grain size coefficient; $\text{MPa} \cdot \text{mm}^2$
L_0	gauge length; mm
M_T	torsional moment; lb.in
m	strain rate sensitivity exponent
N_f	'free' nitrogen content; in wt %
N_f'	volume fractions of precipitate
n	stress dependent constant
n'	strain hardening exponent
P_f	finish of precipitation
P_s	start of precipitation
R	gas constant; cal/mole $^{\circ}\text{K}$
R_f	finish of recrystallization
R_s	start of recrystallization
r	radius; mm
S	fractional softening; %
s	seconds
T	temperature; $^{\circ}\text{C}$
T_c	impact transition temperature; $^{\circ}\text{C}$
t	time; sec
t_i	interruption time; sec
\bar{X}	mean planar intercept diameter of a precipitate; mm
Z	zener-Holloman parameter; sec^{-1}

γ	torsional strain
ΔH	activation energy; cal/mol
ϵ	true strain
ϵ_c	critical strain for dynamic recrystallization
ϵ_p	peak strain
ϵ_s	steady state strain
$\dot{\epsilon}$	strain rate; sec^{-1}
$\bar{\epsilon}$	equivalent strain
ϵ_i	interruption strain
σ	true stress; MPa
σ_D	sub-structural strengthening; MPa
σ_i	stress constant; MPa
σ_p	precipitation strengthening; MPa
σ_s	solid solution strengthening; MPa
σ_y	lower yield strength; MPa
$\bar{\sigma}$	equivalent stress; MPa
τ	shear stress; MPa

CHAPTER 1

INTRODUCTION

The object of this research is to determine the hot working behaviour of low carbon steel and high strength low alloy steel (HSLA) under continuous and interrupted deformation conditions. The literature review therefore will be a background against which the experimental work and results can be compared and analysed.

The experimental method employed in the present hot workability study of low carbon and HSLA steels is the torsion test. The project involves in the determination of the stress-strain curves and ductilities at typical hot working temperatures and strain rates. Interrupted deformation tests are also conducted with different interruption times.

Torsion testing for determining hot working characteristics has two outstanding advantages compared with the more frequently conducted tension or compression test. Test at constant and high deformation rates can be readily made by twisting at a constant rate. In addition, strains can be reached without complications of the kind introduced when necking occurs in the tension test; or when barreling due to frictional end effects arise in compression testing. One disadvantage of the torsion test is that the strain and strain rate vary from zero at the axis to a maximum at the surface.

As a brief introduction to the general characteristics of the HSLA steels, the following subjects are examined in Chapter 2:

1. their development from low carbon steels;
2. their advantages relative to these steels.

The literature which provides the background to the experimental work then follows in Chapter 3, it covers the general hot working characteristics of steels and the recrystallization and precipitation characteristics of HSLA steels.

A brief description of the hot torsion machine along with its operating procedure are presented in Chapter 4. A full description of the experimental procedures adopted in the present study is also given in this chapter. Chapter 5 deals with the experimental results and a detailed analysis of these results follows in Chapter 6. Finally, in Chapter 7 some conclusions are drawn concerning the hot deformation characteristics of low carbon and Nb-bearing steel based on the present work.

CHAPTER 2

DEVELOPMENT OF HSLA STEELS

In order to understand why high strength low alloy (HSLA), or micro-alloyed, steels have been developed we must firstly look at the limitations of its forerunner, low carbon steel.

2.1 LOW CARBON STEELS

Mild, or low carbon steel, is a most important steel product for 94% of the world's metal products are made from iron and steel and 85% of this 94% is low carbon steel [1]. An important use for mild steel was for structural purposes and this will be dealt in this chapter since the major application of HSLA steels [1,2,3] include plate or section for ships, bridges, buildings, pressure vessels, heavy vehicles and tubes and pipelines, especially for the transportation of oil and gas over long distances.

Early mild steels were relatively high in carbon, in the order of 0.3%, since design was then based on tensile strength and good weldability and resistance to brittle fracture were not requirements [2,3]. This was followed by steels with carbon contents around 0.3%. In these steels the main factor which contributes to the tensile strength were:

- (a) the % pearlite,
- (b) the ferrite grain size,
- and (c) solid solution hardening by Mn.

The way in which these factors vary with changing C and Mn content [2] are shown in Figures 2.1 and 2.2.

These figures show that the pearlite content is the major strengthening factor and thus increasing the carbon content is the simplest and cheapest way of increasing the tensile strength. Also by having 1 - 1.5% Mn and 1% Si strengthening by solid solution hardening can be achieved [2].

2.1.1 Weldability

As fabrication by welding became a frequent process many difficulties were experienced using these relatively high carbon steels. The main problem was the heat - affected zone cracking. This was due to low transformation temperature products, in the region of the weld which had been austenitized and cooled sufficient rapidly to produce martensite [2]. This effect was reduced by lowering the carbon content, steel BS 968 : 1941 (C 0.23% maximum and Mn 1.3 - 1.7%) [2]. Silicon was also varied in order to obtain differences in solid solution strengthening. Generally, solid solution strengthening is not very effective (Figure 2.3) and usually expensive [3].

During World War II, major structural failures in shipplate made it necessary to improve weldability and fracture resistance [3]. The effect that carbon, i.e. pearlite, has on impact transition temperature curves of ferritic-pearlitic steels [3] is shown in Figure 2.4. Better weldability and lower impact transition tempera-

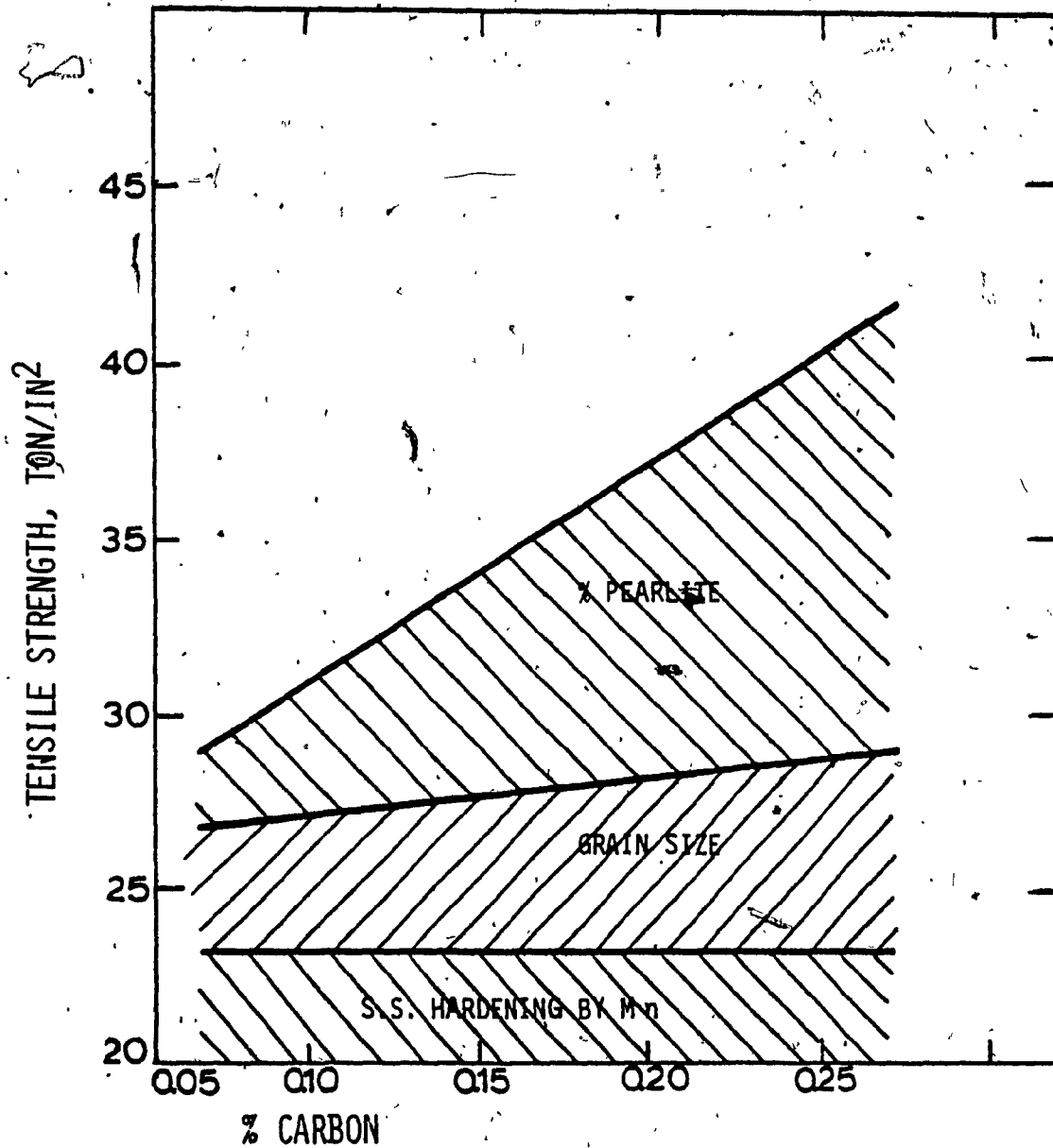


Fig. 2.1: Factors Contributing to the Strength of C-Mn Steel
(After Irvine, Ref. 2).

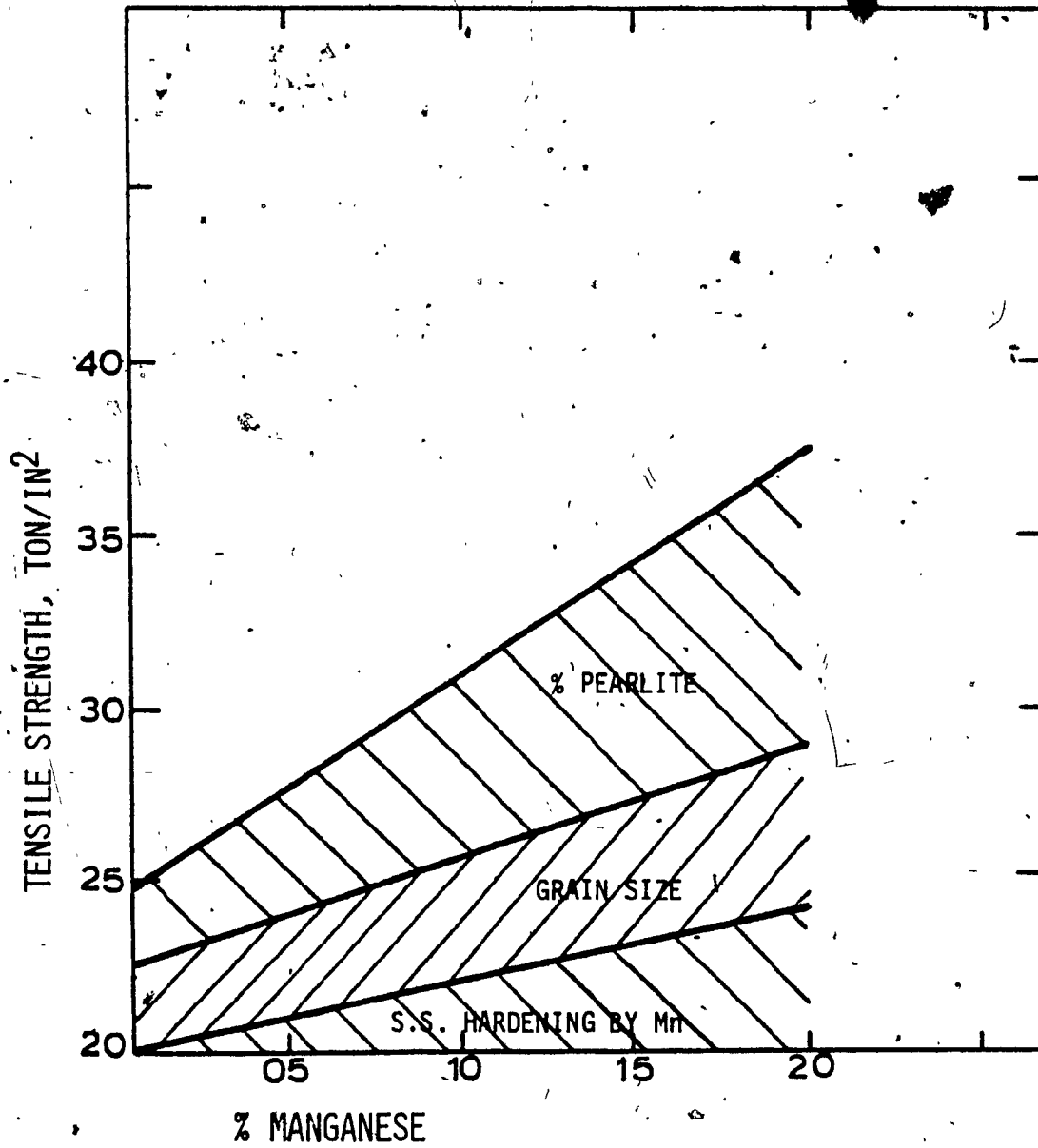


Fig. 2.2: Factors Contributing to the Strength of C-Mn Steel
(After Irvine, Ref. 2).

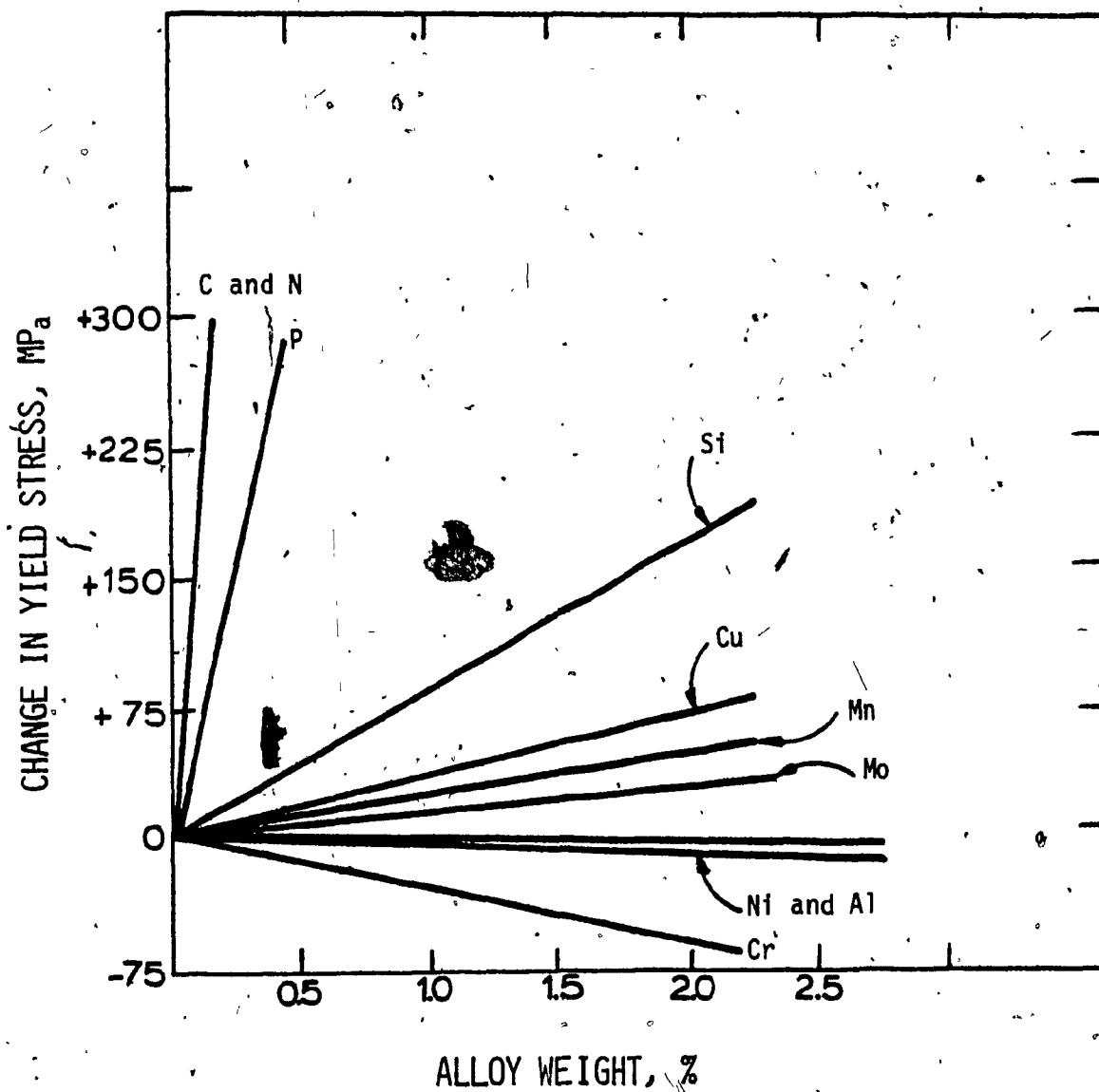


Fig. 2.3: Solid-Solution Strengthening of Ferrite.
(After Pickering, Ref. 3).

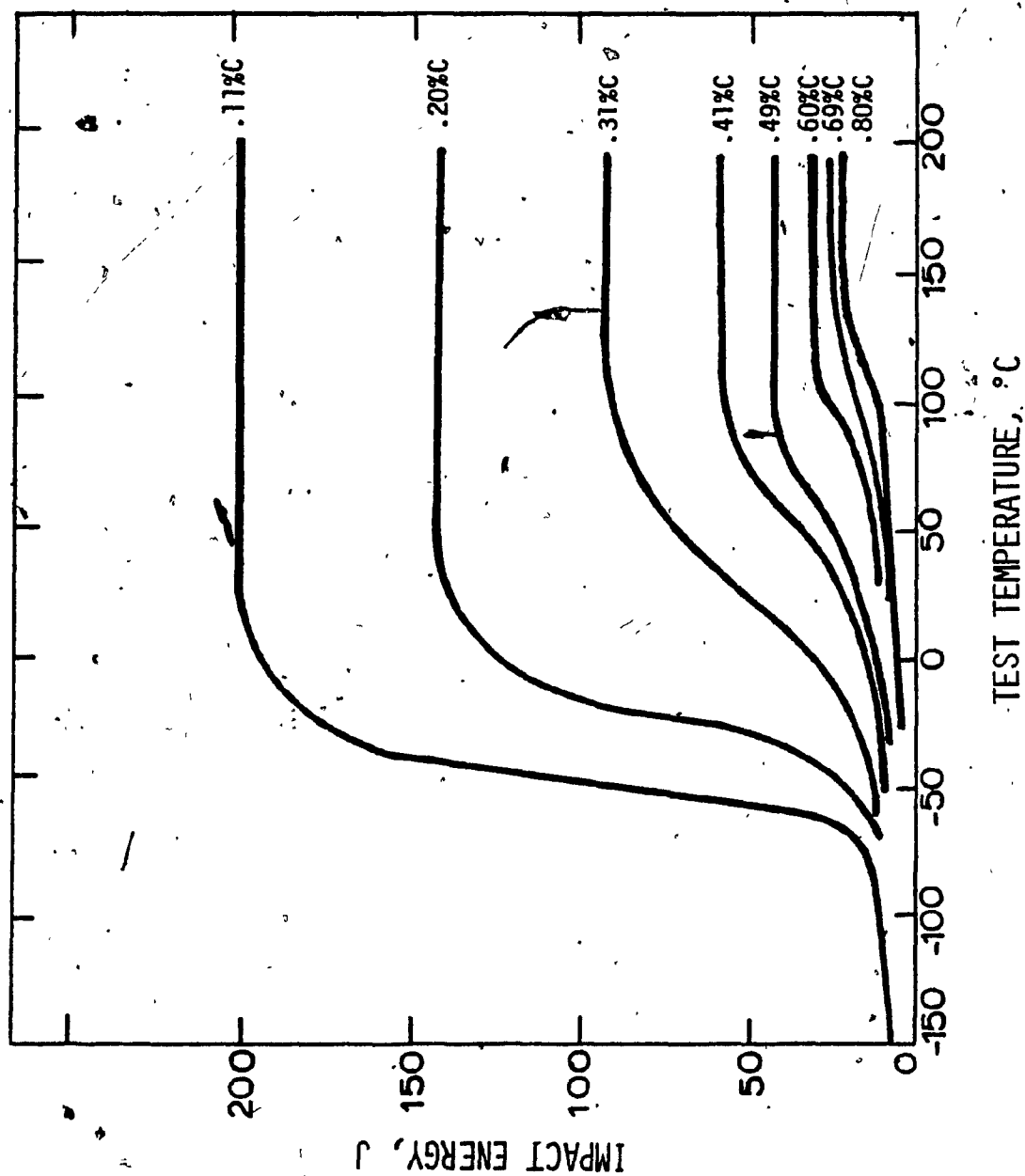


Fig. 2.4: The Effect of Carbon and hence the Pearlite Content on Impact-Transition Temperature Curves of Ferrite-Pearlite Steels (After Pickering, Ref. 3).

ture thus is achieved by having lower carbon contents.

2.1.2 Grain Refined Steels

About this time, it was accepted that designs should be based on yield strength rather than tensile strength. The general requirements therefore for these steels were [3]:

- (a) High yield strength.
- (b) Low impact transition temperature.
- (c) High charpy-shelf energy.
- (d) Minimum toughness and ductility anisotropy.
- (e) Good weldability.
- (f) Good formability.
- (g) Minimum cost.

The yield strength and impact transition temperature have been quantified using micro-structural and compositional parameters in the following relationships [3]:

Yield stress (MP_a)

$$= 15.4[2.5 + 2.1(\% Mn) + 5.4(\% Si) + 23(\% N_f) + 1.13(d^{-1/2})] \quad (2.1)$$

Impact Transition Temperature (T_c)°C

$$= -19 + 44(\% Si) + 700(\sqrt{\% N_f}) + 2.2(\% Pearlite) - 11.5(d^{-1/2}) \quad (2.2)$$

where N_f = the "free" nitrogen content, and

d = the ferrite grainsize in mm.

The compositions are expressed in weight percent.

Since grain refinement increases the yield strength and decreases the impact transition temperature in a ferritic-pearlitic steel, the carbon content should be low and the grain size should be kept as fine as possible. A coarse grain size is ASTM 4-5 and a fine grain size should be between ASTM 10-12 [2]. Figure 2.5 shows the grain size dependence of the yield strength of a 0.15%C, 1.5%Mn steel. As the grain size varies from ASTM 5 to ASTM 11, the yield point increases.

The ferrite grain size developed after allotropic transformation from austenite depends upon the original austenite grain size from which it is formed because of ferritic nucleation on the austenite-grain boundaries. A refined austenite and thus a fine ferrite grain size can be achieved in the following ways:

(1) Depressing the transformation temperature by alloying additions (one disadvantage of this approach is that as the alloy content is increased, the steel tends to be semi-air hardening) [2,4].

(2) Depressing the transformation temperature by increasing the cooling rate as given in T.T.T. diagram provided acicular structures are not produced.

(3) Refining the prior austenite grain size using aluminium-nitride, niobium, vanadium, or titanium additions [3].

(4) Using controlled rolling techniques and thus recrystallizing the austenite [3,4,5].

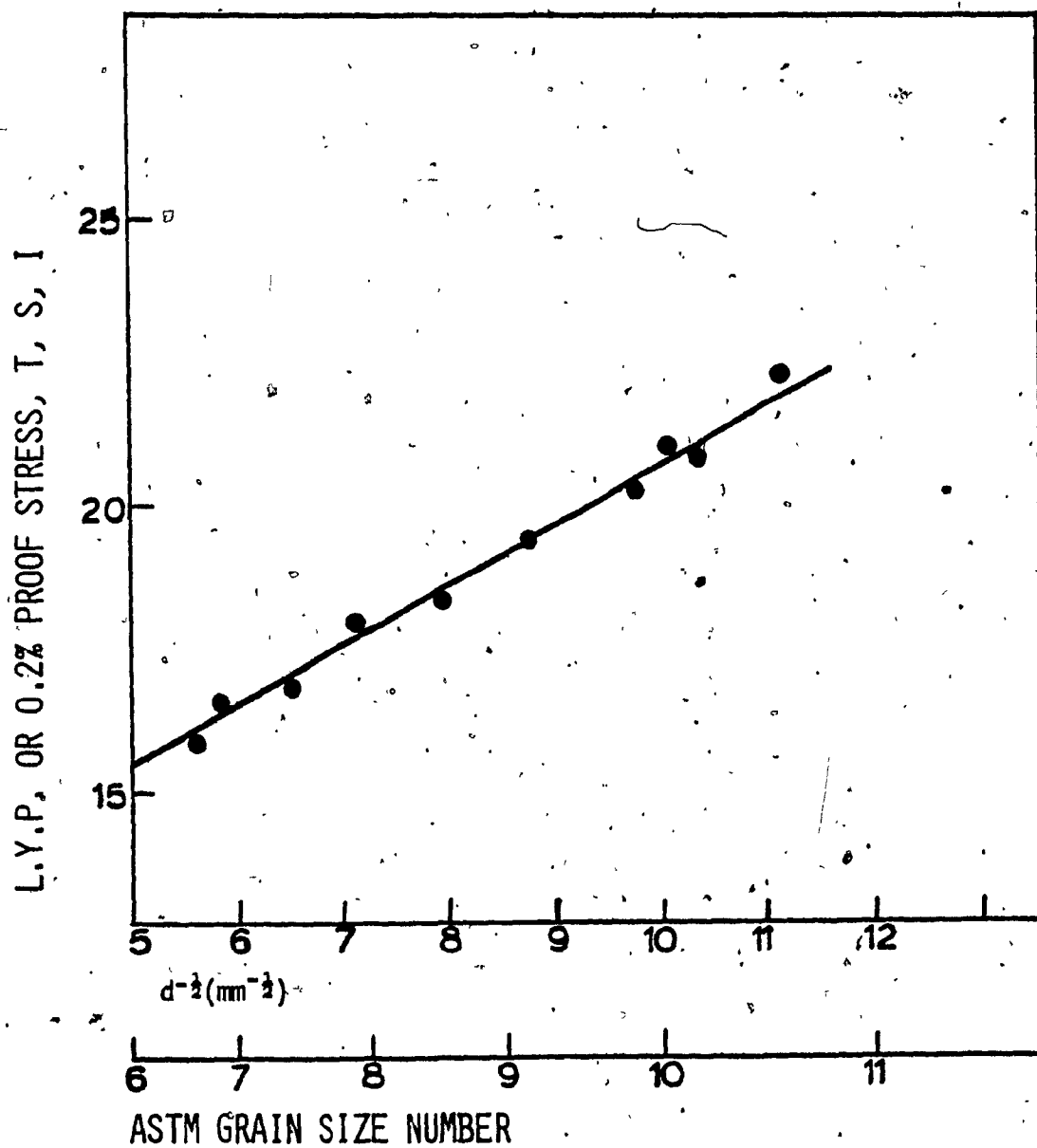


Fig. 2.5: Grain Size Dependence of the Yield Strength of a 0.1% C - 1.5% Mn Steel (After Irvine, Ref. 2).

In the case of the use of aluminium nitride for grain refinement, grain sizes from ASTM 5 to ASTM 11, with increased yield strengths can be achieved with 0.03% or more of AlN [2]. This level of AlN requires 0.015% N and 0.05% Al. The effects of Al and N on impact properties are shown in Figures 2.6 and 2.7. The mechanism which produces this refinement is that particles, precipitated by prior treatment, pin grain boundaries and retard grain growth during reheating. These steels are usually normalized at temperatures between 850°C and 950°C to obtain refinement since at higher temperatures the particles begin to redissolve giving rise to grain coarsening [4].

Titanium is also used for grain refinement but it is not popular, since it produces dirty steels. Also the carbides and nitrides formed by titanium give greater difficulty than aluminium does in producing the correct size of particles for grain refinement. The main disadvantage of using titanium and aluminium as grain refiners is their strong affinity to oxygen [1].

2.2 HIGH STRENGTH LOW ALLOY STEELS (HSLA)

Since 1960, niobium and vanadium are added to steel as grain refiners since only a small amount of these elements are required. These steels have additional strengthening due to precipitation hardening by niobium or vanadium carbides, over and above that resulting from the fine grain size. Early work on their effects on quantitative relationships [equations (2.1) and (2.2)] were carried out by Morrison and Woodhead [6]. The result deviated from the

CHANGE IN TRANSITION TEMPERATURE °C

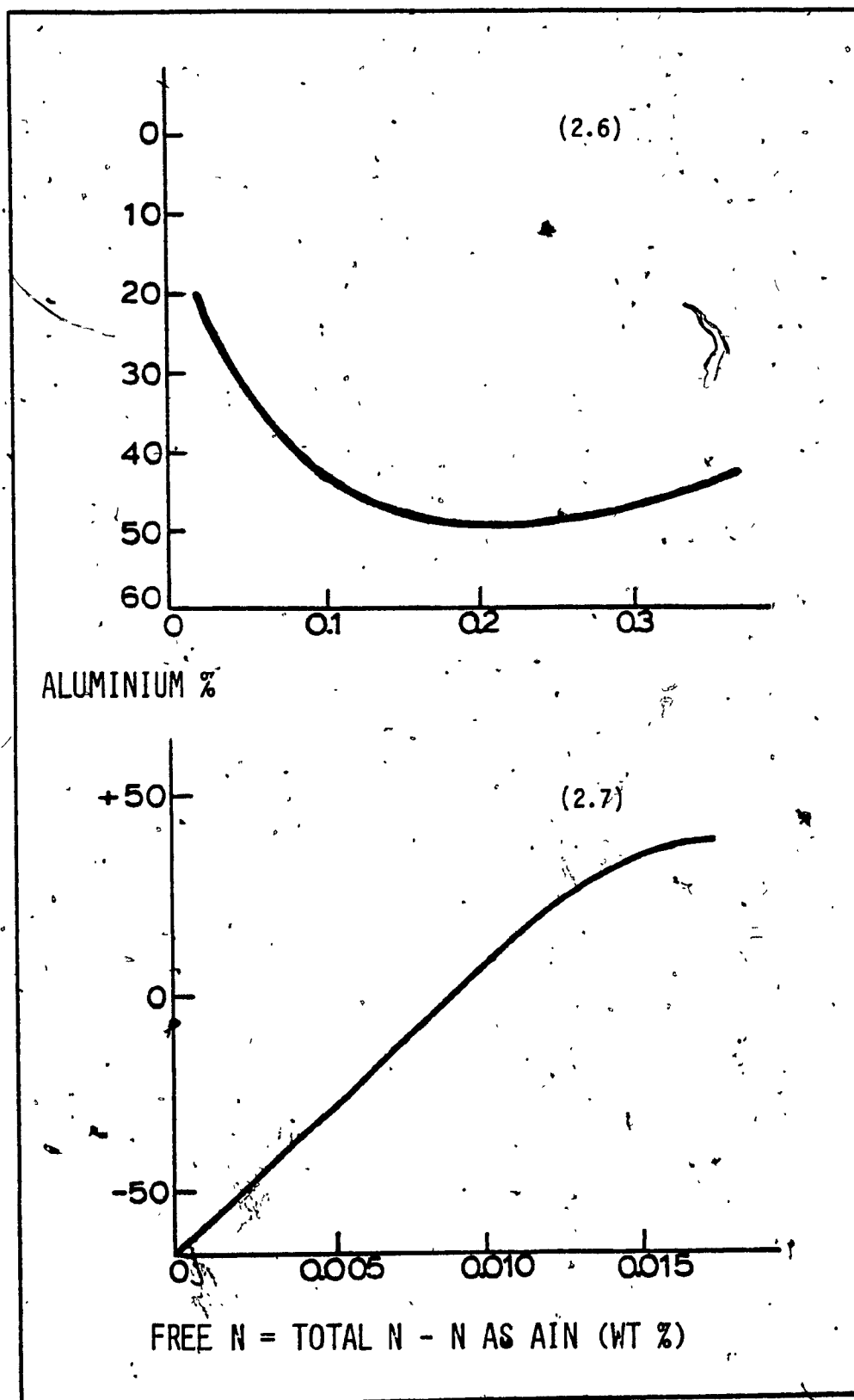


Fig. 2.6 and 2.7: The Effect of Al and N on Impact Properties (After Irvine, Ref. 2).

Classical Hall-Petch relationship [7,8]:

$$\sigma_y = \sigma_i + K_y d^{-\frac{1}{2}} \quad (2.3)$$

$$T_c = f(\sigma_0) - K d^{-\frac{1}{2}} \quad (2.4)$$

where σ_y = lower yield strength

σ_i = a stress constant experiencing the effects of lattice friction and solute atoms

K_y = the grain size coefficient associated to the density of dislocation sources along the grain boundaries

K = a constant

d = mean ferrite grain size,

the graphical construction for Equation (2.3) is shown in Figure 2.5.

Reheating temperature, finish rolling temperature and cooling rate all influence yield stress for a constant grain size as shown in Figure 2.8.

Niobium is effective only at high reheating temperatures as to obtain adequate solution of niobium. But since vanadium carbide is readily soluble at low temperatures such as 950°C, marked precipitation hardening occurs even in the normalized condition. Figure 2.9 shows the effect of variables on the strength-grain size relationship of vanadium steel [2].

A completed Hall-Petch relation has recently been proposed [9]:

$$\sigma_y = \sigma_i + \sigma_s + \sigma_p + \sigma_D + \sigma_t + K_y d^{-\frac{1}{2}} \quad (2.5)$$

$$T_c = f(\sigma_i + \sigma_s + \sigma_p + \sigma_D + \sigma_t) - K d^{-\frac{1}{2}} \quad (2.6)$$

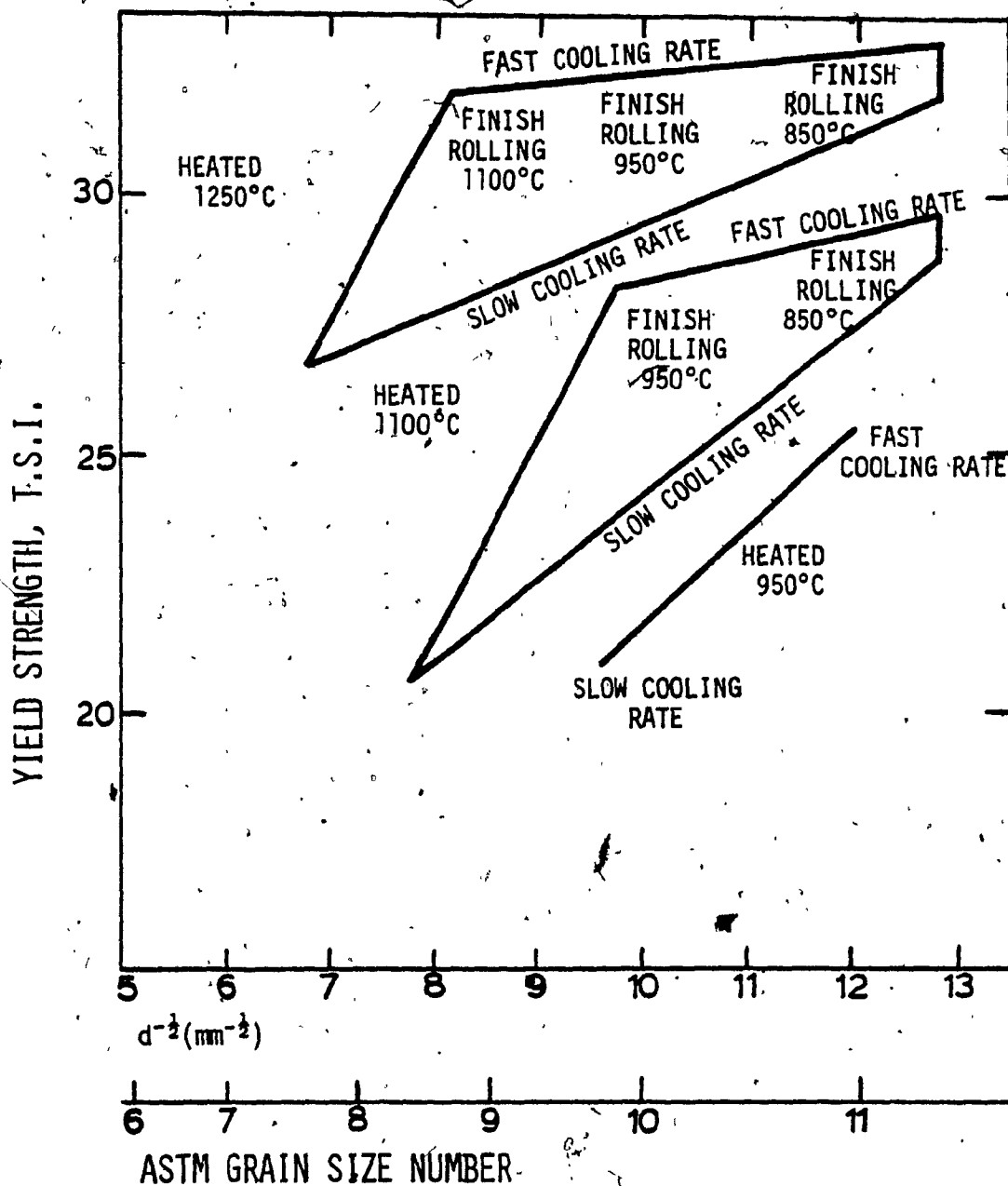


Fig. 2.8: The Effect of Rolling Variables on the Strength-Grain Size Relationship of Nb Steel (After Irvine, Ref. 2).

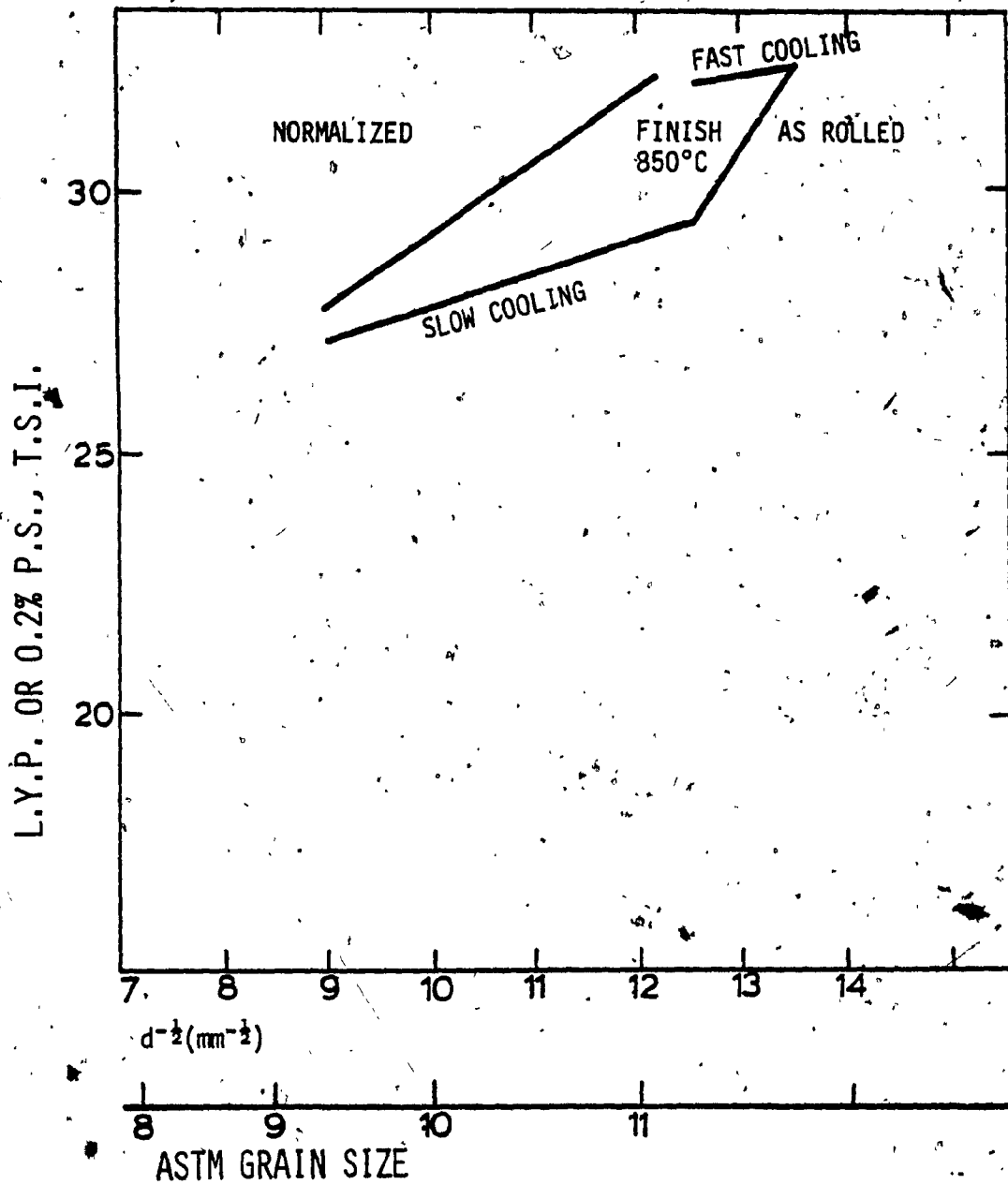


Fig. 2.9: The Effect of Base Composition on the Strength-Grain Size Relationship of V Steel (After Irvine, Ref. 2).

where

σ_f = a small relatively constant term arising from the friction stress of iron,

σ_s = solid solution strengthening,

σ_p = precipitation strengthening,

σ_D = sub-structural strengthening,

K_y = grain size strengthening,

the main strengthening effect comes from grain size and precipitation effect in niobium steel at higher finish rolling temperature. At finish rolling temperatures below 700°C dislocation and texture hardening also played significant roles as in Figure 2.10.

In controlled rolled plates, micro-alloy carbides and nitrides precipitated during rolling in the austenite region. From micro-structural examination, Morrison et al [9] showed niobium carbide precipitates on prior austenite boundaries, on sub-boundaries within the austenite grains and in rows in the ferrite grains.

Gladman et al [11] (using Ashby/Orowan Model) showed precipitation strength:

$$\sigma_p = \frac{5.9 N_f'}{\bar{x}} \ln \left[\frac{\bar{x}}{2.5 \times 10^{-4}} \right] \quad (2.7)$$

where

N_f' = volume fractions of precipitate from the chemical composition

\bar{x} = mean planar intercept diameter of a precipitate from electron microscopy.

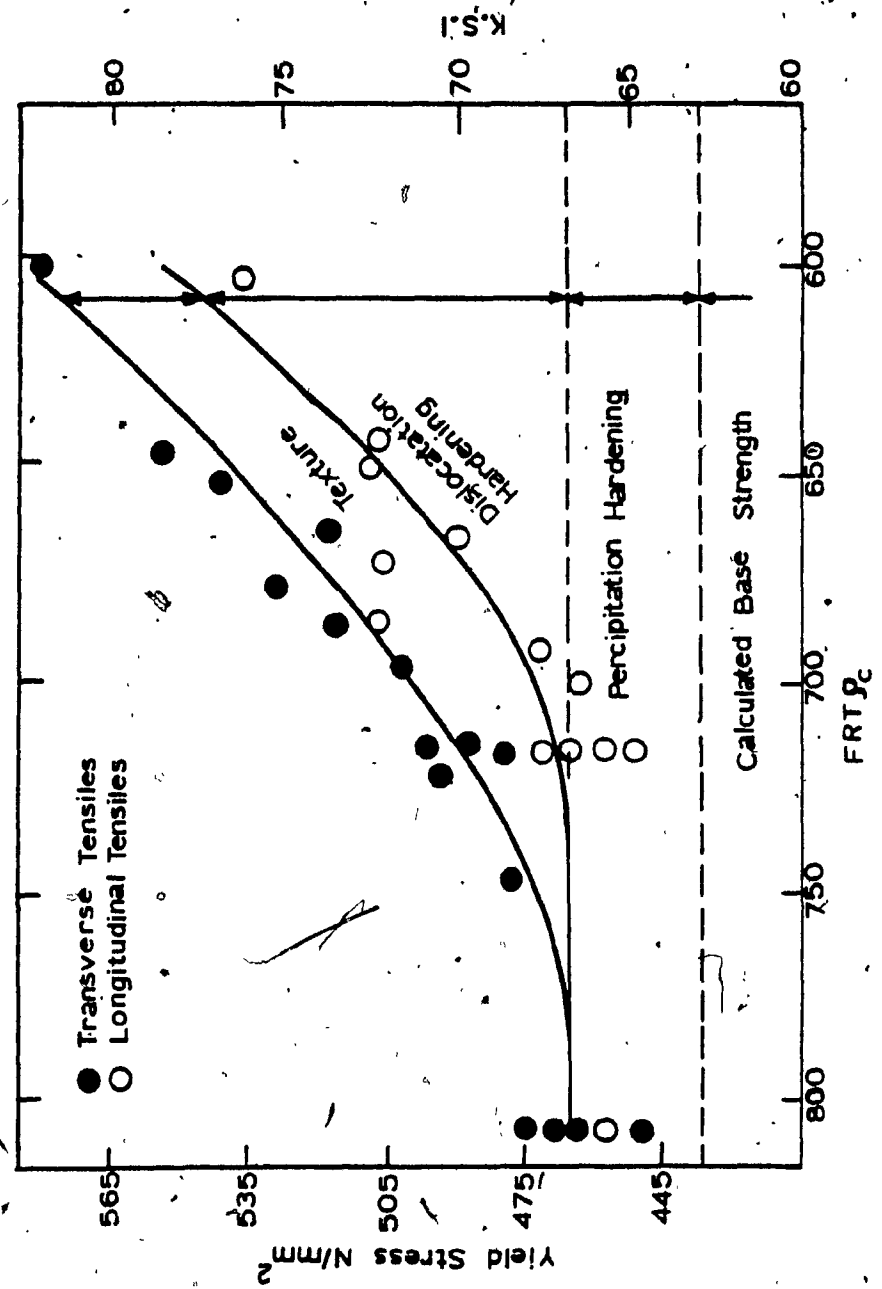


Fig. 2.10: Variation of Yield Strength of X65 Steels as a Function of Finish Rolling Temperature (After Morrison et al, Ref. 9).

It is more difficult to predict impact properties from a knowledge of composition and structural factors than it is to predict yield strength. In niobium and vanadium steels precipitation hardening raises the transition temperature but is counteracted by the grain refinement [9,12].

CHAPTER 3

HOT WORKING CHARACTERISTICS OF STEELS

3.1 INTRODUCTION

Hot working refers to deformation at temperatures above $\sim 0.6 T_m$ (T_m is the melting temperature in $^{\circ}\text{K}$) and at relatively high strain rates (10^{-2} to 10^3 s^{-1}) [13-15]. At these temperatures, most metals have low flow stresses and high ductilities [16]. Both dynamic and static softening processes take place during the entire hot working process [17,18] and this chapter examines the way in which these softening processes change the structure and the mechanical properties of metals and particularly of steels.

3.2 RESTORATION PROCESSES ON HOT WORKING

Recovery and recrystallization have traditionally been considered as mechanisms of restoration through which hot worked metal returns partially or completely to its condition prior to working. The restoration process occurring in the absence of stress or strain is termed static and restoration during straining is called dynamic. The principal factor that determines whether recovery or recrystallization will be the main restoration process during working seems to be the stacking fault energy. It has been proved that for low stacking fault energy metals, the tendency for dynamic recrystallization to occur is more while in metals of medium and high stacking fault energy, dynamic recovery operates as the main restoration process [14,19]. Table 3.1 shows the various high temperature

Table 3.1. High Temperature Softening Processes

Metals	Dynamic Softening Processes		Static Softening Processes	
	At Small Strains	At Large Strains	At Small Strains	At Large Strains
Ni, Ni base super alloys, Cu, γFe, austenitic alloys, brass	Récovery	Recovery and Recrystallization ⁺	Recovery followed by Classical Recrystallization	Recovery and Metadynamic Recrystallization followed by Classical Recrystallization
Al, αFe, ferritic alloys, bcc refractory metals, Zr alloys, hcp metals	Recovery	Recovery	Recovery followed by Classical Recrystallization	Recovery followed by Classical Recrystallization

⁺Under creep conditions, at very low strain rates (i.e. low stresses), dynamic recrystallization may not occur at all.

softening processes occurring in most metals.

3.3 DYNAMIC RECOVERY

The typical flow curve of a metal undergoing dynamic recovery is shown schematically in Figure 3.1. It exhibits an initial work hardening portion up to a strain of 50-100% and a subsequent steady state region with the stress independent of strain. The flow curve is divided into three distinct stages [20]. The first is the micro-strain region, the region in which the plastic strain rate in the sample increases from zero to approximately the applied strain rate. It has been recently found that some dislocation multiplication takes place during this interval, causing an increase in dislocation density [21].

The second stage or the work hardening regime starts with a decrease in the slope of the flow curve at the end of micro-strain interval. The slope of the flow curve here, as well as in the first stage, depends on both temperature and strain rate. During the second stage deformation, the work hardening rate gradually decreases, until finally, in the third or steady state region, the net rate of work hardening becomes zero [22].

3.3.1 Mechanism of Dynamic Recovery

During micro straining some dislocation multiplication takes place and the dislocation density increases slightly. In the strain hardening stage, the dislocations climb, glide and entangle to form a cellular structure. Jonas et al [23] showed that by the time steady

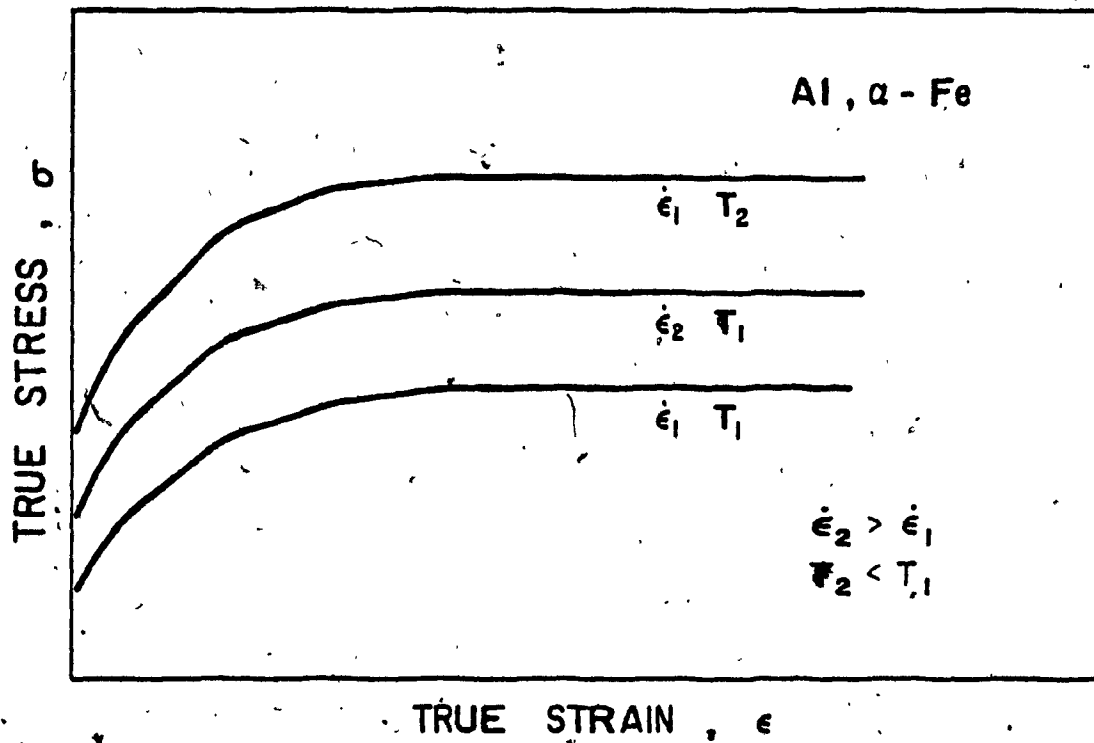


Fig. 3.1: Schematic Representation of the Flow Curve of Metals That Recover Dynamically.

State regime is reached, the dislocations have arranged themselves into subgrains. Dynamic recovery leads to an equilibrium between the rate of dislocation generation and the rate of internal annihilation [24,25], so that a stable dislocation density is maintained during steady state deformation which accounts for the constancy of the temperature, strain rate and flow stress [14]. McQueen et al [14] showed that during steady state deformation the sub-boundaries are continuously breaking up and reforming. This dynamic regeneration termed repolygonization, explains the absence of distorted subgrains even after very large strains. In hot torsion tests, subgrains remained approximately constant in size throughout the steady state deformation [26-29].

3.4 DYNAMIC RECRYSTALLIZATION

The typical flow curves of a material undergoing dynamic recrystallization are shown in Figure 3.2. These curves show a sharp peak at higher strain rate at a particular strain ϵ_p termed peak strain. The work softening region is followed by a steady state region, the minimum strain required for this is denoted by ϵ_s . At lower strain rates in the hot working range, the dynamic recrystallization follow a cyclic flow curve of approximately constant period with declining amplitude [30,31]. New grains appear at the grain boundaries when peak stress is reached, suggesting that the strain to peak stress can be related to the critical strain for dynamic recrystallization (ϵ_c) [32-35]. According to Rossard [36] ϵ_c is given by the approximate relation

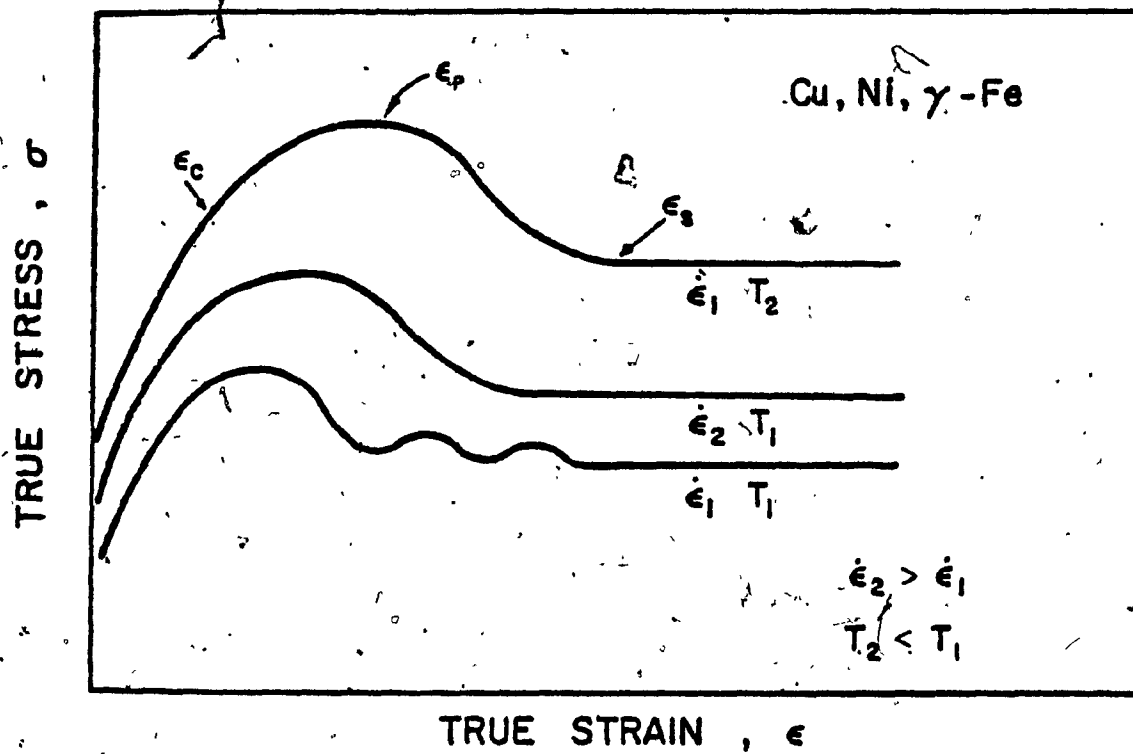


Fig. 3.2: Schematic Representation of the Flow Curves for Dynamic Recrystallization at High and Low Strain Rates.

$$\epsilon_c \approx 5/6 \epsilon_p \approx 0.83 \epsilon_p \quad (3.1)$$

• 3.4.1 Mechanism of Dynamic Recrystallization

In metals and alloys of low stacking fault energy with less dislocation mobility, the rate of annihilation of dislocations is small compared to rate of generation. This leads to high dislocation density which accounts for the nucleation of dynamic recrystallization.

At lower strain rates, the evidence indicates that nucleation occurs by bulging of an existing grain boundary [35,37-38]. As it migrates, it eliminates the dislocations and leaves behind a dislocation free recrystallized structure. Once recrystallization is complete, the dislocation density builds up again, raising the flow stress until recrystallization is again nucleated [30].

At higher strain rates, a fine tangled cellular structure is developed throughout all the grains, which does not leave grain boundary segments long enough to bulge [39]. McQueen et al [40] showed as the strain increases some tangles build up to high mic-orientations, giving rise to nuclei throughout each grain, initiating the dynamic recrystallization. In high strain rate deformation, the gradient of deformation from center to boundary of a recrystallized grain is high. So before recrystallization is complete, the dislocation densities at the centers of the recrystallizing grains have increased sufficiently that another cycle of nucleation occurs. Thus, at any instant, there is a distribution of dislocation sub-structures which maintains the average flow stress at a steady state [30].

3.5 INTERRELATIONSHIPS BETWEEN FLOW STRESS, STRAIN RATE, TEMPERATURE AND GRAIN SIZE

A number of mathematical expressions have been proposed to describe the relationship between flow stress, σ , strain rate, $\dot{\epsilon}$ and temperature, T [26,41-49]. Jonas [42] showed that power law

$$\dot{\epsilon} = A \sigma^n \exp(-\Delta H/RT) \quad (3.2)$$

where A , n are constant

ΔH is activation energy (cals/mole)

R is gas constant

can be used effectively to represent hot working data.

As the dynamic restoration mechanisms are thermally activated, the resultant flow stress depends on both strain rate and temperature. The effect of these variables can be combined by using the Zener-Holloman parameter, [50]

$$Z = \dot{\epsilon} \exp(\Delta H/RT) \text{ sec}^{-1} = f(\sigma) \quad (3.3)$$

which is maintained constant during a hot working experiment.

Both subgrain size and recrystallized grain size produced during deformation vary inversely with Z [14,26,51]. When either the imposed temperature is raised, or the imposed strain rate is decreased, the enhanced mobility of the dislocations leads to a greater rate of annihilation, a lower equilibrium dislocation density, and a greater subgrain size. From Figure 3.3, it can be stated that the subgrain size, d , varies inversely as the logarithm of the

Zener-Holloman parameter (Z). The dependence of the flow stress on the subgrain size (Figure 3.4) was derived as

$$\sigma \propto d^{-1} \quad (3.4)$$

3.6 STATIC RECOVERY

This static softening process takes place after high temperature deformation or between intervals of hot working. During recovery annihilation of dislocations takes place. Static recovery does not replace the deformed grains but leads to structural changes on a fine scale within the existing grains. The driving force for static recovery is the high density dislocation sub-structure which rearranges to attain a lower energy level. The recovery process does not lead to full softening, but saturates at a softening level well below 100% [30].

3.6.1 Effect of Experimental Variables on the Rate of Static Recovery

The main experimental variables affecting the recovery rate after high temperature deformation are the deformation and holding temperature, strain and strain rate. Djaic [34] showed that the recovery rate increased with temperature, strain and strain rate. The effect of high deformation and holding temperature, on the recovery rate is not as marked as on recrystallization rate. The difference is accounted for by the strong dependence of grain boundary mobility on higher holding temperature. Increases in strain lead to increases in the recovery rate until steady state flow is reached. This can be

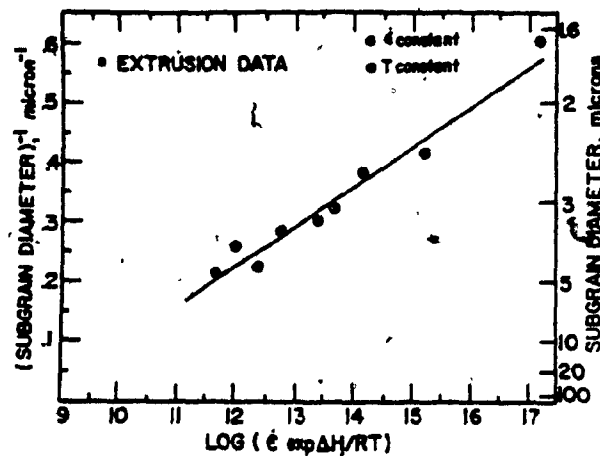


Fig. 3.3

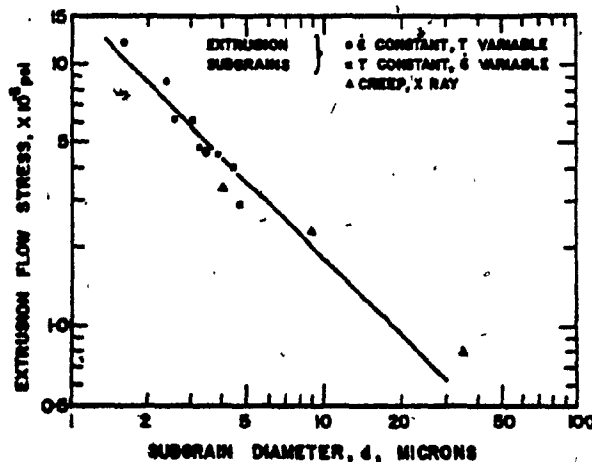


Fig. 3.4

Fig. 3.3: Relationship Between Subgrain Size(d) and Zener-Holloman Parameter(Z). Higher Extrusion Rates and Lower Temperatures (Larger Z) Results in Smaller Subgrains.

Fig. 3.4: Log-Log Plot of Flow Stress Against Subgrain Size in Extrusion and Creep, the Slope of Approximately -1 Indicates an Inverse Proportionality (After McQueen, Ref. 26).

attributed to the attendant increase in dislocation density, and therefore driving force, with strain until equilibrium is reached. The strain rate of prior working also affects the recovery rate. With an increase in strain rate at a fixed temperature, the recovery rate increases [34].

3.7 STATIC RECRYSTALLIZATION

In this classical recrystallization process, dislocations are eliminated in large numbers as a result of the motion of high angle boundaries. Static recrystallization results in new strain free grains nucleated from the strained grains. A critical strain of the order of 10% is required for static recrystallization to take place. The fraction transformed in this process is related to time by a sigmoidal curve (Figure 3.5). The length of the incubation period depends on temperature and on the amount of prior strain, as will be discussed below [52,53]. If the critical strain for recrystallization is exceeded, softening by static recovery takes place during the incubation period.

3.7.1 Experimental Variables Affecting Recrystallization

Inclusions, precipitates, solutes, strain, strain rate, temperature and prior recovery all affects the recrystallization. Inclusions and precipitates have similar effects on recrystallization. Nucleation can be retarded or accelerated, depending on the particle size and inter-particle spacing. If the particles are large and the spacing is coarse, then nucleation is accelerated [55,56]. Such

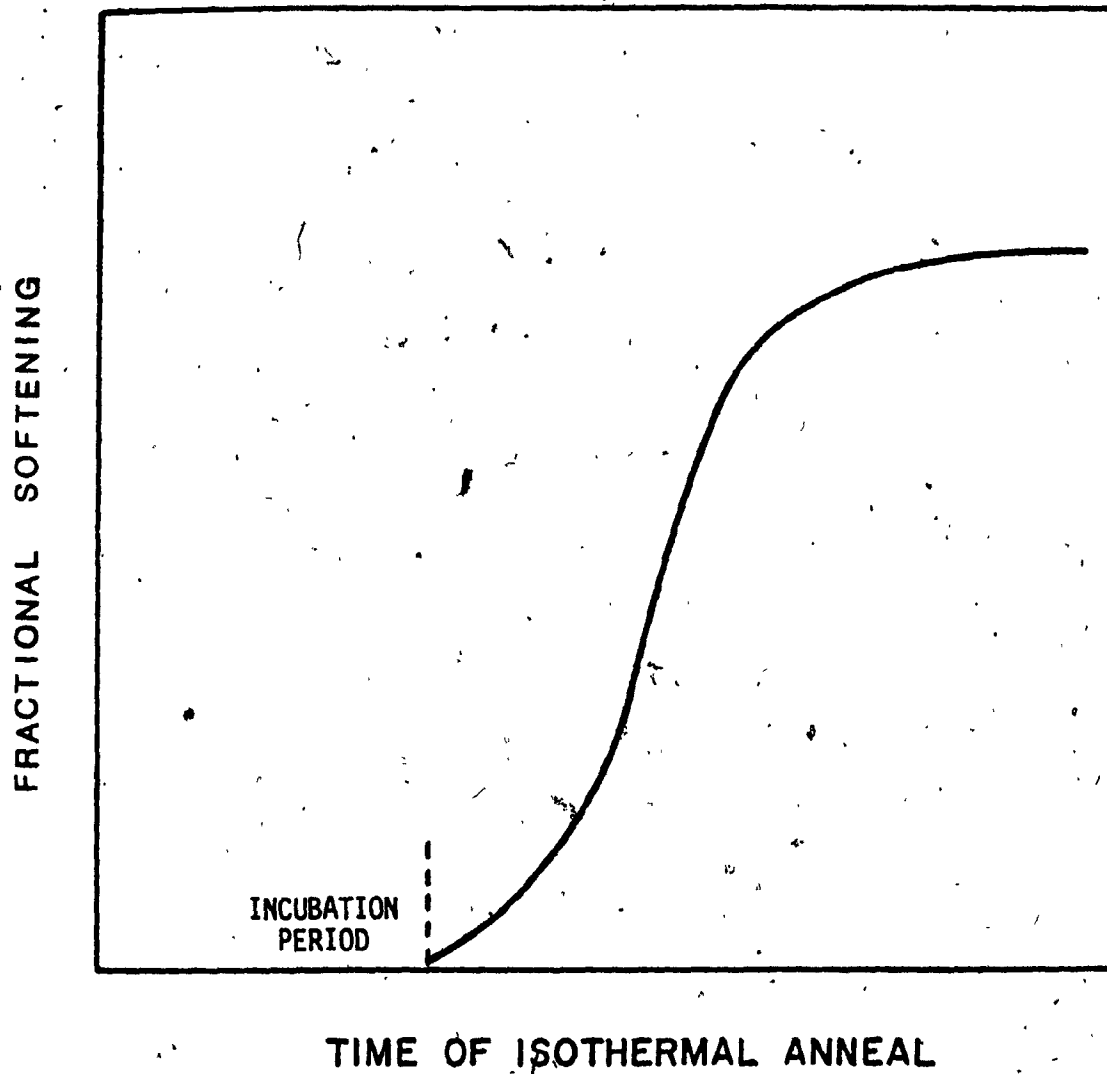


Fig. 3.5: The Progress of Isothermal Annealing After Cold Deformation.

acceleration has been attributed to the high dislocation densities produced in the neighbourhood of the particles by the deformation. But if the precipitates are small and finely spaced, they interfere with the growth of subgrains during the nucleation stage.

Luton and Sellars [35] showed that rate of recrystallization can be reduced by the addition of suitable solutes. There are several reasons why this trend is observed. One is the drag effect of impurity atoms on moving grain boundaries; another is the increase in the density of possible nucleation sites caused by impurity addition.

Fine recrystallized grains are obtained after high strains at high Z particularly if the initial grain size is also fine [57,58]. Both increase of strain rate and temperature increases the recrystallization rate [52]. It has been also found that the rates of nucleation and growth decrease with the amount of prior recovery [57,59].

3.8 METADYNAMIC RECRYSTALLIZATION

When high temperature deformation is halted during dynamic recrystallization, many nuclei are already present within the material, that is some of the grain boundaries are migrating and sweeping regions free of dislocations. These boundaries can continue to migrate and the nuclei to grow without any classical incubation period being required. This softening process resulting from the continued growth of these nuclei is known as metadynamic or post-dynamic recrystallization. Nucleation of static recrystallization

also takes place in regions which do not contain dynamic nuclei [30].

3.9 MULTIPLE DEFORMATION

The plate or strip rolled from the ingot is not usually attained by a single pass. The final product is obtained through a rolling sequence involving a series of passes separated by intervals of time. Figure 3.6 shows schematically the multiple deformations involved in a plate rolling schedule along with their temperatures, amount of deformation produced, strain rate involved, etc. The R_1 , R_2 etc shown in the figure are roughing stands and F_1 , F_2 etc are the finishing stands. Usually, in plate rolling, two high mills are used for roughing and four high mills for finishing. It can be noted that the strain rate of successive passes increases and reaches a very high value during finish rolling. The hot working characteristics of mild steel and HSLA steels are different and are discussed briefly in the forthcoming sections.

3.9.1 Interrupted Tests

Interrupted mechanical tests have been used by many researchers [34,53,60-64] to analyse the progress of softening after hot working of steel. The technique used is based on the principle that the stress at high temperatures is a sensitive measure of the structural state of the material. The samples were loaded at a constant true strain rate to the required deformation and then unloaded and held at no load condition for increasing time intervals. Following the delay

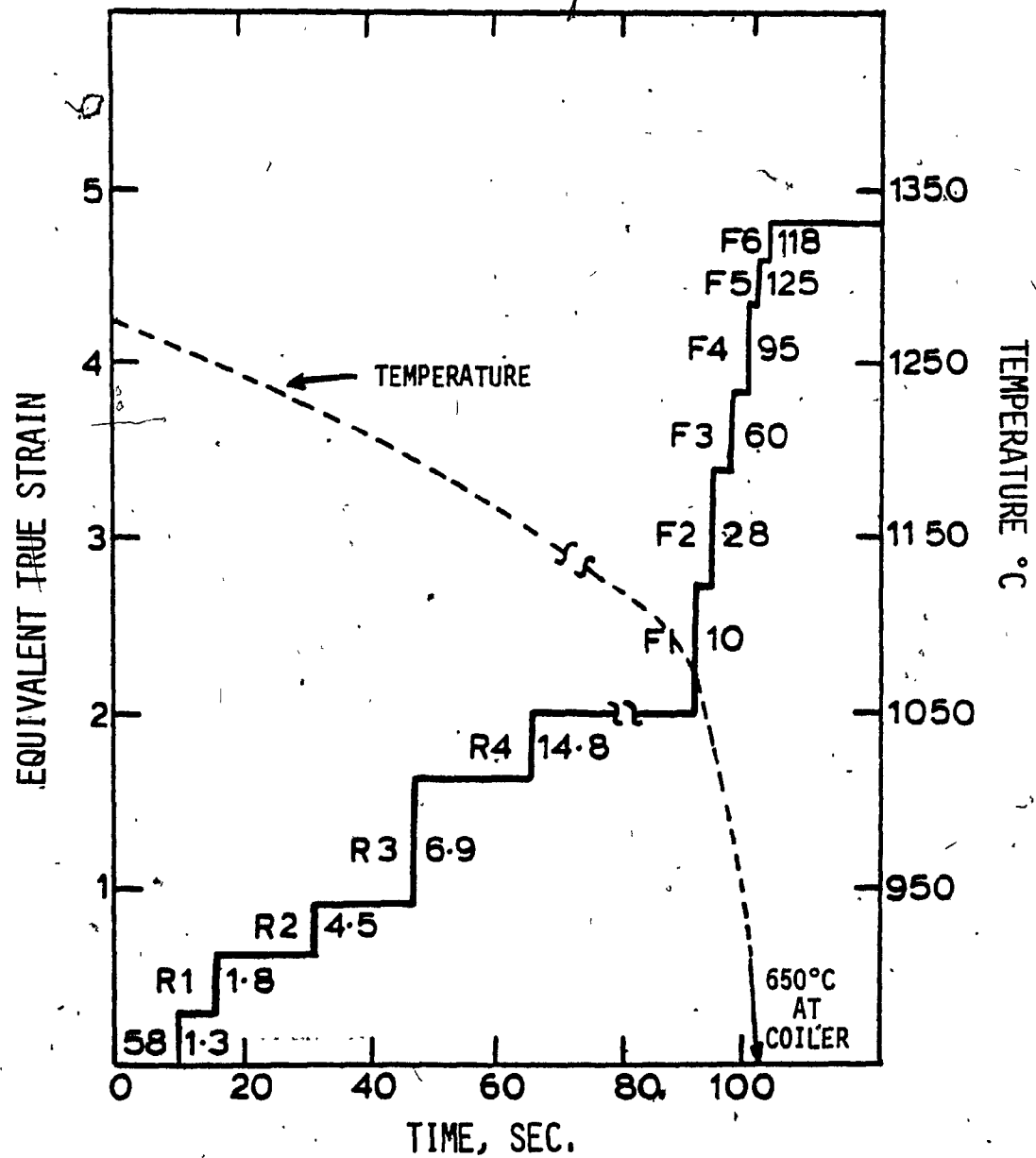


Fig. 3.6: Typical Schedule for Rolling 216 mm Slab to 2 mm Strip (Tinplate) (After Sellars et al., Ref. 58).

time the samples were reloaded at the same strain rate. One such test is shown in Figure 3.7. After a short holding time, t_1 , the flow stress on reloading rises rapidly to a stress level comparable with the unloading stress. On the other hand, the reloaded flow curve after long delay time, t_2 , resembles that of initial loading. The magnitude of the yield stress on reloading is governed by the degree of structural change that has occurred during the holding interval and can therefore be taken as a measure of the progress of softening. Several workers [34,53,60-65] have reported that the softening after hot working can be due to one or two or all the three softening mechanisms discussed before, depending on the strain rate, temperature and interruption strain. A detailed study of the amount austenite softening with increasing time under different test conditions is given by Petkovic et al [65].

Duplex mechanical testing was used by Dunstan et al [63] to study the progress of softening of aluminium after hot working; in this case metallography confirmed the results. Interrupted deformation with equal shear strains and equal rest period was carried out on Al-5% Mg alloy by Farag et al [66] (Figure 3.8). The interrupted curve shows an increase in torque level over that for continuous deformation; this they ascribed to the strengthening associated with the alloy addition which decreased during deformation and returned during the rest periods by strain aging. The ductility was greater in the interrupted tests because the static restoration inhibits the fracture mechanism.

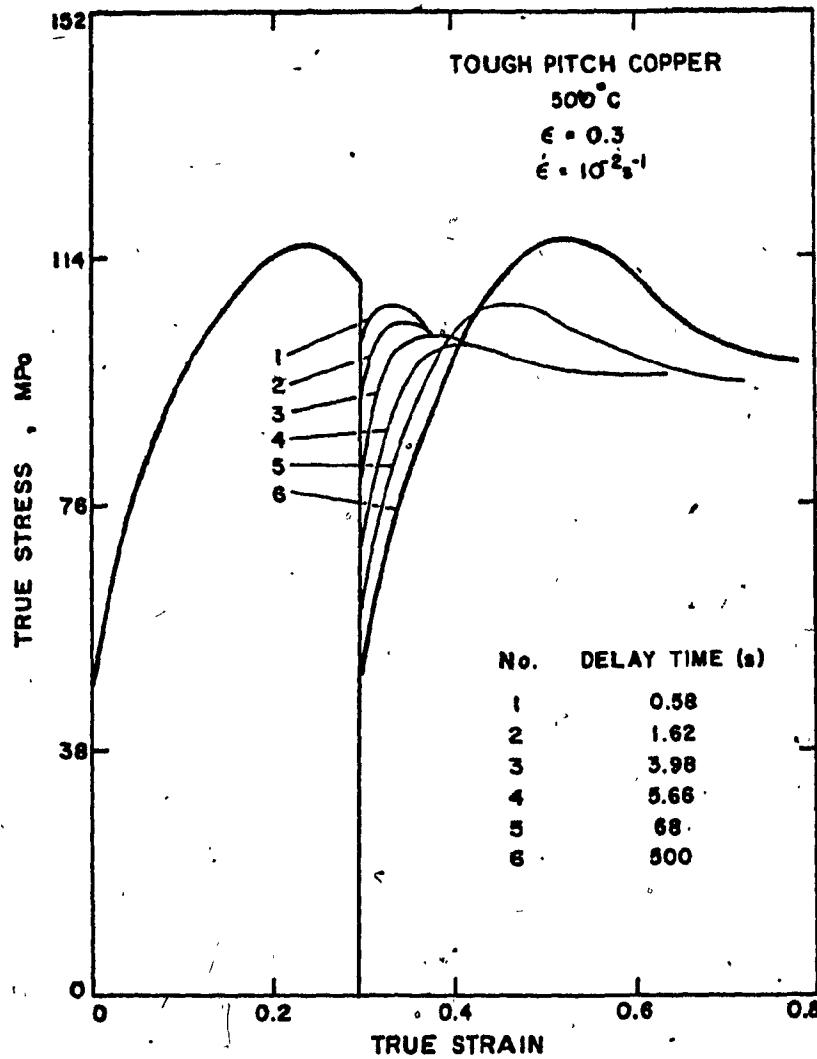


Fig. 3.7: Effect of Increasing Delay Time on the Interrupted Flow Curve (After Petkovic, Ref. 21).

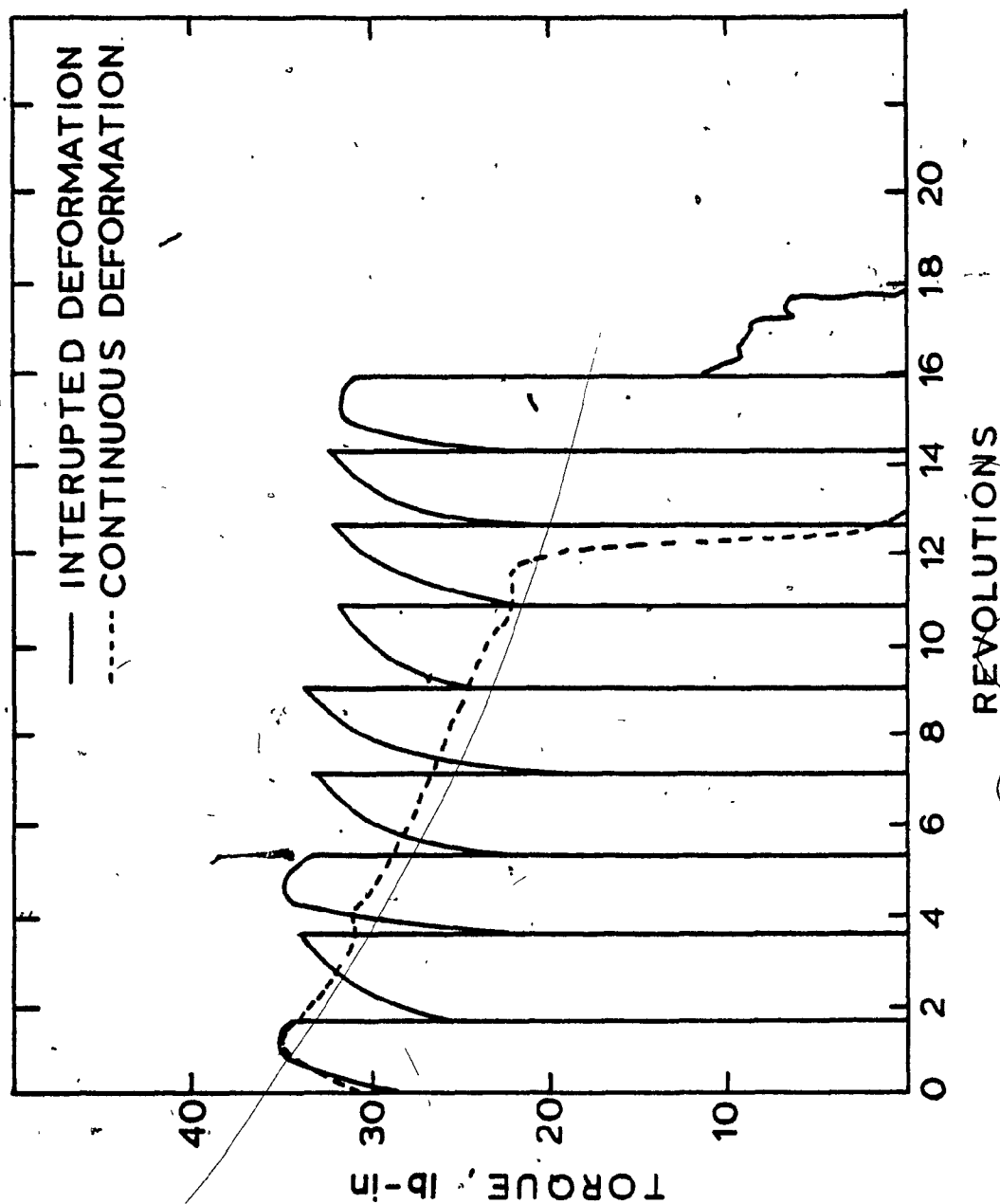


Fig. 3.8: Effect of Interrupted Deformation by Incremental Surface Shear Strains of 1.38 Followed by Rests of 2 min. on the Torque-Revolution Curve for Al-5% Mg at 450°C and a Surface Shear Strain Rate of 3.93 s⁻¹ (After Farag et al. Ref. 66).

3.10 CONTROLLED ROLLING

The effects of hot working and the rate of cooling on the characteristics of recrystallization are utilized in the process known as controlled rolling [5,67-69]. The objective of controlled rolling is to produce a fine grained austenite which is transformed to a fine, uniform ferrite with high yield strength and low transition temperature [5,67-69].

✓ In mild steel, fine grained austenite is produced by static recrystallization following deformation of 50% at the finishing temperature. The finishing temperature here must be low enough so that there is very little grain growth during run-out from the rolling mill. If the strain in the relevant passes is much greater than 50% austenite will recrystallize dynamically during deformation. Such softening cycle can lead to undesirable mixed final grain size [30].

Niobium addition to a steel decreases the recrystallization rate of austenite especially in the static conditions thus giving rise to fine ferrite grains after transformation. The improved strength and lower transition temperature of these steels produced by a lower finish-rolling temperature can be seen from Figure 3.9.

3.10.1 Problems in Controlled Rolling

Major problem in controlled-rolled niobium steel is the occurrence of a mixed or duplex grain size [5,9]. This nonuniform microstructure of ferrite and pearlite have lower strength and much poorer toughness than an equiaxed fine-grained one obtained from the same

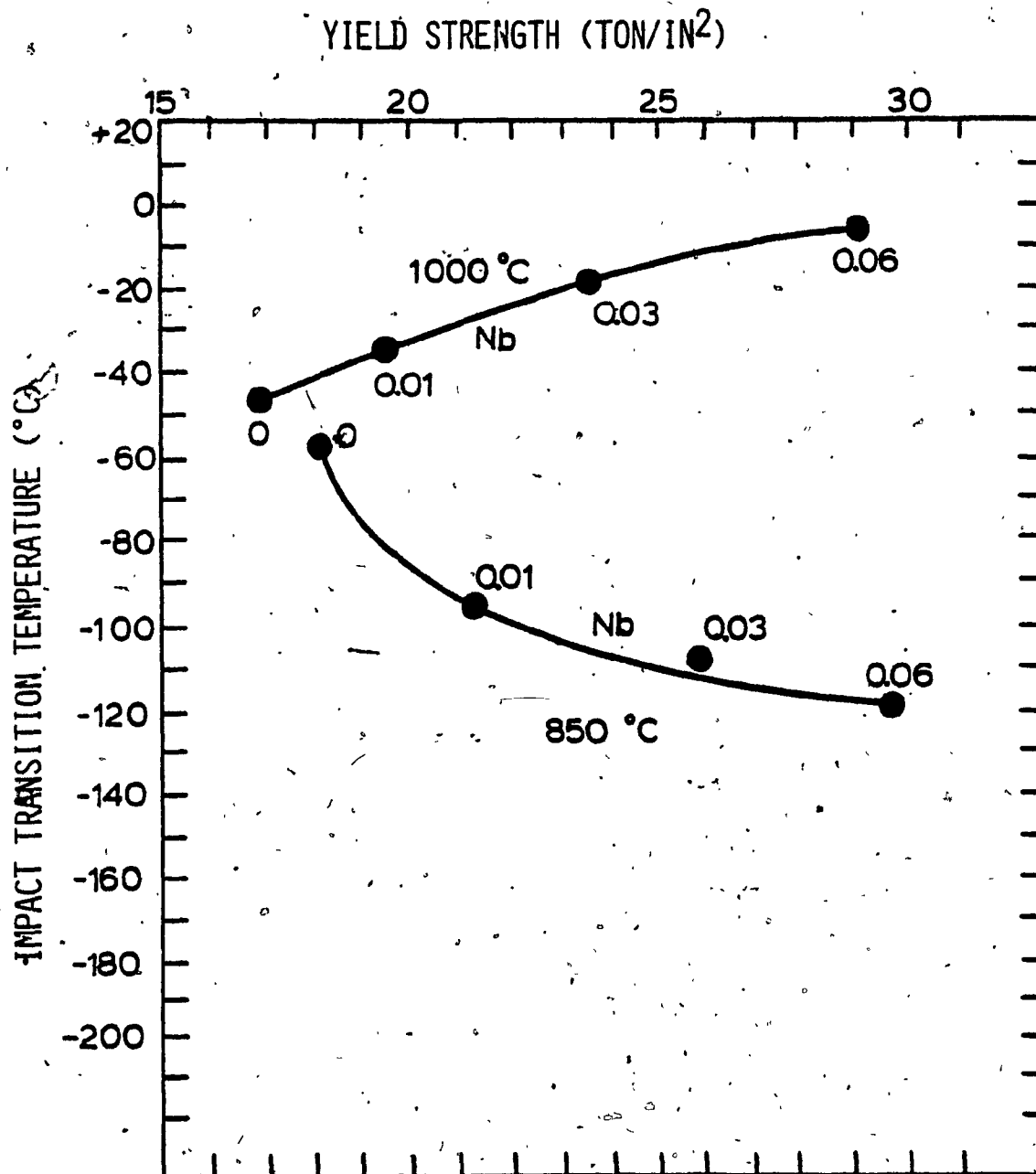


Fig. 3.9: The Effect of Niobium Addition on the Room Temperature Yield Strength and Impact Transition Temperature of a 0.04% C, 6.5% Mn Steel. The Improvement Resulting from a Lower Rolling Temperature is also Shown (After Jones et al., Ref. 70).

finish rolling temperature [1,5].

The difference in the rolling schedule resulted in the difference of microstructure as illustrated in Figure 3.10. The thin commercial material showed a fine, uniform ferrite structure whereas thicker plates exhibited a mixed grain size, due to the occurrence of partial recrystallization during the holding period and absence of recrystallization during subsequent rolling [1].

As the number of rolling passes increases, the temperature decreases below 1100°C and the time for completion of recrystallization increases. During the rolling of thin plates, precipitation of niobium takes place on the subgrain boundaries formed by recovery at each pass and coarsen during subsequent passes thus stabilizing subgrains and restraining recrystallization and grain boundary migration. The overall rate of recrystallization is thus reduced and if the rolling sequence is sufficiently rapid no recrystallization occurs in the austenite in the later rolling stages, and a fine grained ferrite results after transformation.

In thicker plates due to long holding at intermediate stages and temperatures recrystallization occurs partially. The partially recrystallized structure, containing large grains embedded in a matrix of small ones as shown in Figure 3.10 never recrystallizes again into a satisfactory uniform structure, since the temperature drops below that of rapid recrystallization [1,5]. Explanation of the differences arising in the two schedules can be schematically represented as in Figures 3.11 and 3.12 [1].

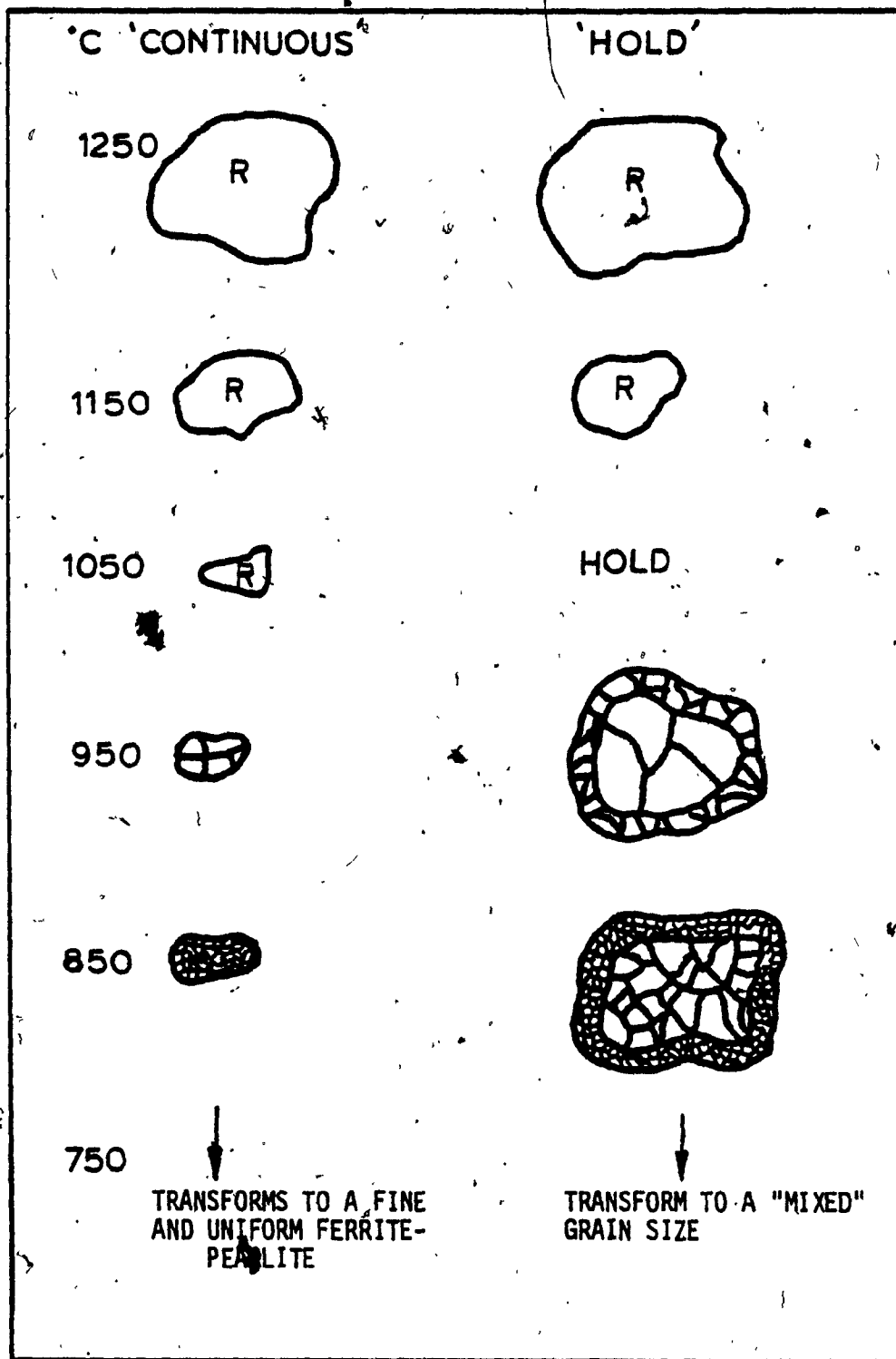


Fig. 3.10: Schematic Diagram Contrasting Recrystallization Effects in the Two Schedules ('Continuous' and 'Rough-hold-finish') for C-Mn-Nb Steel (R = Recrystallized Structure) (After Duckworth et al., Ref. T).

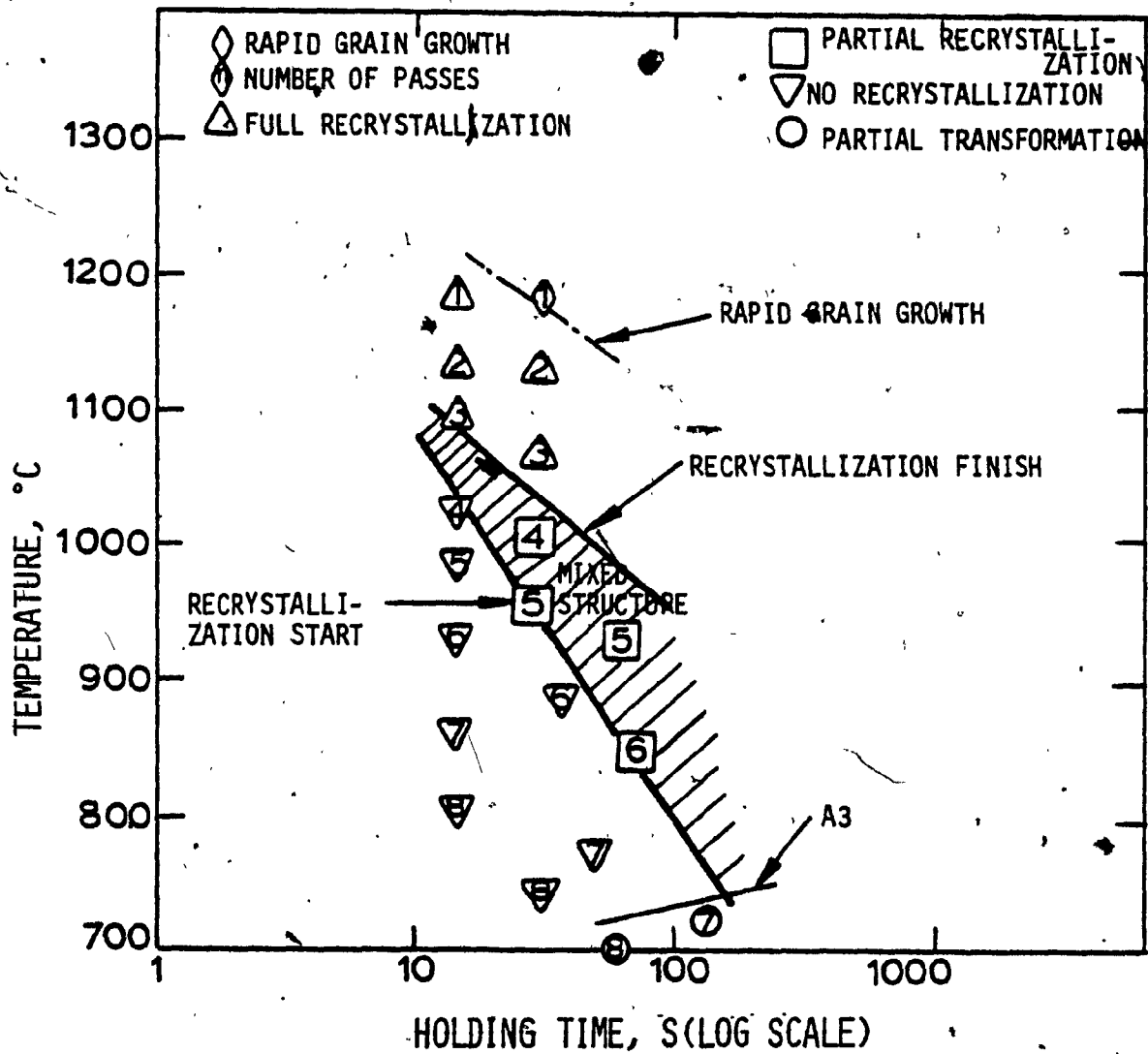


Fig. 3.11: Schematic Representation of State of Recrystallization During Hot Rolling of C-Mn-Mn Steels (After Duckworth et al., Ref. 1).

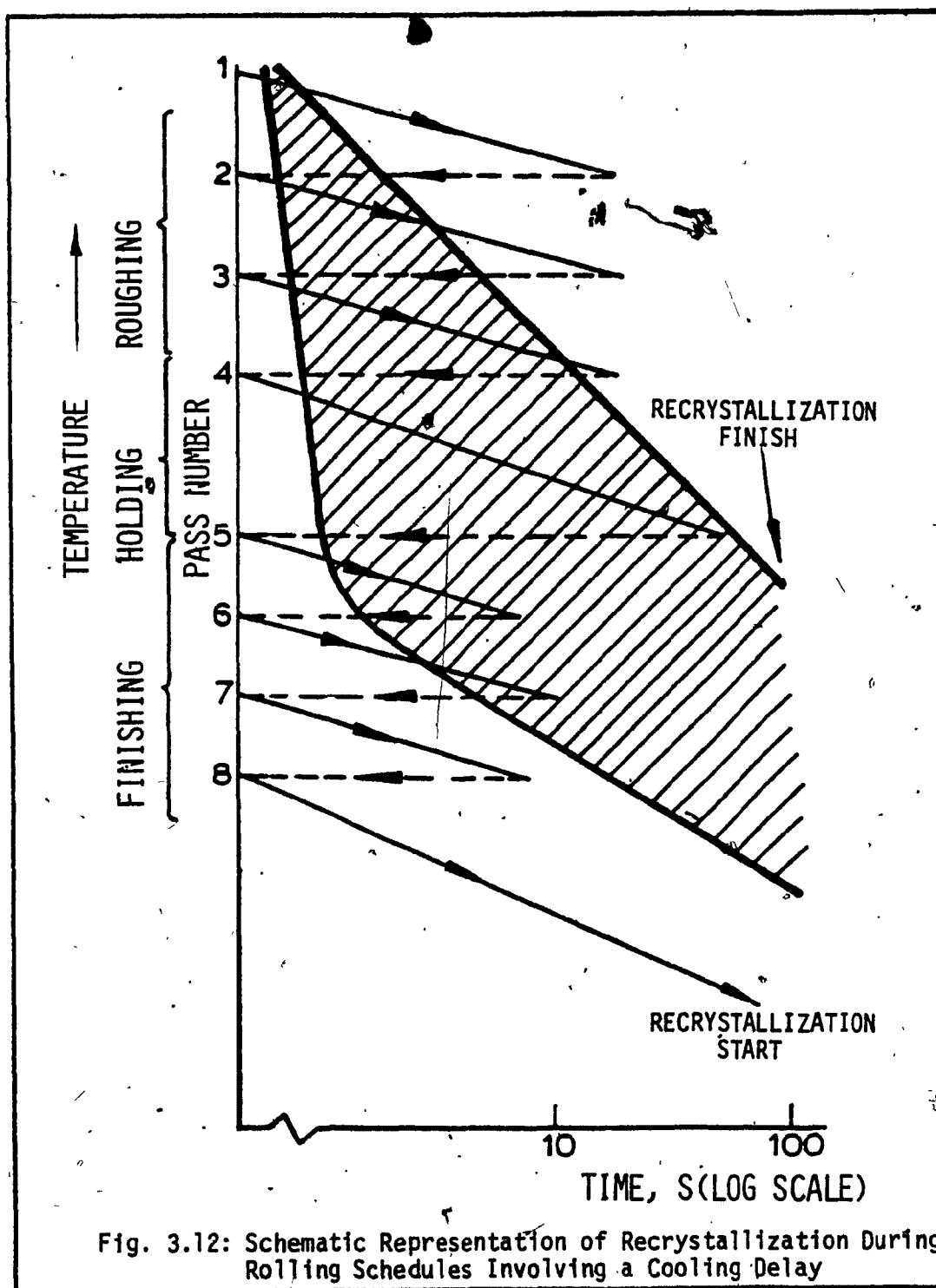


Fig. 3.12: Schematic Representation of Recrystallization During Rolling Schedules Involving a Cooling Delay

(After Duckworth et al., Ref. 1).

To avoid mixed grain size, the material should not be held in the temperature range of 1080°C down to 950°C. Continuous deformation in this range is essential for producing uniform grains and this can be achieved by [1,5].

(1) Using lower reheating temperature of 1200°C rather than the usual +1300°C and rolling continuously to finish at 900-850°C.

(2) If reheating temperature is fixed at +1300°C, the rolling schedule is modified such that the "hold" is made above 1100°C or below 950°C. The former case gives a rapid recrystallization and in the latter it is too low for any recrystallization - in both cases, there is small chance of an inhomogeneous grain size [1,5].

3.11. METALLURGY OF STEELS ON HOT ROLLING CHARACTERISTICS

3.11.1 Strength and Ductility of Mild Steel

The strength and ductility exhibited by a hot worked steel depends on both temperature and carbon content of the steel [71,72]. Increase of temperature and increase of carbon content in the austenite range increased the ductility and decreased the strength of mild steel. This is due to the fact that carbon increases the self-diffusion of iron in austenite. When hot worked in the alpha-plus-cementite range, where dynamic recovery is the softening mechanism, increase of temperature increases the ductility and decreases the strength of mild steel for a particular carbon content. In this range, increasing carbon content (>0.1% C) decreased the ductility and increased the strength, due to the increasing amount of the hard, brittle cementite.

In the two phase alpha-plus-gamma region increasing temperature decreases the ductility of mild steel because the amount of the harder γ phase increases. However, in the lower part of this range strength continues to decrease because of the softer α phase but started to increase as the temperature approaches that for complete austenite.

3.11.2 Restoration Processes During Plate Rolling of Mild Steel

Comparison of the usual strains in a rolling pass with strain to the onset of dynamic recrystallization in austenite indicates that some dynamic recrystallization could occur during early rolling passes of mild steel. During the initial rolling (i.e. at high temperatures and low strain rate) of mild steel complete static recrystallization occurs between passes in less than a second. Although this is followed by grain growth, the overall effect in roughing is such that the grain size is reduced in each successive pass. Later in the rolling sequence, where temperature is lower, individual pass strains are too small to cause the onset of dynamic recrystallization and this process is likely to occur only if strain accumulates over several passes because static recrystallization has not taken place between previous passes [58,73]. Holding between roughing and finishing produces considerable grain growth in mild steel. In finish rolling due to high strain rate again complete static recrystallization between passes is found to occur in mild steel [58,73].

3.11.3 Effects of Nb on Hot Rolling

The main features, differentiating the behavior of Nb bearing from that of low carbon steel during hot rolling are [74]:

(1) At a given temperature the deformation required to initiate dynamic recrystallization of austenite is higher in HSLA steels.

(2) After deformation static recrystallization of austenite generally proceeds at slower rate in HSLA steels.

After solution treatment in HSLA steels at $\sim 1260^{\circ}\text{C}$ the Nb(C,N) precipitation in constrained austenite proceeds very slowly [75]. Under deformation, dynamic precipitation occurs, retarding the nucleation of dynamic recrystallization, thus increasing the strain to the peak [75,76].

In static condition, Nb steels starts to recrystallize after ~ 10 seconds and complete recrystallization is expected only after 10^3 - 10^4 seconds [75]. So during the holding periods of roughing operations, only a small amount of static recrystallization is expected in Nb steels. The delay in static recrystallization is due to the pinning action of the precipitates on grain boundaries and sub-boundaries. At high strain rate, it has been found that retardation effect results from 'solute-drag effect' rather than precipitation [76,62]. During the initial period, precipitation is occurring and consequently recrystallization proceeds slowly. As the time increases precipitation is complete and the static recrystallization accelerates [75]. In HSLA steels during the intervals between the first few

passes, static recrystallization frequently do not occur. However, it is found to occur when high strains have been accumulated after several passes [73,75].

CHAPTER 4

EXPERIMENTAL PROCEDURE

4.1 TORSION TESTING

Hot torsion of solid bars has been extensively used as a deformation mode in hot working studies [48,77-78]. Torsion that permits deformation up to high strains at a constant shear strain rate, but is complicated by the variation in strain and strain rate across the section. Since the dimensions remain constant, the true strain rate and the engineering strain rate are equal and constant [16]. Both multi-pass processes, such as slab rolling and total deformation, as in planetary rolling mill, are readily simulated in torsion machine [71,79-81]. In the present work, both the above processes are simulated for low carbon and HSLA steel to determine their hot deformation characteristics.

The data obtained in torsion testing were of the form of graph, drawn between torque and total angle of twist. Torque was converted to torsional shear stress by using the maximum shear stress formula [82,83]:

$$\tau = M_T(3 + m + n')/2\pi r^3 \quad (4.1)$$

where

M_T : torsional moment

m : strain rate sensitivity exponent

n' : strain hardening exponent

r : radius of the specimen gauge section

At temperatures above $0.5 T_m$, n' is extremely small and m is the dominant parameter, whereas at low temperatures the reverse is true [81-83].

Torsional strain is defined as the amount of relative rotation under an applied torque, by reference points on the surface of the specimen divided by the distance between them. Thus, the torsional strain on the surface, γ , is [71]:

$$\gamma = \frac{\pi D}{L_0} \times N \quad (4.2)$$

where

$\pi D N$: the amount of rotation

D : the gauge diameter, and

L_0 : the original gauge length

In order to compare the present torsion results with other tension and compression tests, the torsional shear stresses and strains were converted to effective stresses and strains using the Von Mises criterion of plastic yielding [84,85]. These relations are:

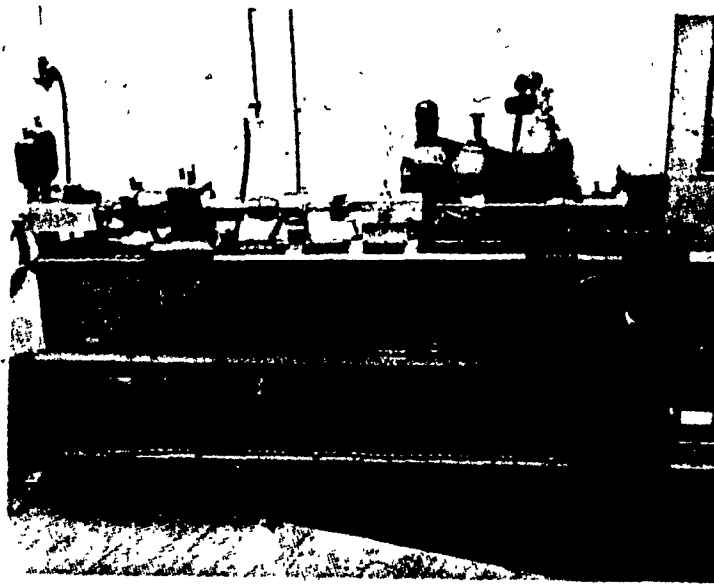
$$\bar{\sigma} = \tau \sqrt{3} \quad (4.3)$$

$$\text{and } \bar{\epsilon} = \gamma / \sqrt{3} \quad (4.4)$$

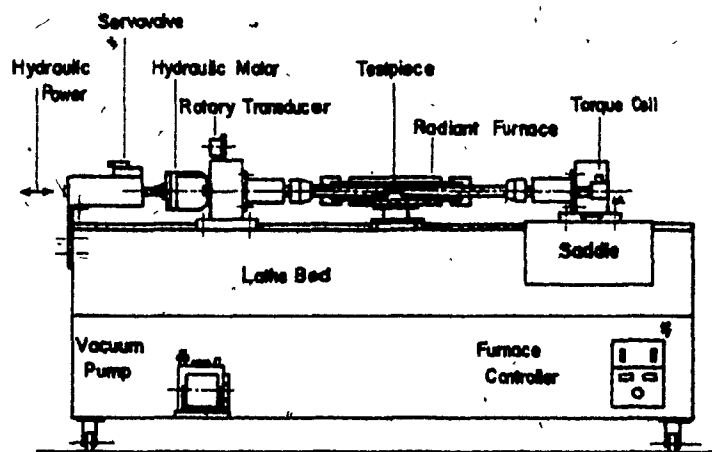
where $\bar{\sigma}$ and $\bar{\epsilon}$ are equivalent stress and equivalent strain respectively.

4.2 TORSION TESTING SYSTEM AND PROCEDURE

A servo controlled closed loop torsion tester was used for the hot deformation studies (Figure 4.1). The torsion machine is capable of applying a maximum of 100 revolutions of twist at



(a)




(b)

Fig. 4.1 Servo-Controlled Hydraulic Torsion Machine

velocities up to 15 revolutions/second with a maximum torque of 110 Nm. On the torsional frame the test piece was held by superalloy loading members. One end of the test piece was twisted by a measured amount by a hydraulic motor controlled by a servo valve, while the other end was held fixed by a torque cell.

The displacement of the motor is controlled by a closed-loop "MTS" control system (Figure 4.2). The rotary displacement is measured by a dual gang potentiometer, which provides the feedback signal to the controller. The torsion tester can be operated on either rotary displacement or torque feedback mode. The former was used for the present experiments. A Hewlett-Packard X-Y recorder was used for plotting torque against angular displacement. A detailed description of this machine has been given by Fulop et al [86].

A water cooled radiant split furnace was used and tests can be made from room temperature up to 1100°C in either air or in an inert atmosphere (argon in the present investigation). The temperature was measured by a thermocouple extending into the test piece shoulder through the reaction bar. A 15 mm wide strip of the parabolic mirror of the furnace was shaded by carbon black so that the temperature variation along the gauge length of the specimen was no more than $\pm 1^\circ\text{C}$ at any temperature. Before experiments, a correlation between the controlling thermocouple and the gauge length temperature was found by embedding external thermocouples along the test piece's length. The output of the reaction torque cell was also calibrated with a lever system and known weights.



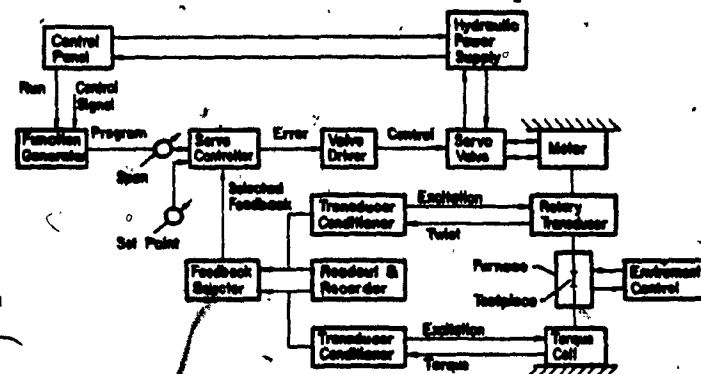


Fig. 4.2 -The Control System

Based on the initial calibration, the actual experimental values of temperature and torque were within $\pm 0.5\%$ and 2.0% of the recorder values.

4.3 TEST MATERIALS AND TEST PROCEDURES

4.3.1 Test Materials and Its Preparation

The test materials, low carbon and Nb-bearing steel (HSLA) used in the present studies were supplied by Sidbec-Dosco Steels Ltd, Quebec. The materials were in the form of rolled plates of sizes $42'' \times 11\frac{1}{2}'' \times 0.717''$ and $37'' \times 12''-15'' \times 0.625''$ for low carbon and HSLA steels respectively. The chemical composition of both the steels are given in Table 4.1. Torsion test pieces were removed from the plate with their axes in the rolling direction with close tolerances especially in the gauge section to insure that twisting would be uniform. The test piece design is shown in Figure 4.3. One end of the test piece was threaded, and the other had a rectangular section, which slipped into a slot in the grip that allowed easy removal without accidentally straining the specimen. For all the samples transition shoulders of intermediate diameter were provided between the gauge length and the grip sections in order to reduce the heat flow and the temperature gradient in the gauge length.

As the maximum temperature reached in the radiant furnace was only 1100°C , the niobium steel specimens were presoaked in an outside furnace for 30 minutes at 1250°C to dissolve niobium carbide. This was done by placing the samples with some zirconium pieces in a Sen-Pak⁺

⁺ Registered trade mark of the Sentry-Co., Foxboro, Mass.

Table 4.1. Chemical Composition in wt% of the Materials Tested.

	C	Mn	S	P	Si	Cu	Ni	Cr	Mo
Low carbon Steel	.14	.56	.025	.004	.009	.20	.09	.06	.012
Niobium Bearing Steel	.12	.94	.016	.003	.007	.09	.04	.04	.007
	Sn	Ti	Al	V	Nb	N ₂ (ppm)			
	.00	.000	.049	.000	.00	48			
	.01	.000	.005	.002	.05	45			

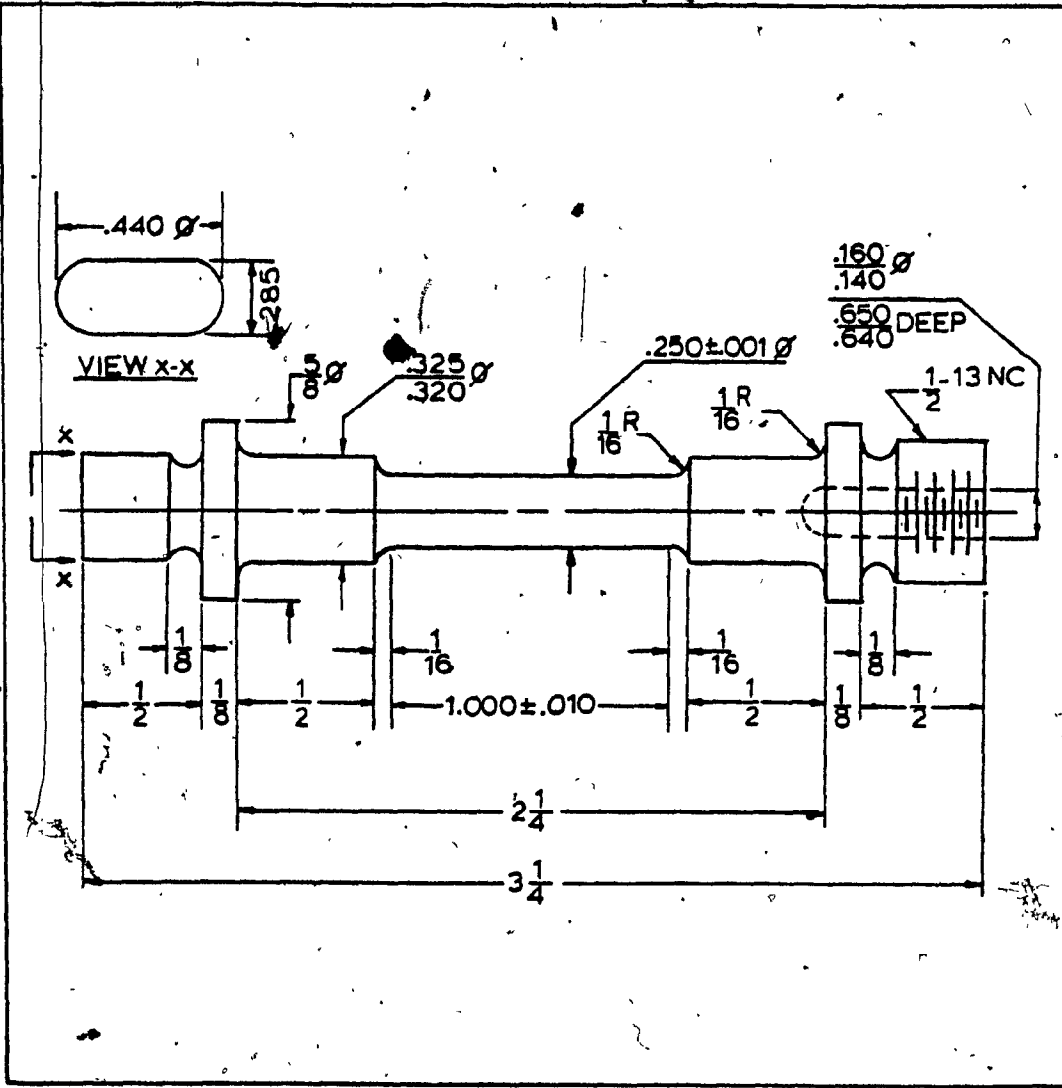


Fig. 4:3: Test Piece Design(1n inches).

stainless steel annealing envelope. Zirconium was used as a sacrificial oxidizer as they have strong oxidizing capacity compared to steel. After 30 minutes of heating at 1250°C, the specimens were quenched in water in order to keep the niobium in solution. The samples treated in this way were quite bright and showed very little of surface oxide.

4.3.2 Test Procedures

Prior to starting of any test the mirror of the furnace was cleaned so that the test temperature could be reached as quickly as possible. Specimens were inserted into the grips of the bars with high temperature anti-seize agent⁺. All tests were carried at temperatures of 900°C, 950°C and 1000°C and at torsional shear strain rate of 0.1 s^{-1} and 1 s^{-1} in a controlled atmosphere of argon. Continuous and interrupted deformation tests were performed for both low carbon steel and HSLA steel (Nb-bearing steel).

In the continuous deformation tests, the samples were twisted without interruption to fracture or to the capacity of the machine.

In the interrupted tests, experiments were conducted such that the interruptions were of equal time duration at equal strain intervals. For both the steels, at lower strain rate (0.1 s^{-1}), the experiments were carried out at all three temperatures of 900°C, 950°C and 1000°C with equal interruption strain of 20%. At each particular temperature

⁺ Registered trademark of the Releasall Ltd., Montreal.

three different tests were conducted so that each had a constant interruption time of either 10, 20 or 40 seconds. Interruptions were made by switching off the hydraulic power after the required amount of straining and stopping the machine for the required amount of interruption time.

Tests were also conducted for both the steels at temperatures of 900°C and 950°C at a higher strain rate of 1.0 s^{-1} with interruptions at equal intervals of 40% deformation. Here also the interruption time were either 10, 20 or 40 seconds in a particular test.

The difference in the level of stress at the instant of unloading and of that at the beginning of reloading was measured to assess the amount of restoration taking place during the delay period. Figure 4.4 shows the method of data analysis. The amount of restoration has also been expressed as the fractional softening by calculating the rate of the above drop in stress to the increase in stress due to strain hardening during the first cycle of strain.

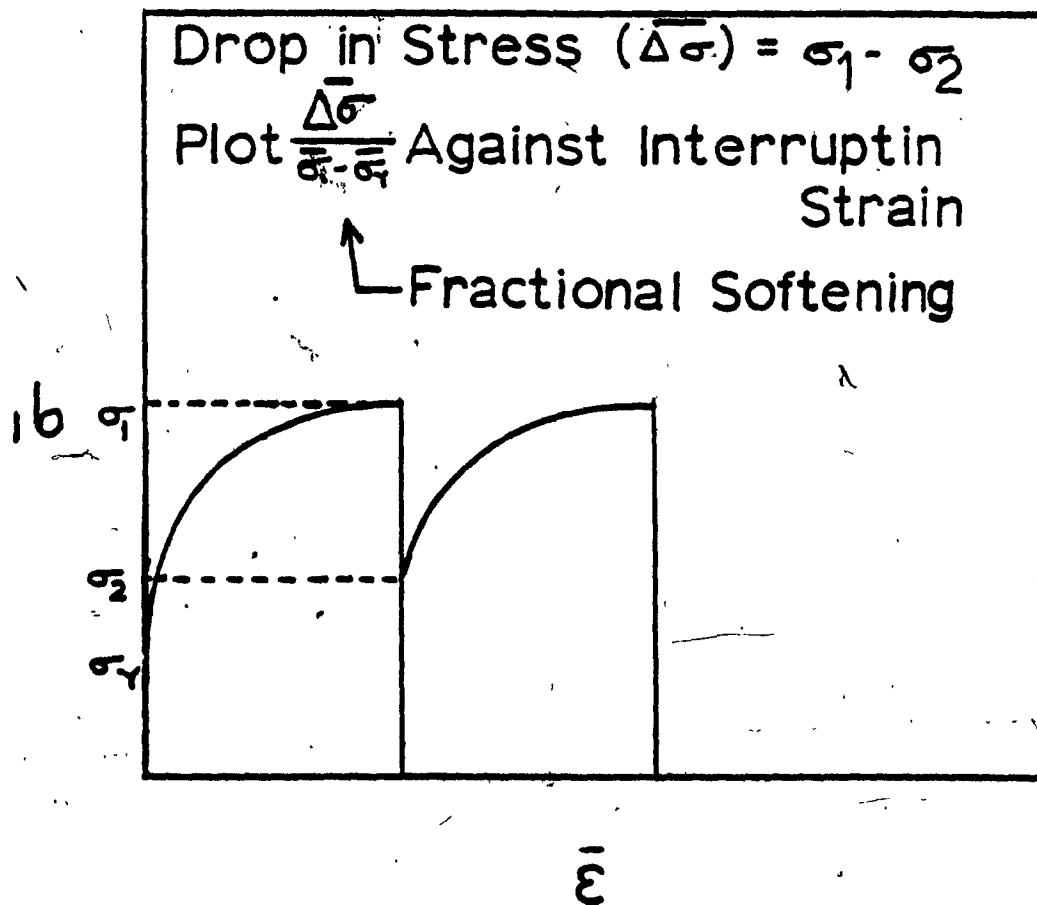


Fig. 4A: Method of Data Analysis.

CHAPTER 5

EXPERIMENTAL RESULTS

In the present research, the recorded torque and twist data were converted to equivalent stress ($\bar{\sigma}$) and strain ($\bar{\epsilon}$) using the Equations (4.1) to (4.4) in order to compare the torsion results with tension and compression results. In Equation (4.1), the value of m is selected as 0.15 based on Rossard's analysis [87] and that of n as zero [71,82].

5.1 CONTINUOUS DEFORMATION

The equivalent stress - strain plots for low carbon steel under continuous deformation at various test conditions are presented in Figure 5.1. The curves obtained on continuous deformation of Nb-bearing steel are shown in Figure 5.2.

In torsion tests, the number of turns to fracture represent the ductility of a material. The number of turns taken by the two steels to fracture are presented in parentheses above the right end of each flow curve. It is observed that for both low carbon and Nb-bearing steels, the ductility increased with increase of strain rate and temperature. For the same test conditions, low carbon steel always showed a higher ductility than Nb-bearing steel.

In order to analyze the effect of test variables on equivalent strain to the peak ($\bar{\epsilon}_p$) during continuous deformation, a graph is drawn between $\bar{\epsilon}_p$ and the test temperatures (Figure 5.3). In both steels, $\bar{\epsilon}_p$ decreased with increase of temperature and decrease of

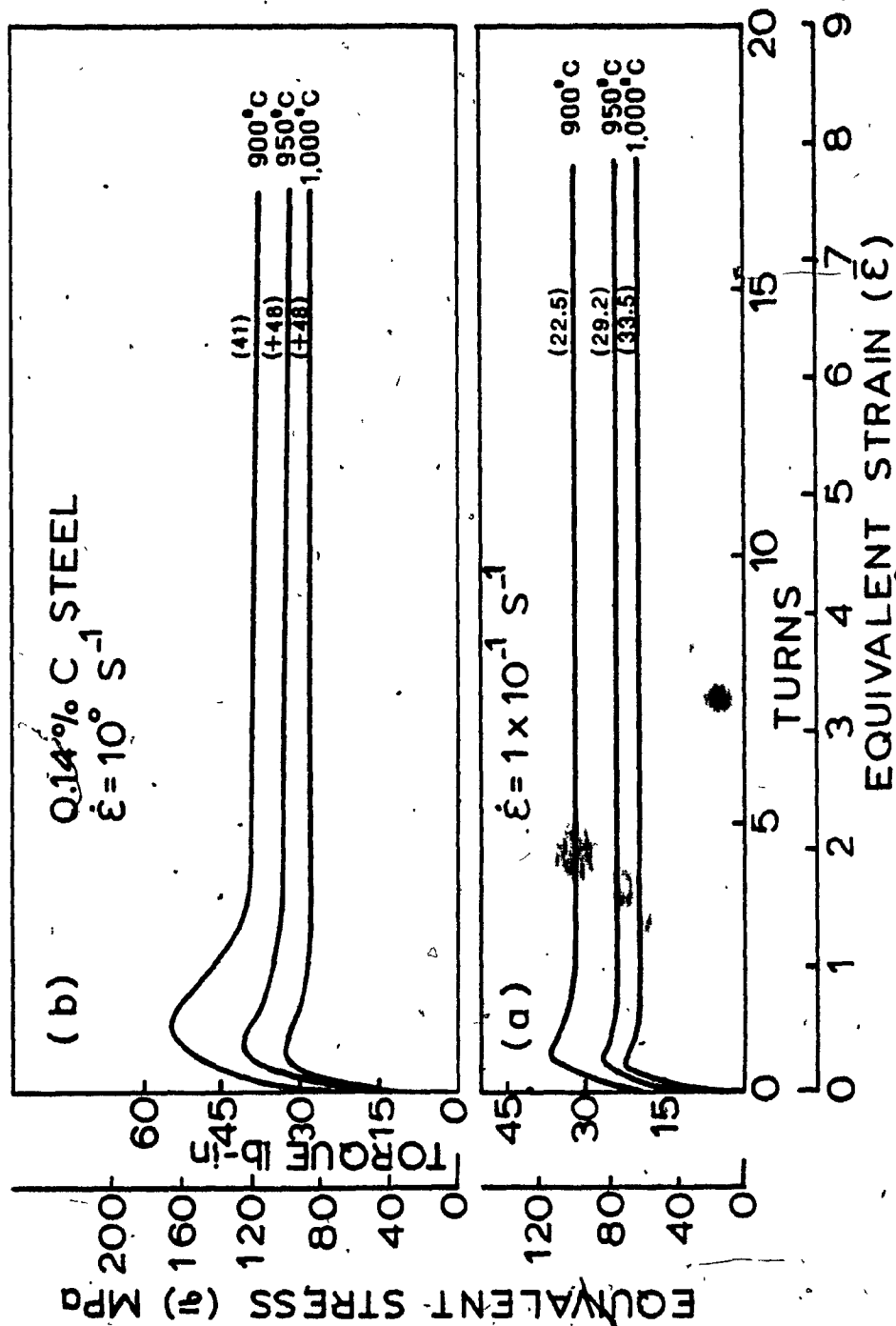


Fig. 5.1: Equivalent Stress/ Equivalent Strain Curves for a 0.14% C Steel on Hot Working at Strain Rates of (a) 0.1 s^{-1} (b) 1.0 s^{-1} .

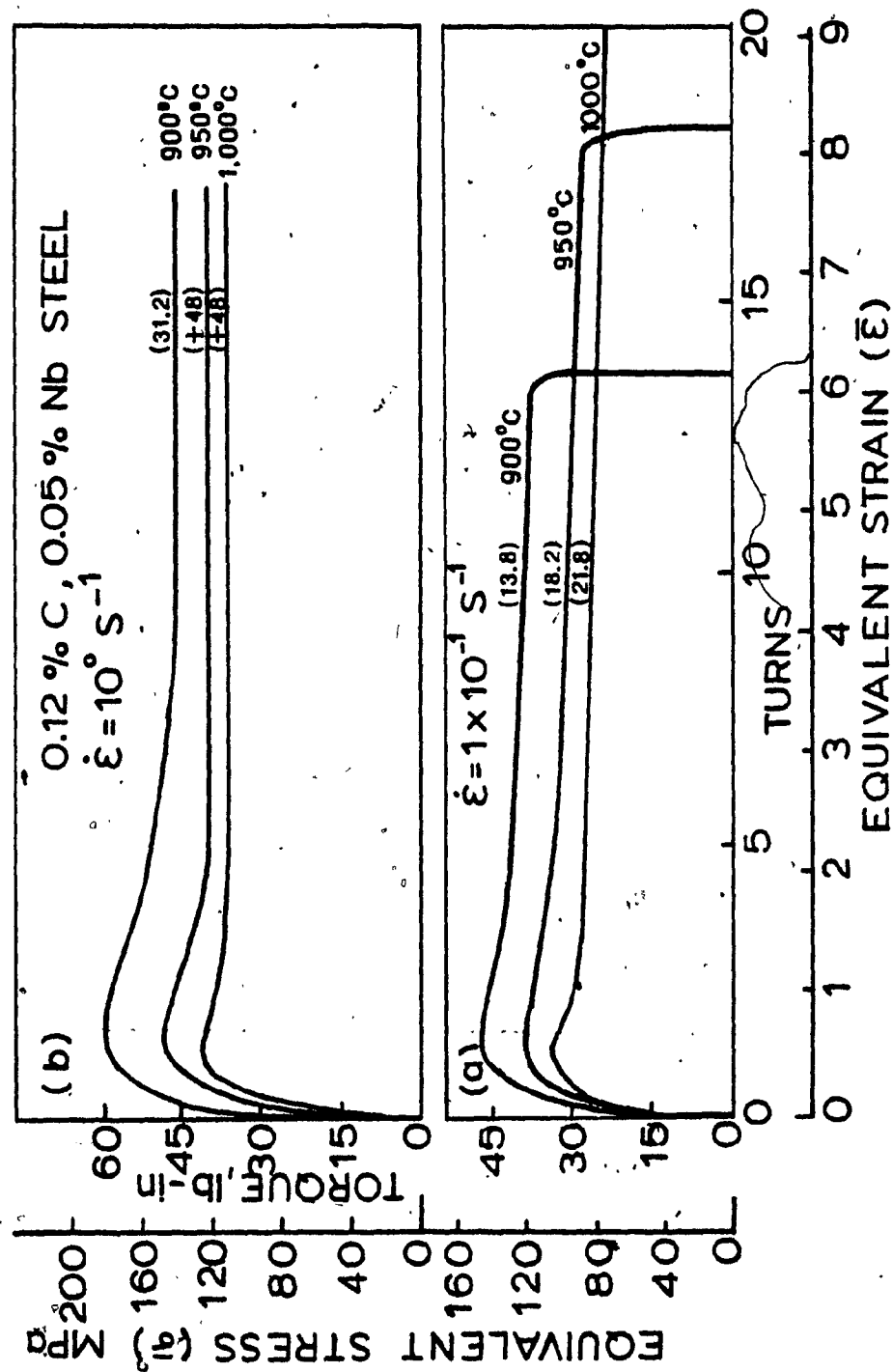


Fig. 5.2: Equivalent Stress/Equivalent Strain Curves for 0.12%C, 0.05%Nb Steel on Hot Working at Strain Rates of (a) 0.1 s^{-1} (b) 1.0 s^{-1} .

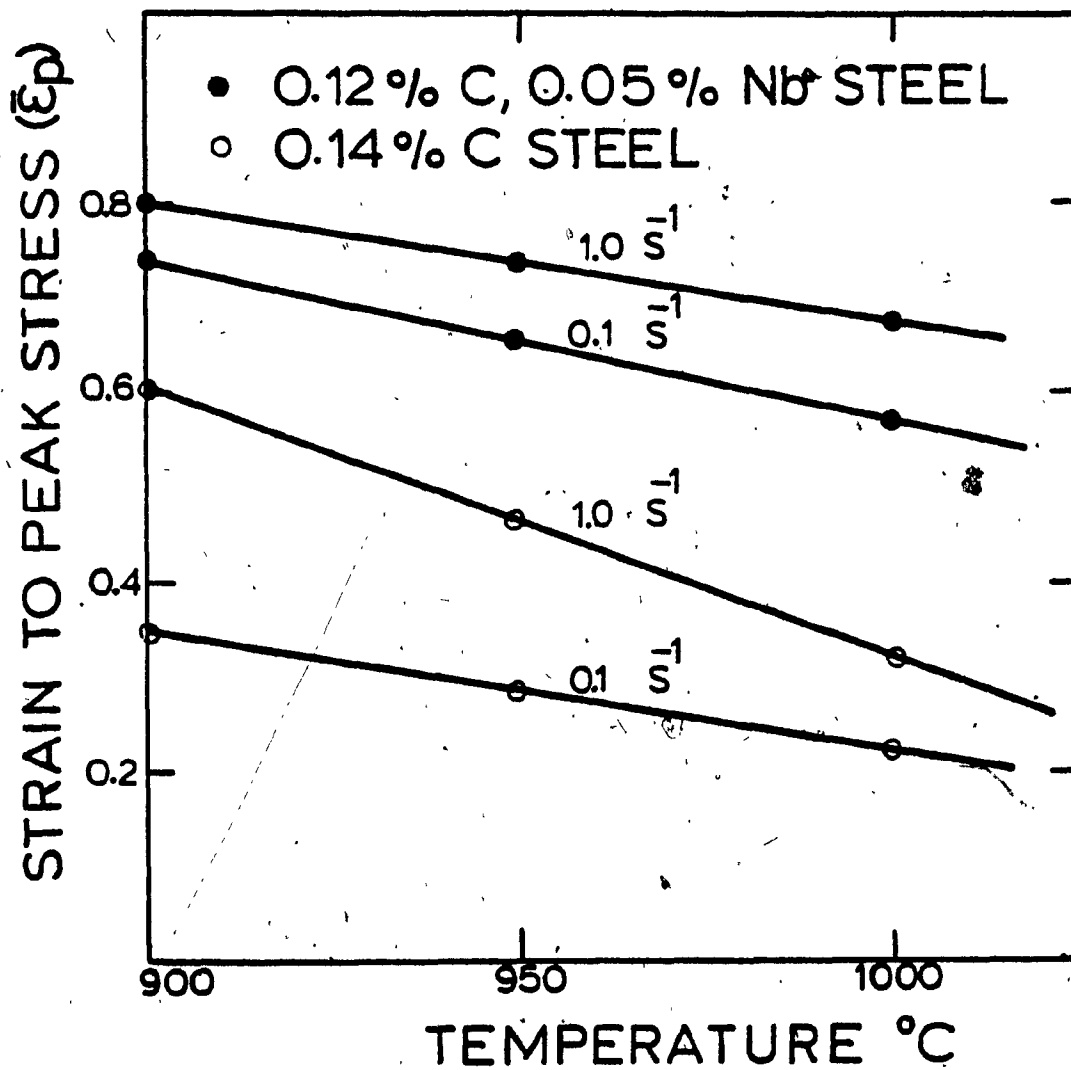


Fig. 5.3: Effect of Temperature and Strain Rate on Equivalent Strain to the Peak.

strain rate. For identical test conditions, Nb-bearing steel showed a higher $\bar{\epsilon}_p$ than low carbon steel.

In order to determine the dependence of the flow stress on temperature and strain rate, plots of $\log \dot{\epsilon}$ vs $\log \bar{\sigma}$ at constant temperature and $\log \bar{\sigma}$ vs $1/T$ at constant $\dot{\epsilon}$ were constructed (Figures 5.4 to 5.7). This is done for both the peak stress and the steady state flow stress. Since there is often a slight decline in flow stress with increasing strain because of the specimen heating or dimensional change, the steady state value is taken after the work softening region at a strain of about 2.5. The presence of parallel straight lines for each of the steels in the graphs indicate a power law relationship:

$$\dot{\epsilon} = A \sigma^n \exp(-\Delta H/RT) \quad (5.1)$$

Figures 5.4 and 5.5 show that the values of n for the steels are as follows:

$$\text{low carbon steel } n_{L.C} = 5.0$$

$$\text{Nb-bearing steel } n_{Nb} = 8.3$$

Use of these values in conjunction with Figures 5.6 and 5.7 permits calculation of ΔH for each steel:

$$\text{low carbon steel } \Delta H_{L.C} = 72.4 \text{ Kcal/mole}$$

$$\text{Nb-bearing steel } \Delta H_{Nb} = 101.2 \text{ Kcal/mole}$$

5.2 INTERRUPTED DEFORMATION

The test curves of interrupted deformation conducted at strain rates of 0.1 s^{-1} and 1.0 s^{-1} (strains of 0.2 and 0.4 respectively)

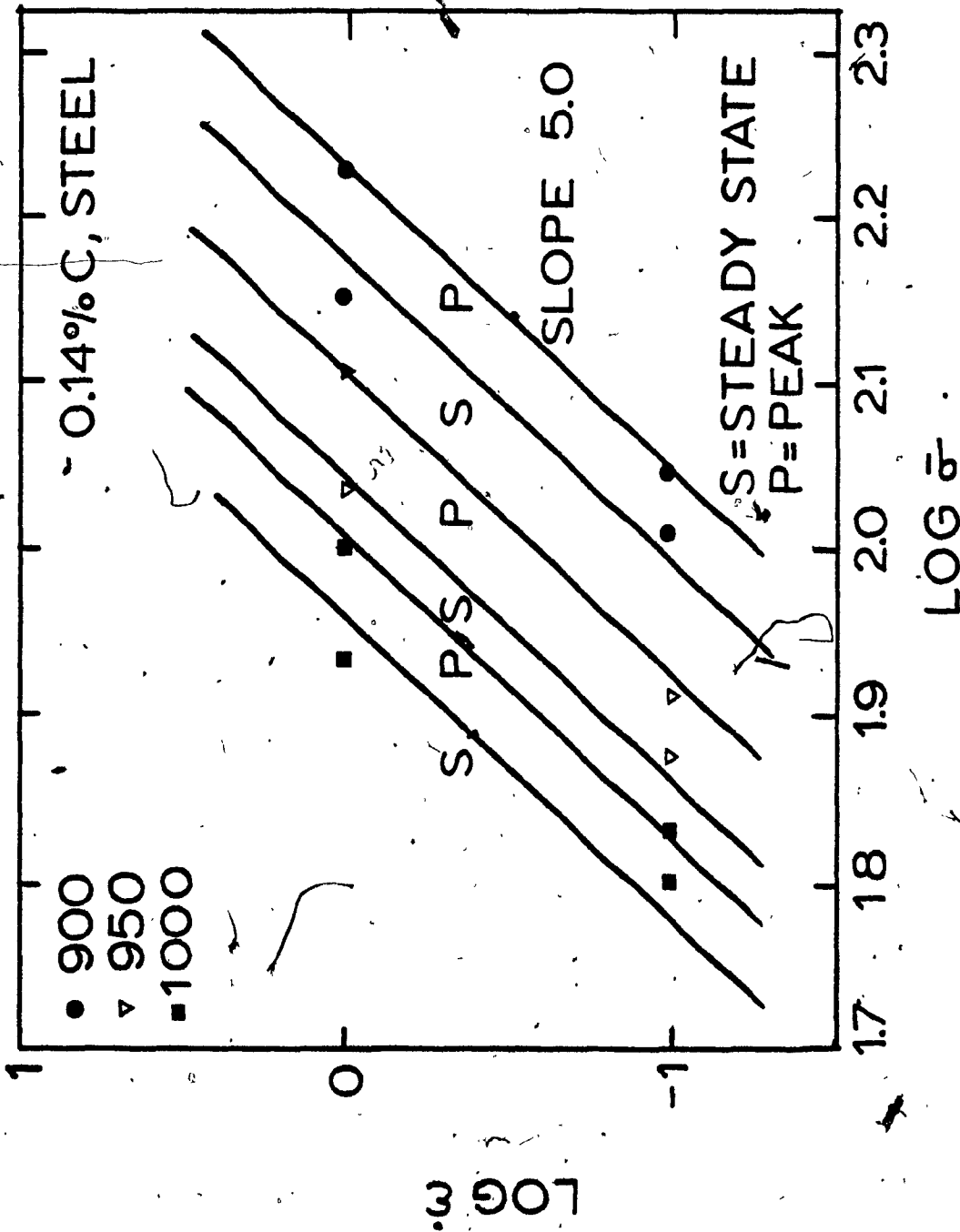


Fig. 5.4: The Stress Dependence of the Strain Rate for a 0.14% C Steel at Various Temperatures Plotted to Demonstrate the Power Law Relationship.

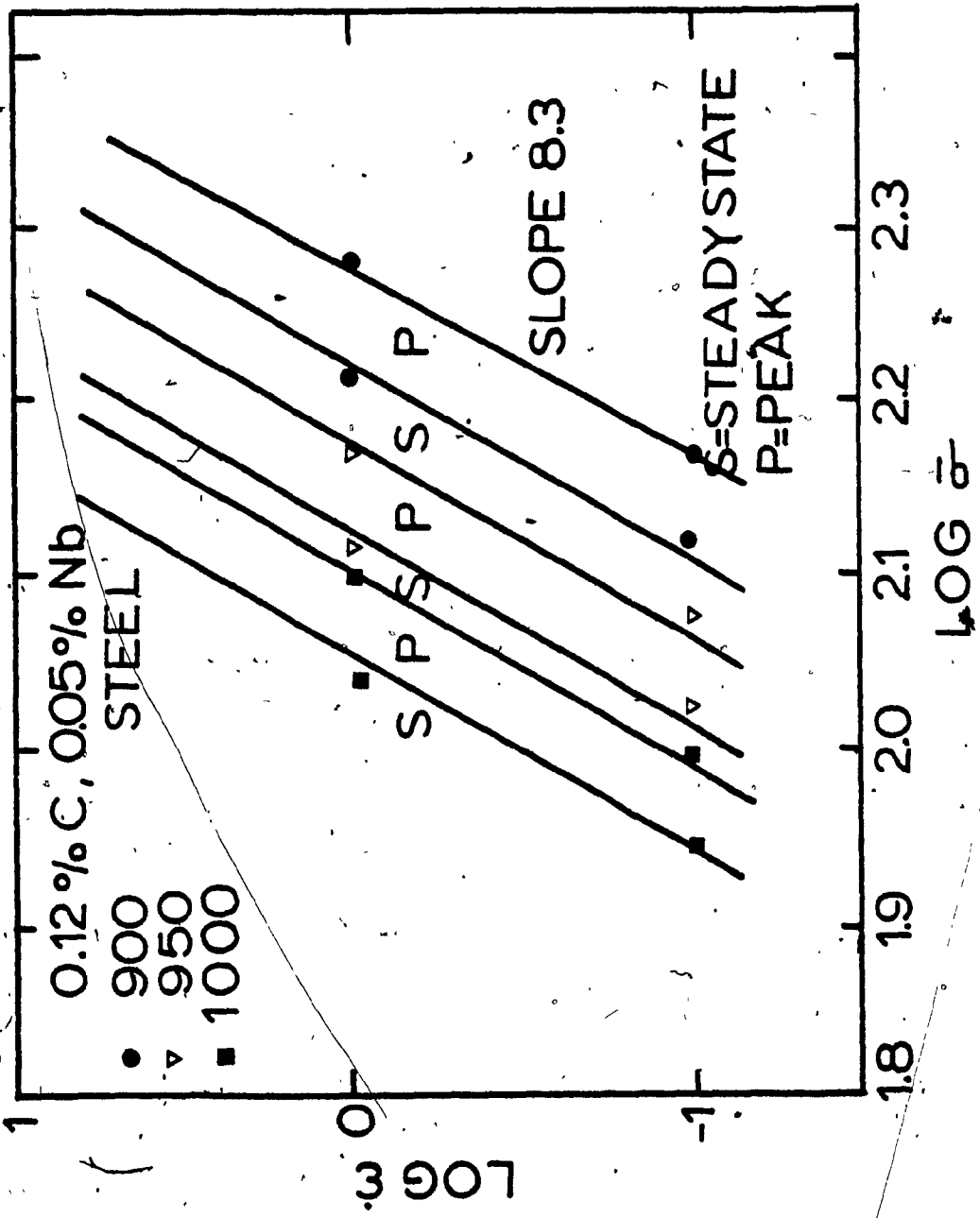


Fig. 5.5: The Stress Dependence of the Strain Rate for a 0.12%C, 0.05%Nb Steel at Various Temperatures Plotted to Demonstrate the Power Law Relationship.

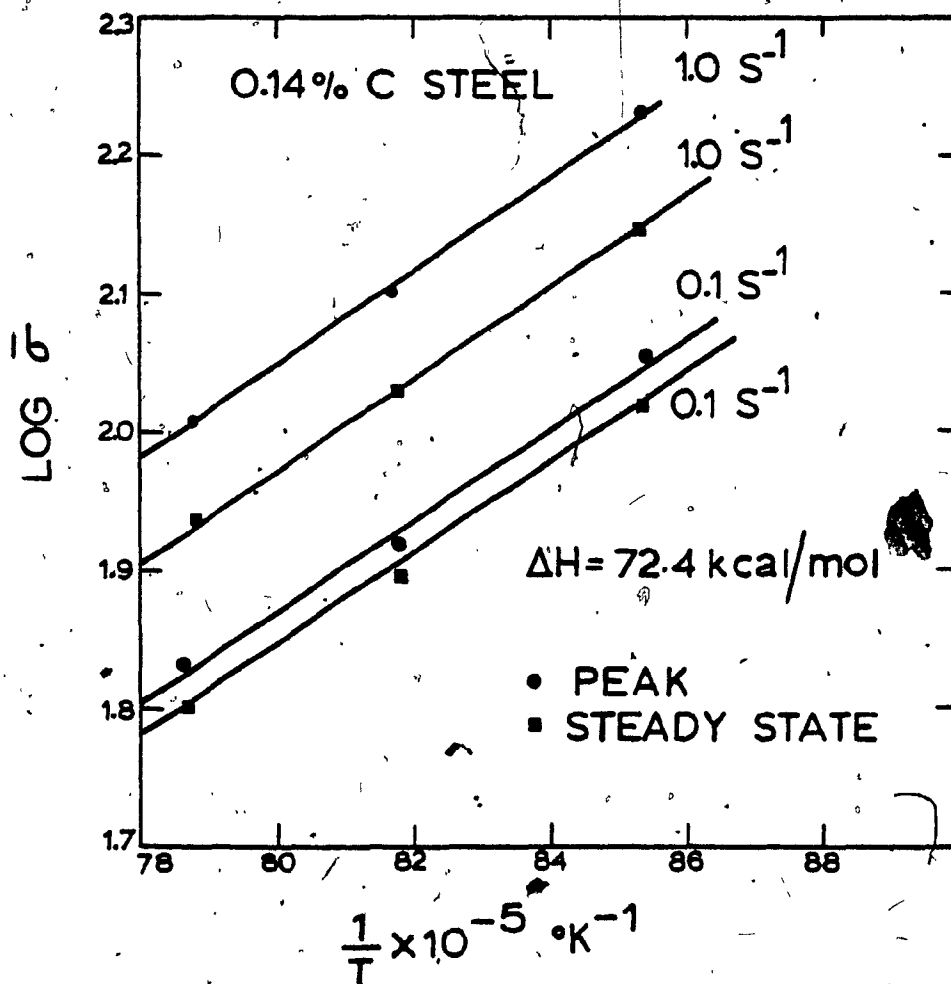


Fig. 5.6: The Temperature Dependence of the Stress for a 0.14% C Steel at Various Strain Rates Plotted to Demonstrate an Arrhenius Law Relationship.

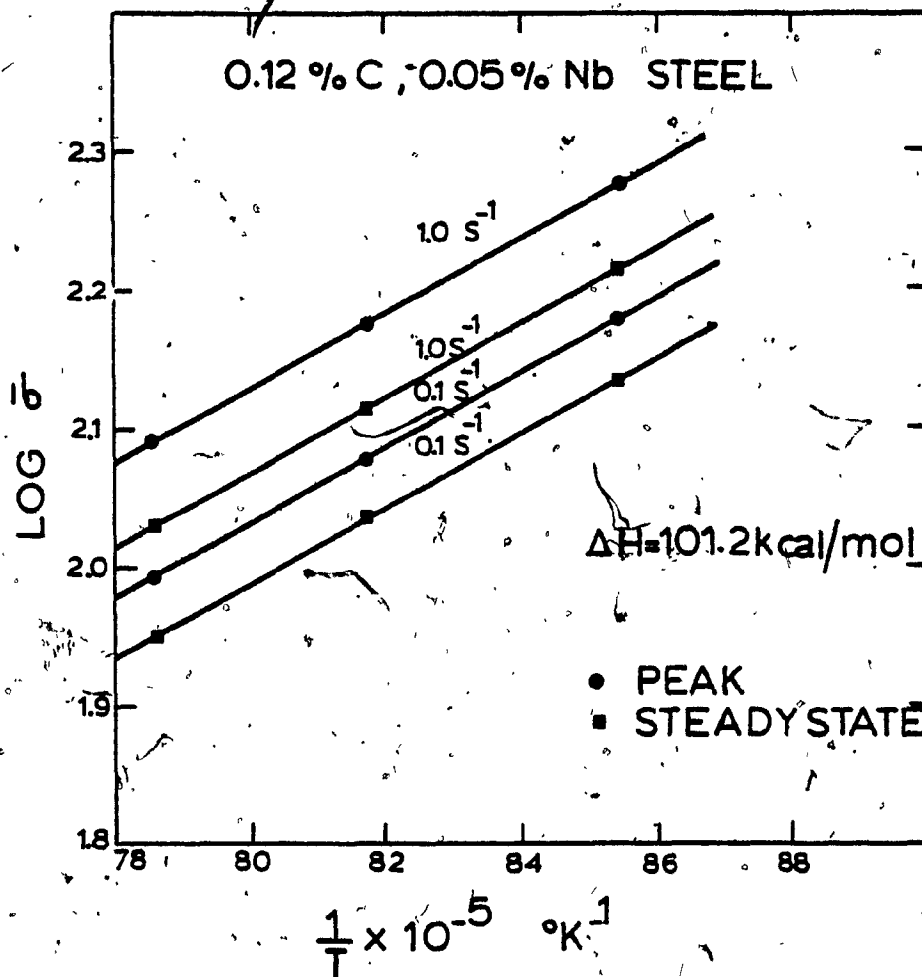


Fig. 5.7: The Temperature Dependence of the Stress for a, 0.12%C, 0.05%Nb Steel at Various Strain Rates Plotted to Demonstrate an Arrhenius Law Relationship.

for low carbon and Nb-bearing steels are given in Figures 5.8 to 5.17 with corresponding continuous deformation curves superimposed on them. The amount of softening at each interruption against strain for the above steels are presented in Figures 5.18 to 5.21. From these figures it is evident that the rates of restoration between passes are quite different for the low carbon and niobium-bearing steel.

For low carbon steel at a strain rate of 0.1 s^{-1} , large amounts of softening are obtained which increase with the temperature and interruption time (t_i). On the other hand, in Nb-bearing steel relatively small amounts of softening and only a slight increase with temperature and interruption time are observed. The relationship between the envelope curve connecting the stress maxima of the interrupted curve and the continuous one is different for each steel. For the low carbon steel the envelope is generally higher whereas for the Nb-bearing steel it is generally the same as the continuous.

At strain rate of 1.0 s^{-1} , low carbon steel shows a high amount of softening in the initial interruption followed by some cyclic pattern of softening. Somewhat similar phenomena seem to operate in Nb-bearing steel. One interesting feature is the increase in the stress level of the envelope curve over that of the continuous one, an effect, which diminishes with temperature especially in low carbon steel.

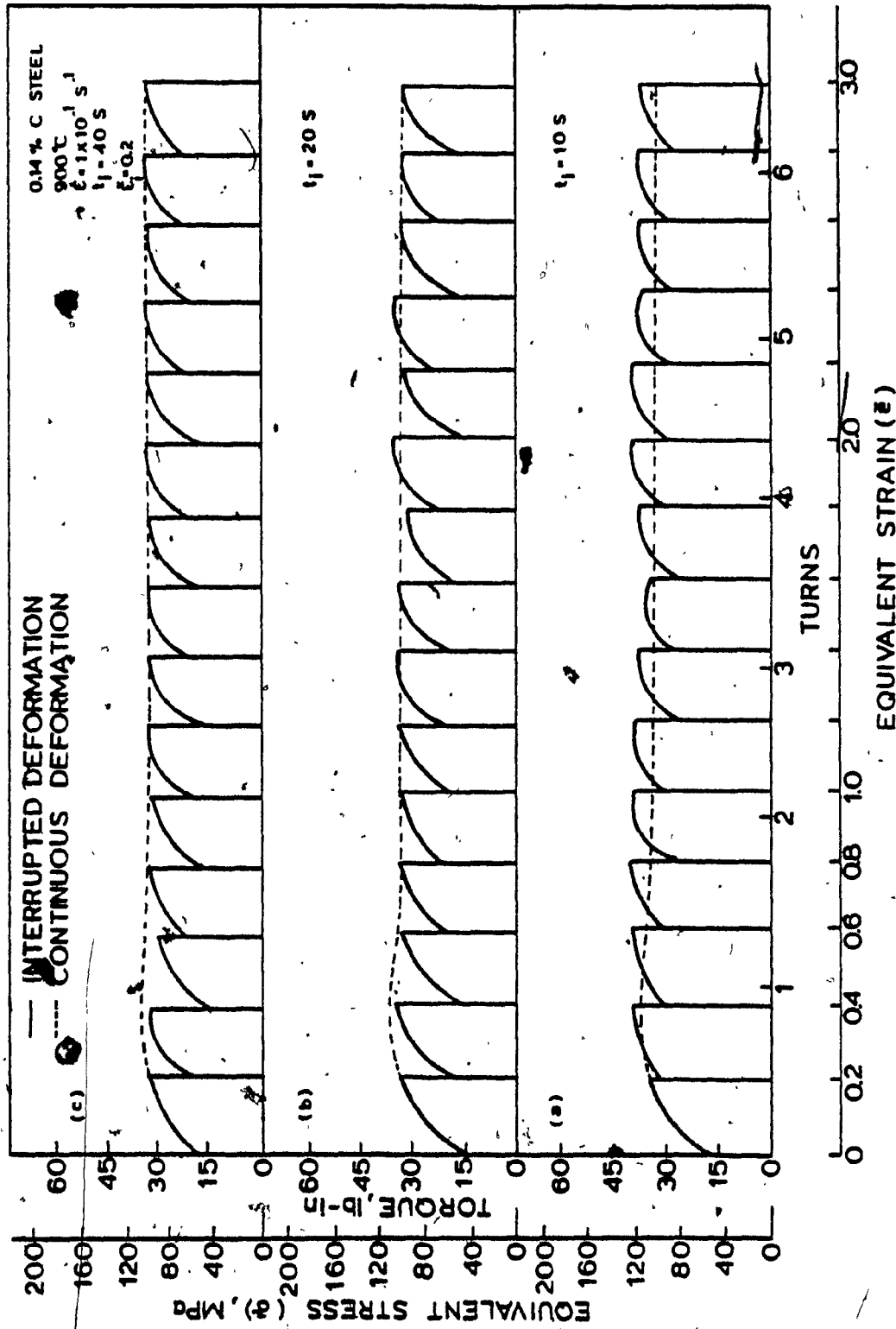


Fig. 5.8: Interrupted Flow Curves for a 0.14% C Steel at 900°C and 0.1 s^{-1} at Pass Strains of 0.2 and Interruption Times of 40, 20 and 10 s.

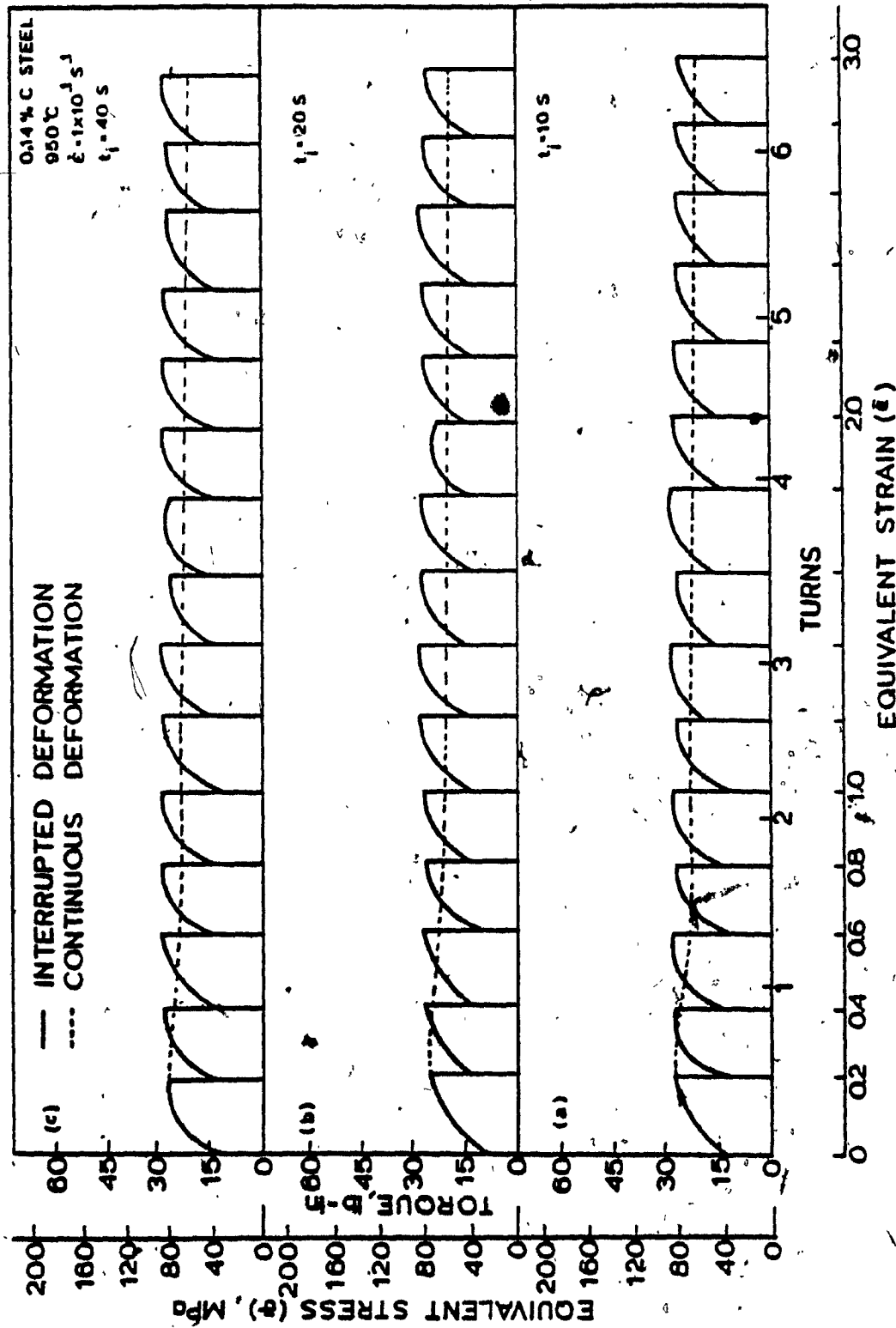


Fig. 5.9: Interrupted Flow Curves for a 0.14% C Steel at 950°C and 0.1 s^{-1} at Pass Strains of 0.2 and Interruption Times of 40, 20 and 10 s.

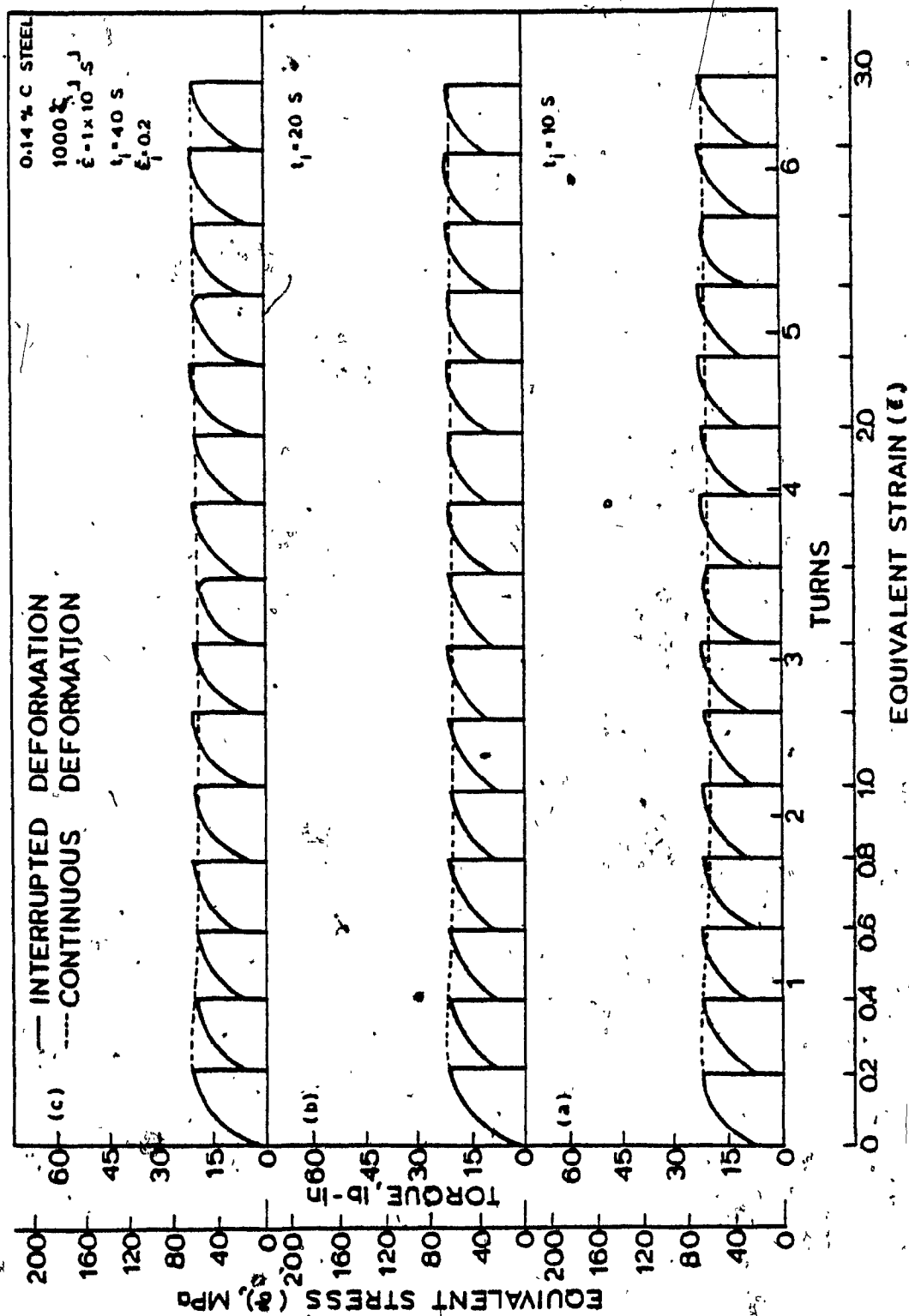


Fig. 5.10: Interrupted Flow Curves for a 0.14% C Steel at 1000°C and 0.1 s^{-1} at Pass Strains of 0.2 and Interruption Times of 40, 20 and 10 s.

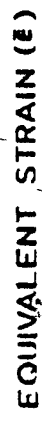


Fig. 5.11: Interrupted Flow Curves for a 0.12%C, 0.05%Nb Steel at 900°C and 0.1 s⁻¹ at Pass Strains of 0.2 and Interruption Times of 40, 20 and 10 s.

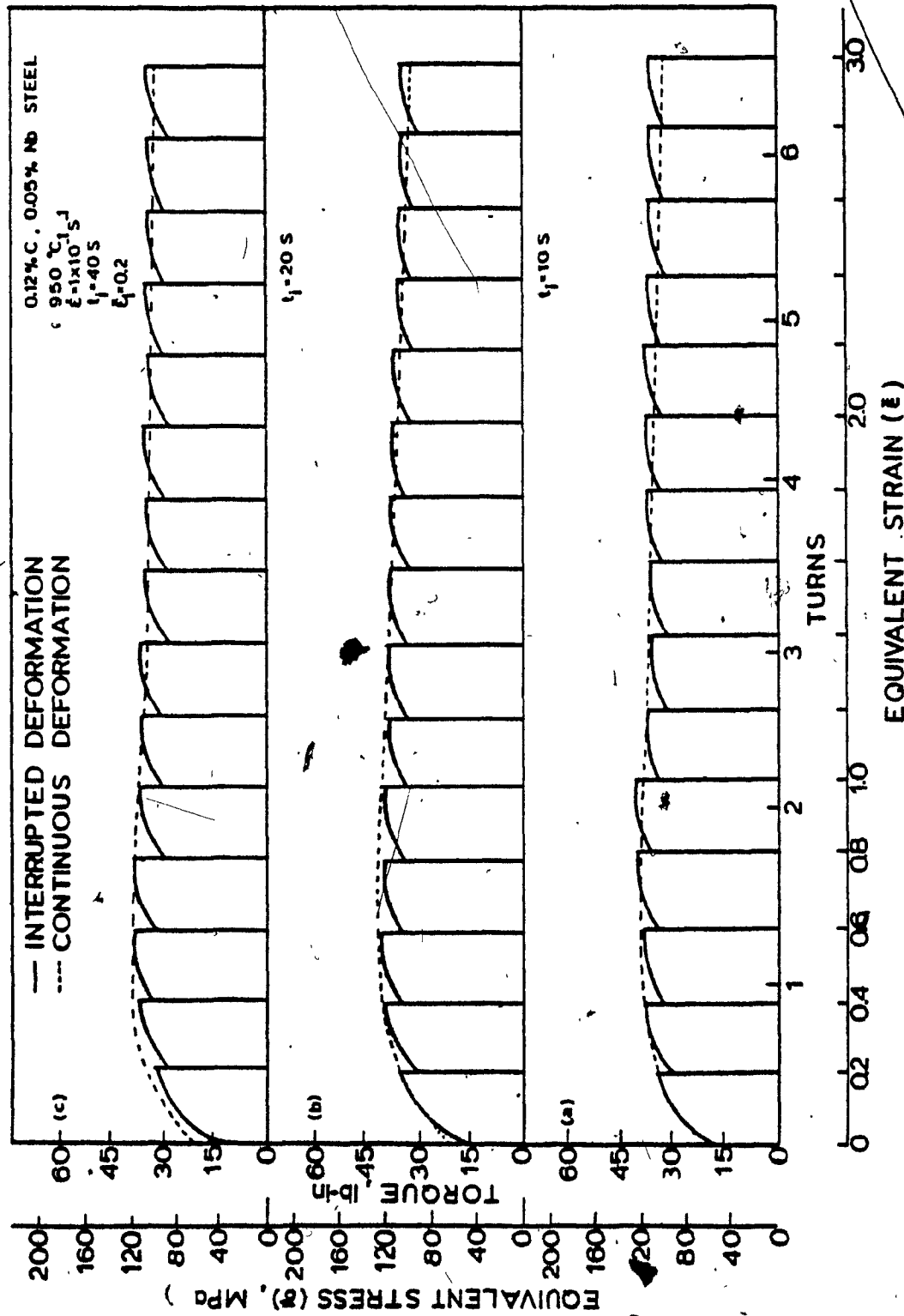


Fig. 5.12: Interrupted Flow Curves for a 0.12%C, 0.05%Nb Steel at 950°C and 0.1 s^{-1} at Pass Strains of 0.2 and Interruption Times of 40, 20 and 10 s.

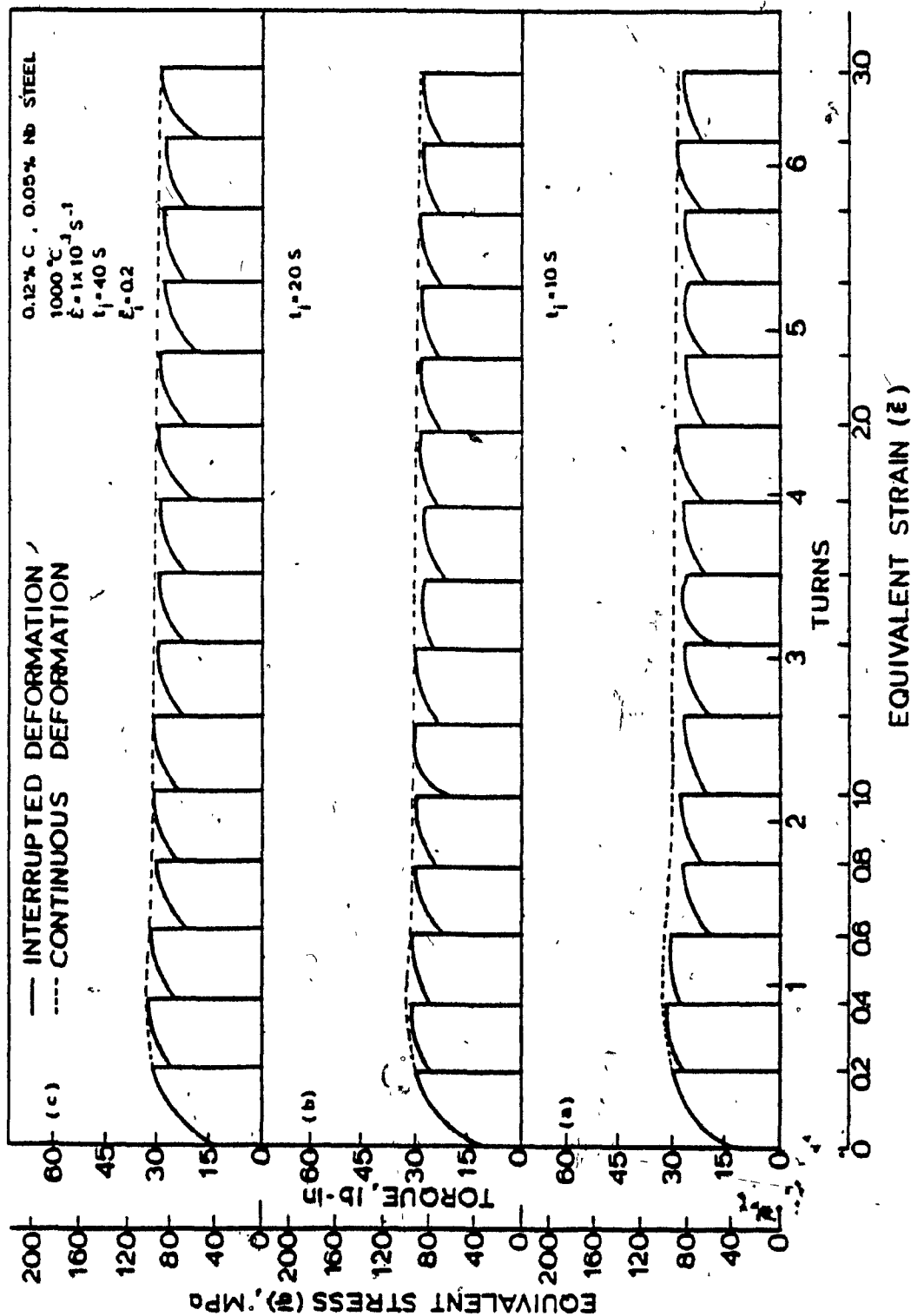


Fig. 5.13: Interrupted Flow Curves for a 0.12%C, 0.05%Nb Steel at 1000°C and 0.1 s⁻¹ at Pass Strains of 0.2 and Interruption Times of 40, 20 and 10 s.

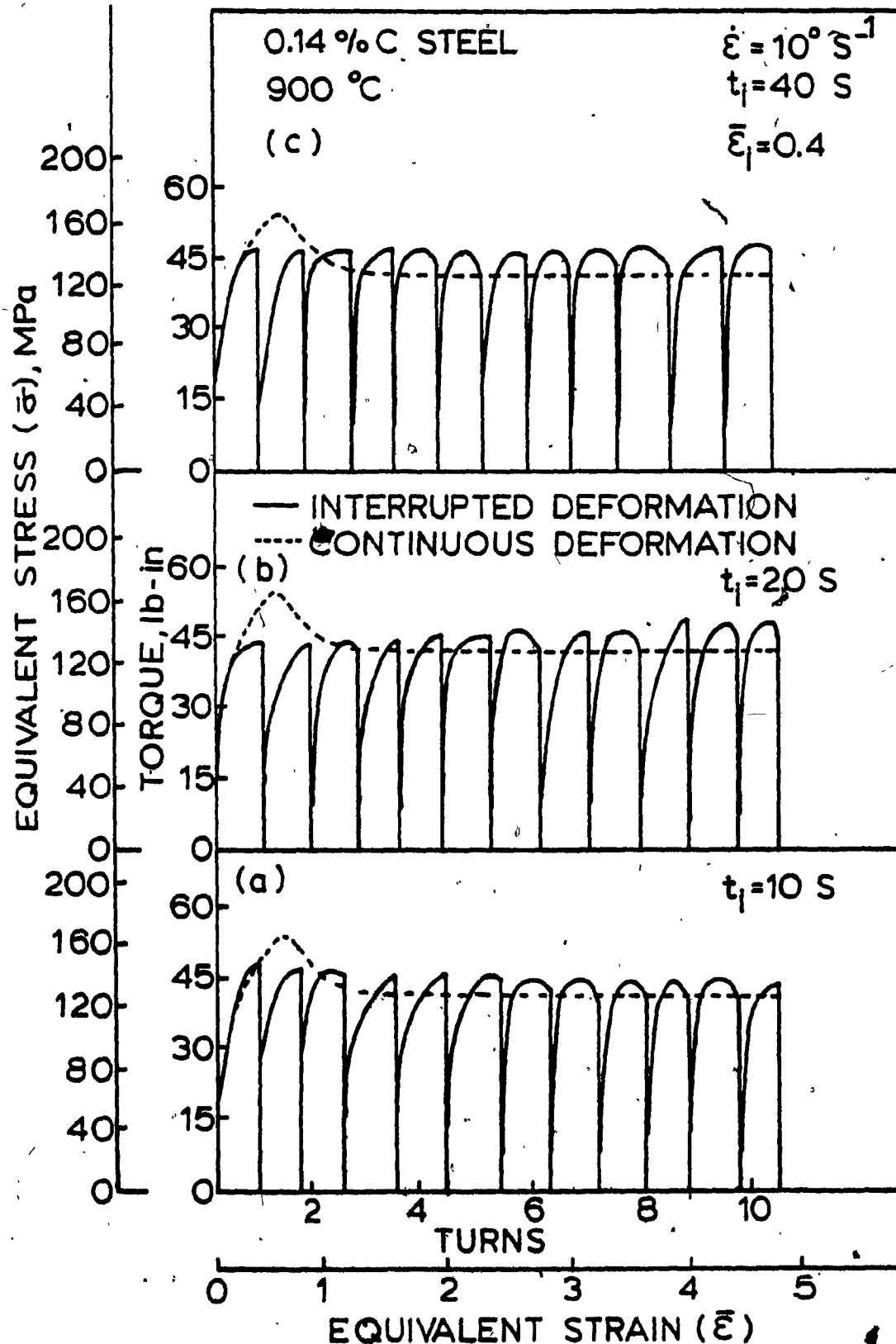


Fig. 5.14: Interrupted Flow Curves for a 0.14%C Steel at 900°C and 1.0 s^{-1} at Pass Strains of 0.4 and Interruption Times of 40, 20 and 10 s.

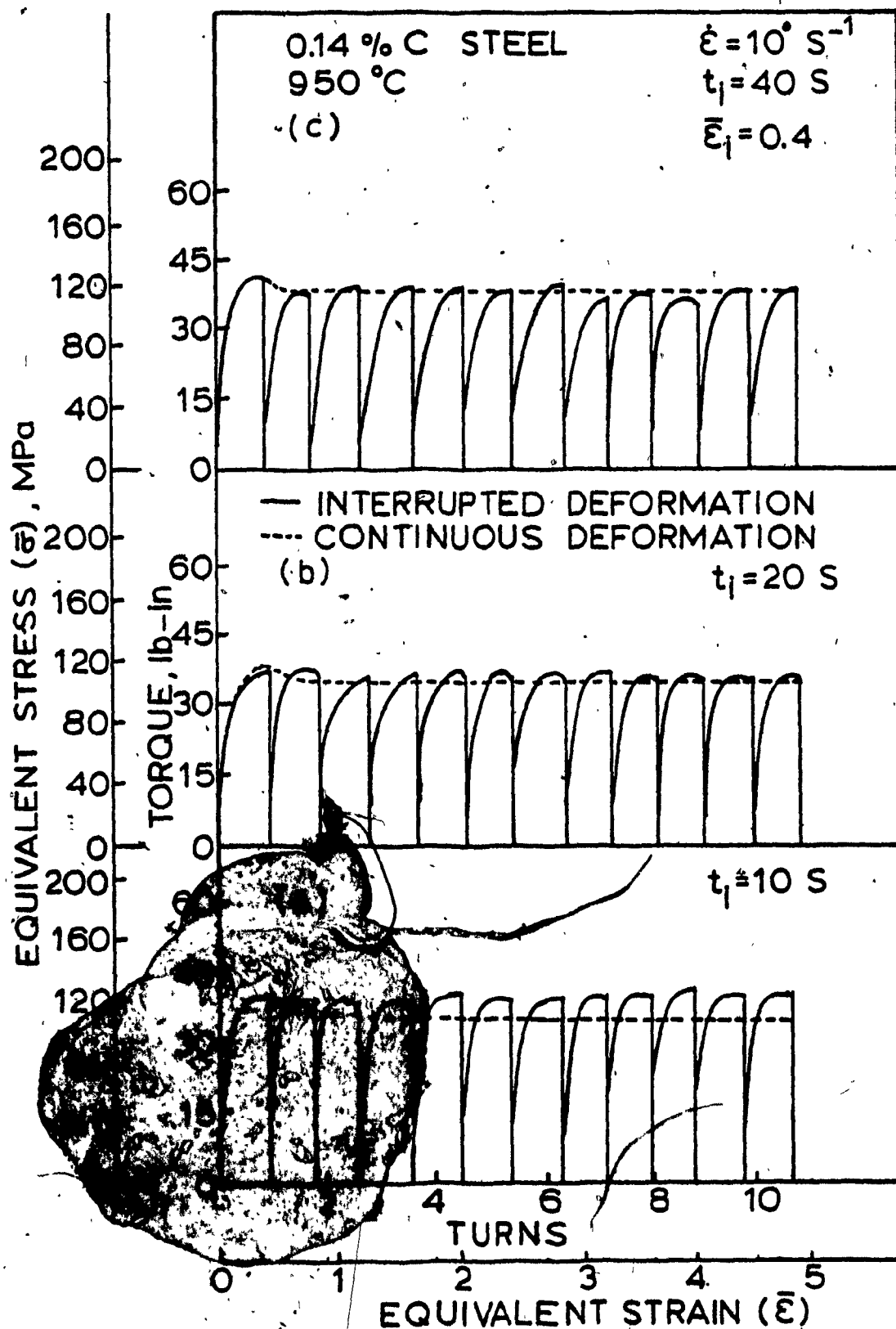


Fig. 5.15: Interrupted Flow Curves for a 0.14% C Steel at 950°C and 1.0 s^{-1} at Pass Strains of 0.4 and Interruption Times of 40, 20 and 10 s.

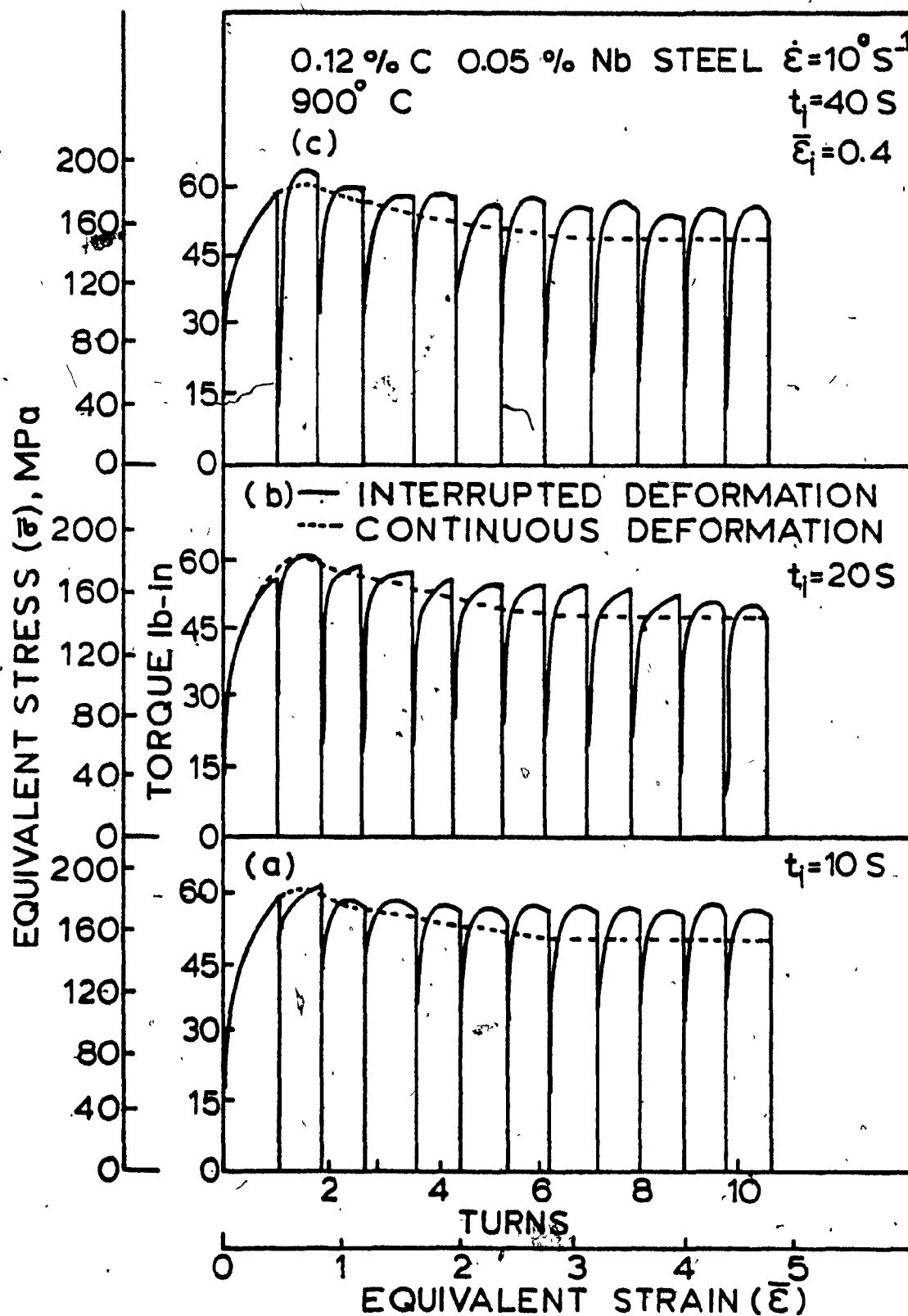


Fig. 5.16: Interrupted Flow Curves for a 0.12%C, 0.05%Nb Steel at 900°C and 1.0 s^{-1} at Pass Strains of 0.4 and Interruption Times of 40, 20 and 10 s.

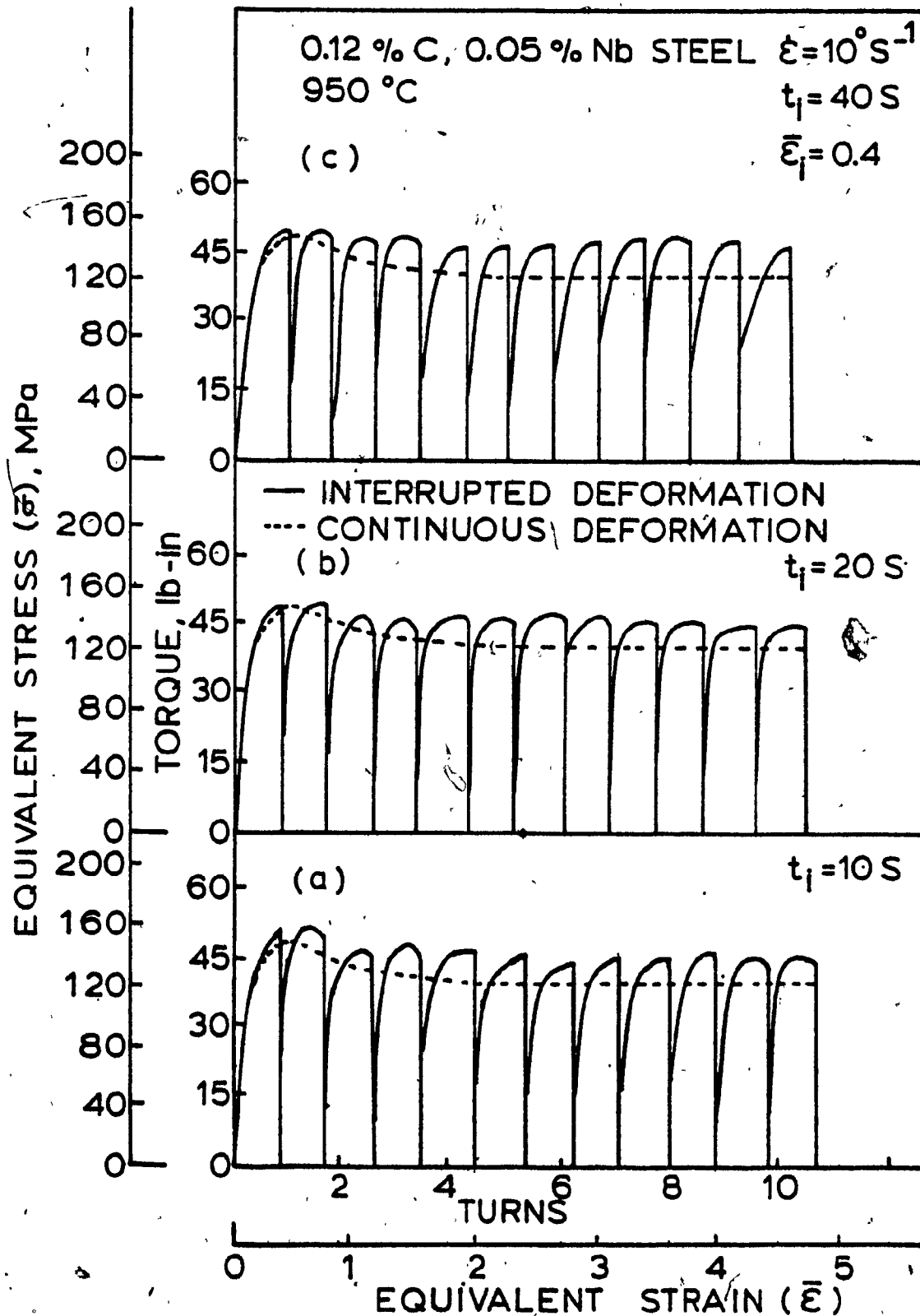


Fig. 5.17: Interrupted Flow Curves for a 0.12%, 0.05%Nb Steel at 950°C and 1.0 s^{-1} at Pass Strains of 0.4 and Interruption Times of 40, 20 and 10 s.

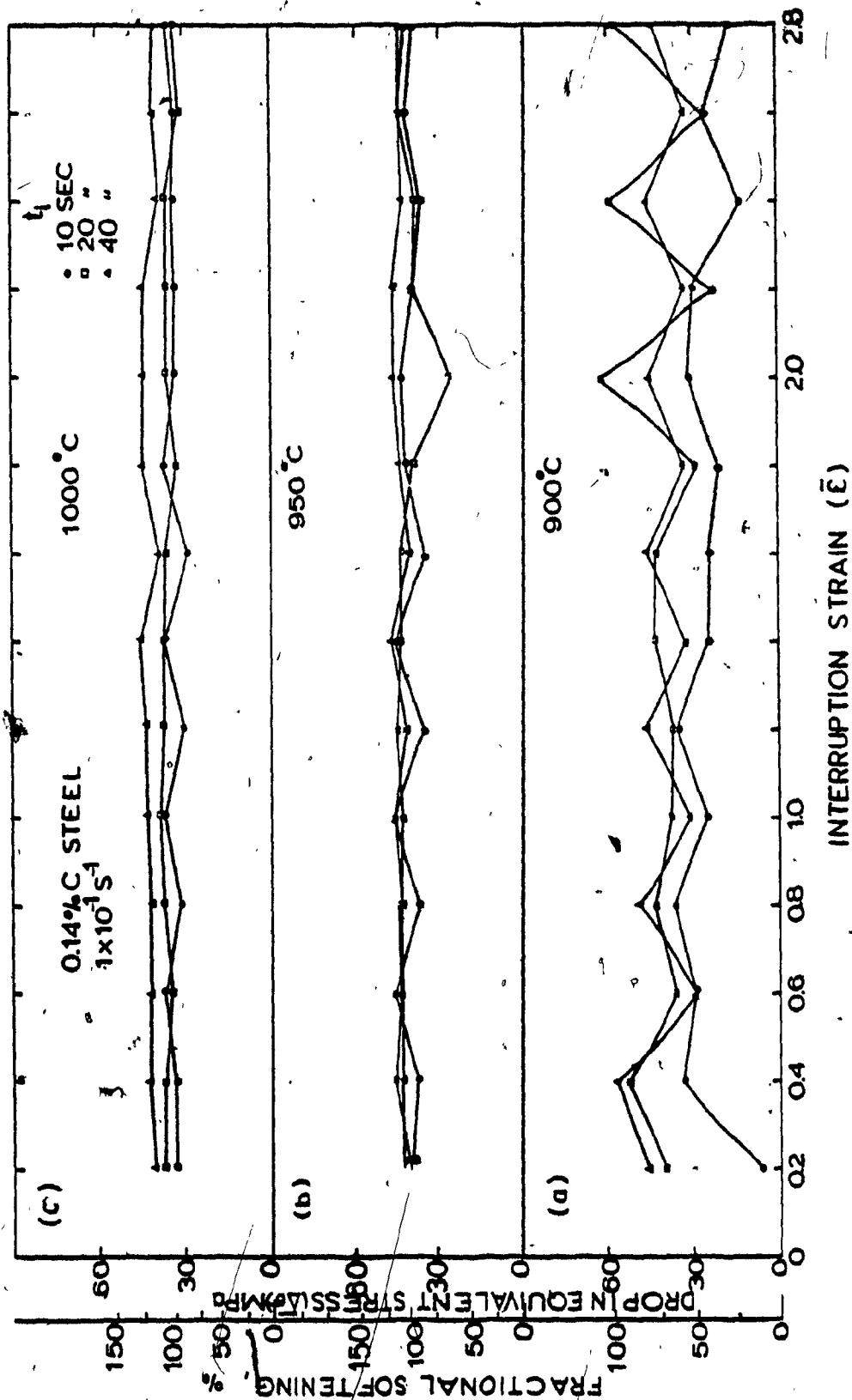


Fig. 5.18: Variation of Fractional Softening with Temperature, Interruption Time and Accumulated Strain for a 0.14% C Steel at 0.1 s^{-1} .

(2) The degree of softening depends on the previous deformation:

- a. if the critical strain (ϵ_c), i.e. 0.83 of the peak strain, has not been passed; dynamic recrystallization has not started; only a dynamically-recovered substructure is present,
- b. accumulation of strain, in several passes without dynamic recrystallization yields a substructure which moves rapidly through the different degrees to produce a finer recrystallized grain size,
- c. high strain rate or a low temperature produces a microstructure which behaves as in b,
- d. accumulation of strain or raising the temperature can lead to surpassing ϵ_c and to dynamic recrystallization so pre-formed nuclei are available for nucleation and hence more rapid progress through the stages of softening,
- e. the presence of precipitate stabilizes the substructure slowing both static recovery and static recrystallization.

(3) The degree of softening depends on the holding temperature and length of the interruption:

- a. increase of temperature or the time permits greater progress through the degrees of softening,
- b. at higher temperature softening by recrystallization occurs before precipitation of niobium [74-76].

(4) The degree of softening controls the shape of the flow curve on reloading. The pattern of successive softening helps to define the series of these curves as a whole. The interrupted curve is considered as a whole by means of an 'envelope' curve, i.e. a continuous imaginary curve connecting the stress maxima of the successive deformation curves:

- a. static recovery lowers the initial flow stress but permits the low curve to rejoin the continuous flow curve, possibly with small variations,
- b. complete recrystallization to the initial grain size leads to a repetition of the initial flow curve before the peak which is higher than the steady state portion of the continuous flow curve;
- c. recrystallization to grains finer than the initial size leads to a flow curve higher than the initial whereas
- d. recrystallization to a coarser grain size leads to a lower flow curve which may be equal or below the steady state value depending on the amount of coarsening.

A detailed analysis of the results obtained for the interrupted tests are given in Table 6.2. The results there are consistently referred to the above principles in parentheses so that a clear explanation of the softening mechanisms can be made. From these results, it can be seen how the over-all softening rate is affected by prior strain, temperature, interruption time, strain rate and

Table 6.2. Softening, S , During Interruption, t_i and Relation of Interrupted to Continuous Curve

(a)

		LOW STRAIN RATE (0.1 s^{-1}), $\bar{\epsilon}_i = 0.2$	
$T^\circ\text{C}$	$t_i \text{ sec}$	Low Carbon Steel	Nb-Bearing Steel
900		$\bar{\epsilon}_i < \bar{\epsilon}_c$	$\bar{\epsilon}_i < \bar{\epsilon}_c$
	10	S_{large} -partial recrystallization(1b)(2c)[except t_i , S_{small} -recovery(1a)(2a)] envelope $>$ continuous(4c)	Repeated Constant S_{small} -recovery (1a)(2e) envelope = continuous(4a)
	20	S_{higher} -recrystallization (1a to 1c) or (1e) envelope \approx continuous (4d)	Same as above
	40	Same as above	Same as above
IN ALL TESTS		envelope \geq continuous(4c)(4d)	envelope = continuous(4a)
950		$\bar{\epsilon}_i < \bar{\epsilon}_c$	$\bar{\epsilon}_i < \bar{\epsilon}_c$
	10	S_{medium} -partial recrystallization(1b)(3a)	S_{small} (1a)(2e); envelope \geq continuous(2e)
	20	S_{large} -recrystallization (1c)(3a)	S_{small} (1a)(2e); envelope = continuous(3a)
	40	repeated S_{constant} -recrystallization to a constant grain size(1c)	Same as above except after accumulation of strain $S_{\text{slightly higher}}$ (1b)(2d) envelope = continuous(4a)
IN ALL TESTS		envelope $>$ continuous(4c)	envelope \geq continuous(4a)
1000		$\bar{\epsilon}_i > \bar{\epsilon}_c$	$\bar{\epsilon}_i < \bar{\epsilon}_c$
	10	S_{large} -recrystallization (1d or 1e)(3a) envelope $<$ continuous(4c)	S_{small} initially(1a)(2e); S_{large} after accumulation of strain (1b)(2d) envelope $<$ continuous(4a)
	20	Same as above but constant S_{large} with some grain growth (1e)(3a)	Same as above
	40	Repeated constant S_{large} -grain growth(1e)(3a) envelope = continuous(4d)	Same as above - effect more pronounced; envelope = continuous(3a)
IN ALL TESTS		envelope \geq continuous(4c)(4d)	envelope \leq continuous(4a)(3a)

(b)

HIGH RATE STRAIN (1.0 s^{-1}), $\bar{\epsilon}_f = 0.4$			
		Low Carbon Steel	Nb-Bearing Steel
900		$\bar{\epsilon}_f < \bar{\epsilon}_c$	$\bar{\epsilon}_f < \bar{\epsilon}_c$
	10	S_{large} -recrystallization(1c) cycles in amount of softening	S_{small} initially(1a); with accumulation of strain
	20	Same as above	S_{large} (1c)(2b) cycles in softening
	40	Same as above(1c)(3a)	Same as above with effect of (3a)
IN ALL TESTS		envelope $>$ continuous(4b)(4c)	envelope $>$ continuous(4b)
950		$\bar{\epsilon}_f > \bar{\epsilon}_c$	$\bar{\epsilon}_f < \bar{\epsilon}_c$
	10	S_{large} -recrystallization(1d) envelope $>$ continuous(4b)(4c); cycles in softening	S_{large} (1c)(3b); cycles in softening
	20	S_{large} -large grains(1e) envelope \geq continuous(4d)	Same as above
	40	S_{large} -grain growth(1e) envelope = continuous(4d)	Same as above + (3a)
IN ALL TESTS		envelope \geq continuous(4b)(4c)(4d)	envelope $>$ continuous(4b)(4c)

alloying elements.

6.2.1 Softening Mechanisms of Low Carbon and Nb-Bearing Steel During Low Strain Rate Interrupted Deformation

At low strain rate (0.1 s^{-1}) when interrupted for 10 sec at 900°C (Figure 5.8a) low carbon steel shows a small amount of softening due to recovery. But it can be seen from Figure 5.18a as the interruption time increases to 20 and 40 sec the softening also increases. This is because of the greater progress through the degrees of softening taking place with increasing amount of time. From Figure 5.9 to 5.10, it is observed as the temperature increases to 950°C and 1000°C , the percent fractional softening (Figure 5.18b and c) also increases for a particular interruption time. This is due to the fact that softening is a thermally activated mechanism. In general, whenever a pre-strained metal is reloaded after an interruption period, the flow curve developed depends on its grain size. By producing a recrystallized grains finer or equal to the initial grain size during interruptions leads to an envelope of higher stress level than that obtained on continuous deformation (Figures 5.9a to 5.10a). Although the recrystallized grains are produced more quickly at a higher temperature and as a result of metadynamic recrystallization a longer interruption time coarsen the dynamically and statically recrystallized grains thus decreasing the general stress level of the envelope relative to that of continuous deformation. This is why the stress level of the envelope curve in Figures 5.10b and c decreases relative to continuous deformation curve.

On the contrary, in Nb-bearing steel at all test conditions, it can be seen that (Figures 5.11 to 5.13 and 5.19) only small amount of softening takes place. This is because of the presence of niobium precipitate stabilizing the substructure slowing both static recovery and static recrystallization. This also leads to the higher $\bar{\epsilon}_p$ observed in the envelope over that of continuous deformation. But at high temperature and especially a higher interruption times (Figure 5.13c) the softening has increased showing that precipitation is not as effective. One can also see that the fractional softening shows a sudden increase after a series of low values. This is due to the accumulation of strain which leads to a strain high enough to produce recrystallization nuclei and hence more softening. Since, generally, in all these tests recovery takes place as the softening mechanism, the envelope curve approximately matched that of the continuous deformation curve.

6.2.2 Softening Mechanisms of Low Carbon and Nb-Bearing Steel During High Strain Rate Interrupted Deformation

In low carbon steel at a strain rate of 1.0 s^{-1} for all test conditions (Figures 5.14 and 5.15) large amount of softening is observed (Figure 5.20). This occurrence is due to the faster softening kinetics following higher strain rates. Due to this softening by recrystallization, the envelope of the interrupted curves shows a higher stress level than the continuous one. But it can be observed from Figures 5.15b and 5.15c the above does apply when both temperature and interruption time increases. In this case, the finer

recrystallized grains due to higher interruption strain and strain rate starts to grow in the longer interruption periods thus pushing the envelope down towards the continuous one.

In Nb-bearing steel at strain rate of 1.0 s^{-1} , it can be seen from Figures 5.16, 5.17 and 5.21 that high amount of softening takes place during the interruptions in all tests except the first 10 sec interruption at 900°C where recovery operates. The above phenomenon is due to the formation of new strain free grains by static recrystallization. From Figures 5.21a and b, it can be observed that the amount of softening increases with deformation temperature and interruption time. This is because at higher temperature the precipitation of niobium is slow leading to faster softening. This delayed precipitation retards the growth of the recrystallized grains thus leading to a high stress level interrupted curves above those of the continuous ones.

6.3 EFFECT OF STARTING GRAIN SIZE AND PRE-HOLDING TIME ON THE INITIAL FLOW CURVE

Both grain size and holding time before deformation affects the stress level of the flow curve and the strain to peak flow stress [32,76]. In the interrupted curves especially in Nb-bearing steel it can be observed that the initial portion of the interrupted curve and that of the corresponding continuous deformation curve does not coincide with each other. Sah et al [32] showed that the work hardening and dynamic recovery portions of the torque/twist curves

are steeper and peak torque and strain to peak stress decrease with decreasing grain size. Petkovic [21] studied the effect of grain size on the high temperature yield stress of tough-pitch copper. She observed an increase in yield stress with decrease of grain size. Weiss et al [76] showed that increase of holding time before deformation in Nb-bearing steel reduces the peak stress and as well as the peak strain. This is due to the fact that increase in holding time increases the amount of prior static precipitation thus diminishing the potential for dynamic precipitation.

6.4 STATIC RESTORATION STUDY OF PREVIOUS WORKERS ON LOW CARBON AND Nb-BEARING STEEL

It is clear from the results obtained, different amount of softening takes place at different temperatures and interruption times. An attempt can be made to correlate the present results with the restoration model found by previous researchers. Although Lebon et al [74,75] tested steels of 0.17%C, 0.04%Nb, at strain rate of 4 s^{-1} , their results on the recrystallization characteristics of carbon and Nb-bearing steel can be considered to give an approximate indication of the degree of recrystallization that may occur in the present work. The RTT diagram determined by Lebon et al is shown in Figure 5.22. PTT curve determined by Weiss et al [76] for a Nb-bearing steel is given in Figure 5.23. The steel used for this study had a composition of 0.05%C, 0.035%Nb and the tests were conducted at a lower strain rates than the present study. From Figures 5.22 and 5.23, it can be observed that at 900°C precipitation of niobium occurs

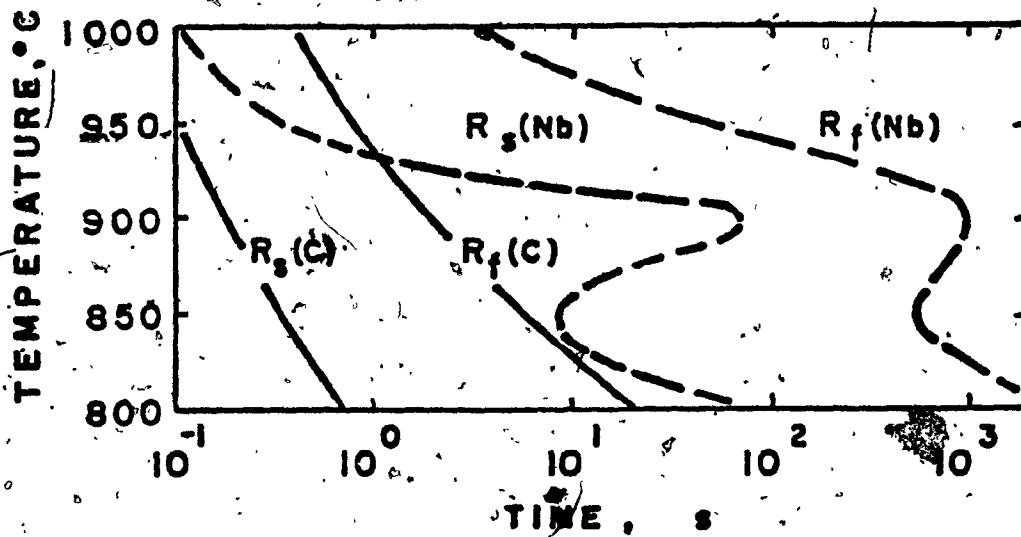


Fig. 5.22: Recrystallization - Temperature - Time Diagram for a 0.17%C - 0.04%Nb Steel (After Le Bon et al, Ref. 74).

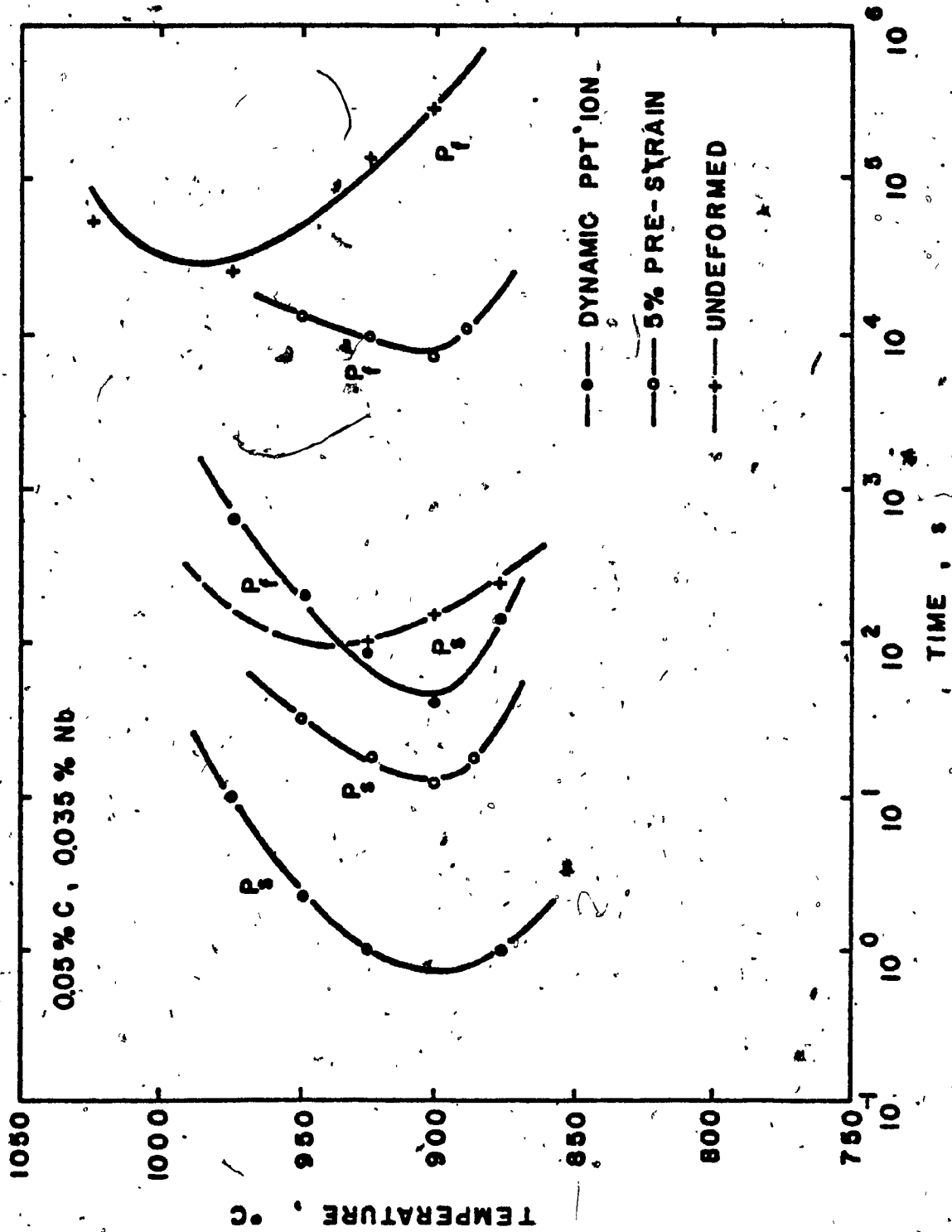


Fig. 5.23: Precipitation - Temperature - Time Diagram for a 0.05%C-0.035%Nb Steel (After Weiss et al, Ref. 76).

rapidly and delays recrystallization compared to what it would be if precipitation did not occur. But at 1000°C, precipitation of niobium is slow and so recrystallization starts and is completed quickly. In the case of low carbon steel, since there is no precipitation, recrystallization starts to occur quickly at all temperatures especially at the higher ones.

Static softening results as a function of time were determined by Cordeau et al [62], Capeletti et al [60] for Nb-bearing steel and by Petkovic [65] for both low carbon and Nb-bearing steel. The present results can be compared to these by determining the softening as a function of time of interruption from the first interruption in each of three interrupted tests, at the same temperature and strain rate. The present results when considered this way (Figure 5.24 and 5.25) agree closely with those of the above workers.

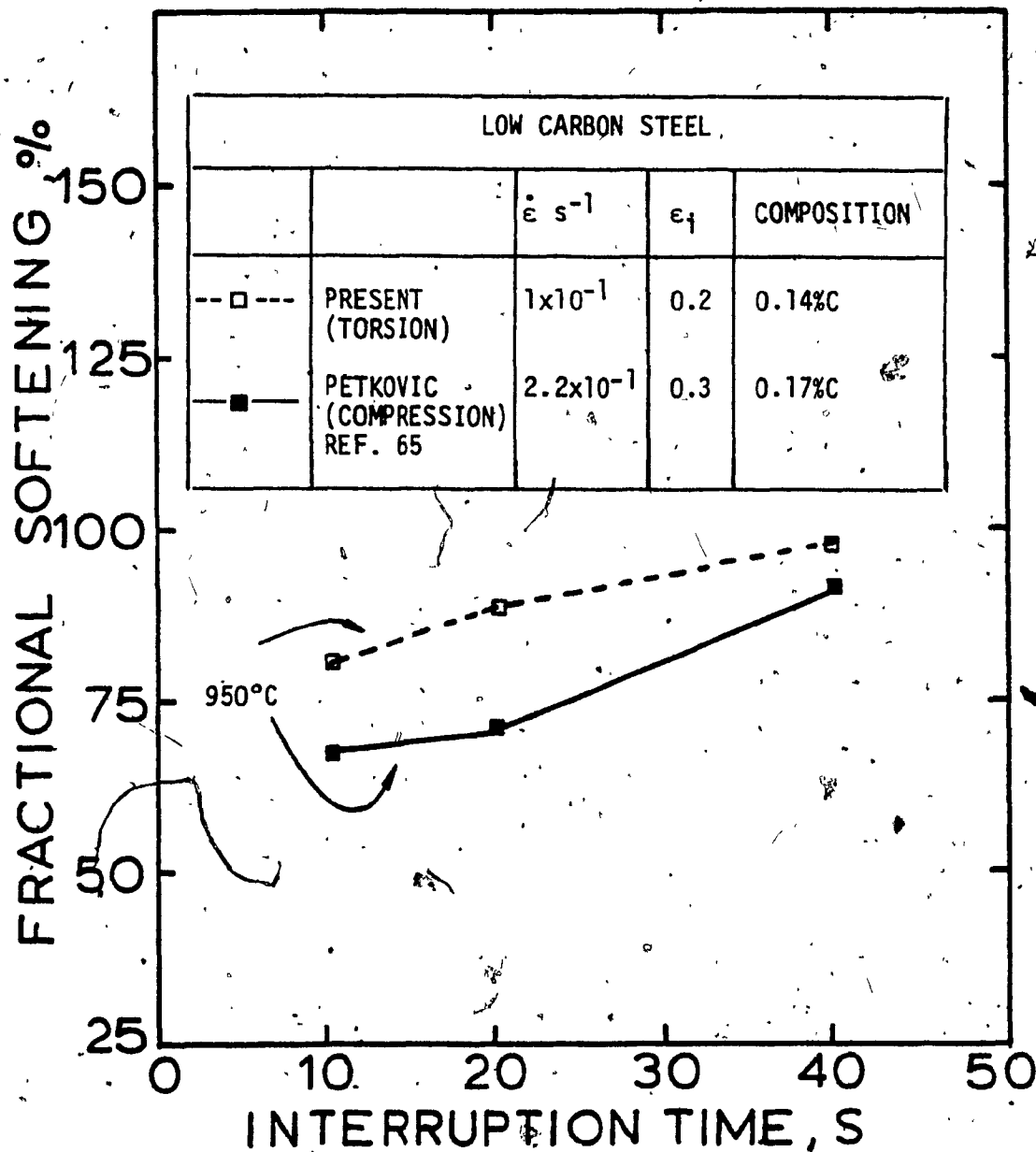


Fig. 5.24: Correlation of the Static Softening Observed in the First Interruption of the Present Study with that of Petkovic (Ref. 65) for low Carbon Steels.

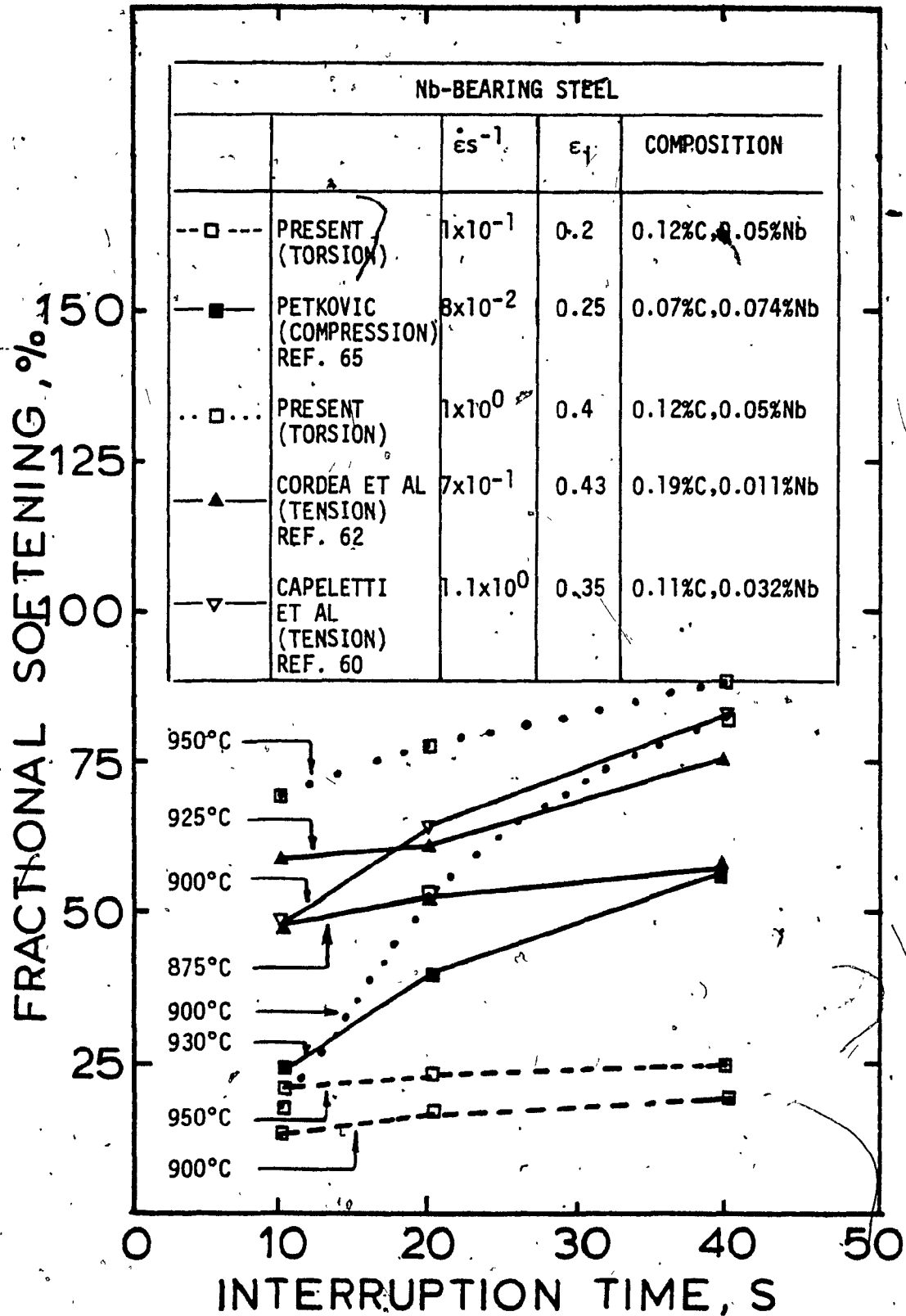


Fig. 5.25: Correlation of the Static Softening Observed in the First Interruption of the Present Study with Previous Workers for Nb-Bearing Steels.

CHAPTER 7

CONCLUSIONS

From the present research, the following general conclusions were reached:

1. Both low carbon steel and Nb-bearing steel undergo dynamic recrystallization under the present test conditions. The strain to the peak flow stress increases with increase of strain rate and decrease of temperature.

2. The flow stress of the steels is strongly strain rate and temperature dependent and can be effectively related by a power law of the form:

$$\dot{\epsilon} = A \sigma^n \exp(-\Delta H/RT)$$

for hot working.

The values of 'n' and ΔH are found to be:

$$n_{LC} = 5.0, \Delta H_{LC} = 72.4 \text{ Kcal/mole}$$

$$n_{Nb} = 8.3, \Delta H_{Nb} = 101.2 \text{ Kcal/mole}$$

3. The ductility of either steel increases with increase of temperature and strain rate.

4. In comparison with low carbon steel, niobium bearing steel always has a higher flow stress, higher strain to peak stress and lower ductility.

5. The amount of restoration during an interruption increases with strain rate, amount of pre-straining, deformation temperature and interruption time.

6. When recovery operates during the intervals between deformation, the flow curve on reloading matches that of continuous deformation as exhibited by the Nb-bearing steel at the low strain rate.

7. When recrystallization takes place during an interruption period, the flow curve on reloading overshoots that of the continuous one. This behaviour is exhibited by the Nb-bearing steel at high strain rates and by the low carbon steel at short interruption times preferentially at low temperatures.

8. When grain growth follows recrystallization during an interruption period, the flow curve on reloading is lower than that for continuous deformation as shown by the low carbon steel at long interruption times preferentially at high temperatures.

9. In comparison with the low carbon steel, niobium precipitates are effective in inhibiting either recrystallization at the low strain rate or growth of the recrystallized grains at the high strain rate.

REFERENCES

1. W.E. Duckworth and J.D. Baird, J. of Iron Steel Inst., 207, 854-871 (1969).
2. K.J. Irvine, "Strong, Tough Structural Steels", Publ. No. 104, Iron Steel Inst., London, 1-10 (1967).
3. F.B. Pickering, "Micro Alloying 75", Washington, D.C., Session 1, 3-24 (1975).
4. A.P. Coldren, Y.E. Smith and R.L. Cryderman, "Processing and Properties of Low Carbon Steel", AIME, Session 2, 163-189 (1972).
5. J.J. Irani, D. Burton, J.D. Jones and A.B. Rthowell, "Strong, Tough Structural Steels", Publ. No. 104, Iron Steel Inst., London, 110-122 (1967).
6. W. Morrison and J.H. Woodhead, *ibid.*, 201, 43-46 (1963).
7. E.O. Hall, Proceedings of the Physics Society, B64, 747-753 (1951).
8. N.J. Petch, J. Iron Steel Inst., 174, 25-28 (1953).
9. W.B. Morrison, B. Mintz and R.C. Cochrane, "Controlled Processing of High Strength Low Alloy Steels", York Conference, England, 1-39 (1976).
10. J.H. Little, B. Mintz, W.B. Morrison and J.A. Chapman, 'Third International Conference on Strength of Metals and Alloys', Cambridge, P. 80 (1973).
11. T. Gladman, D. Dulleu and I.D. McIvor, "Micro Alloying 75", Washington, D.C., Session 1, 25-48 (1975).
12. J.M. Gray, Met. Trans, 3, 1495-1500 (1972).

13. W.A. Wong and J.J. Jonas, Trans. TMS-AIME, 242, 2271-2280 (1968).
14. H.J. McQueen, W.A. Wong and J.J. Jonas, Can. J. Phys., 45, 1225-1233 (1967).
15. J.L. Uvira and J.J. Jonas, Trans. TMS-AIME, 242, 1619-1626 (1968).
16. H.J. McQueen and J.J. Jonas, in Metal Forming, Interrelation Between Theory and Practice, Ed. A.L. Hoffmann, Plenum Publ. Corp., N.Y. 393-428 (1970).
17. R.W.K. Honeycombe, in "The Plastic Deformation of Metals", Edward Arnold (Publ) Ltd., London (1968).
18. R.W. Cohen, in "Physical Metallurgy", North-Holland Publishing Company, Amsterdam (1965).
19. H.J. McQueen, Trans. Japan Inst. Met., 9, 170-177 (1968).
20. M.J. Luton and J.J. Jonas, Proc. Int. Conf. Strength Metals Alloys, 2nd, 1100-1105 (1970).
21. R.A. Petkovic, Ph.D. Thesis, McGill University, Montreal (1975).
22. J.P.A. Immarigeon and J.J. Jonas, Acta. Met., 22, 1235-1247 (1974).
23. J.J. Jonas, C.M. Sellars and W.J. McG. Tegart, Met. Rev. 14, 1-24 (1969).
24. H.P. Stuwe, "Deformation Under Hot Working Conditions"; (Special Rep. No. 108) London (Iron and Steel Institute), 1-6 (1968).
25. H.P. Stuwe, Acta. Met., 13, 1337-1342 (1965).
26. H.J. McQueen, J. of Metals, 20, 31-38 (1968).
27. D. Hardwick and W.J. McG. Tegart, J. Inst. Met., 90, 17-21 (1961-62).

28. C.M. Sellars and W.J. McG. Tegart, *Mém. Scient. Revue Métall.*, 63, 731-746 (1966).
29. H. Ormerod and W.J. McG. Tegart, *J. Inst. Met.*, 92, 297-99 (1963-64).
30. H.J. McQueen and J.J. Jonas, Recovery and Recrystallization During High Temperature Deformation in "Plastic Deformation of Materials", ed. R.J. Arsenault, Academic Press, N.Y., 393-493 (1975).
31. C.M. Sellars and W.J. McG. Tegart, *Acta. Met.*, 14, 1136-1138 (1966).
32. J.P. Sah, G.J. Richardson and C.M. Sellars, *Metal Science*, 8, 325-331 (1974).
33. G. Glover and C.M. Sellars, *Met. Trans.*, 4, 765-775 (1973).
34. R.A. Petković (Previously Djaic), M. Eng. Thesis, McGill University, Montreal (1971).
35. M.J. Luton and C.M. Sellars, *Acta. Met.*, 17, 1033-1043 (1969).
36. C. Rossard "3rd Int. Conf. on Strength of Metals and Alloys", Inst. of Metals and Iron Steel Inst., London, Vol. II, 175-203 (1973).
37. G.J. Richardson, C.M. Sellars and W.J. McG. Tegart, *Acta. Met.*, 14, 1225-1236 (1966).
38. H.J. McQueen, *Materials-Technology - An Inter-American Approach*, A.S.M.E. (N.Y.), 379-388 (1968).
39. J.E. Bailey, "Electron Microscopy and Strength of Crystals", New York and London (Interscience) 535-574 (1963).

40. H.J. McQueen and S. Bergerson, Metal Science J., 6, 25-29 (1972).
41. J.J. Jonas, H.J. McQueen and W.A. Wong, "Deformation Under Hot Working Conditions", 49-59. Iron Steel Inst., London (1968).
42. J.J. Jonas, Trans. A.S.M., 62, 300-303 (1969).
43. C.M. Sellars and W.J. McG. Tegart, Int. Met. Rev., 17, 1-24 (1972).
44. H.J. McQueen, R. Petkovic, H. Weiss and L.G. Hinton in A.I.M.E. Seminar on The Hot Deformation of Austenite, Cincinnati, Nov. 1975.
45. R.R. Arnold and R.J. Parker, J. Inst. Met., 88, 255-259 (1959-60).
46. J.A. Bailey and A.R.E. Singer, J. Inst. Met., 92, 404-08 (1963-64).
47. J.F. Alder and V.A. Phillips, J. Inst. Met., 83, 80-86 (1954-55).
48. F.A. Hodierne, J. Inst. Met., 91, 267-73 (1962-63).
49. H. Ormerod and W.J. McG. Tegart, J. Inst. Met., 89, 94-96 (1960-61).
50. C. Zener and J.H. Hollomon, J. Appl. Phys., 15, 22-32 (1944).
51. H.J. McQueen and J.E. Hockett, Met. Trans., 1, 2997-3004 (1970).
52. G. Glover and C.M. Sellars, Met. Trans., 3, 2271-2280 (1972).
53. R.A.P. Djaic and J.J. Jonas, J. Iron and Steel Inst., 210, 256-261 (1972).
54. W.A. Johnson and R.F. Mehl, Trans. AIME, 135, 416-428 (1939).
55. J.G. Byrne in Recovery, Recrystallization and Grain Growth, MacMillan, N.Y., 90 (1965).

56. F.J. Humphrey and J.W. Martin, *Acta. Met.*, 14, 775-781 (1966).
57. J.E. Bailey and P.B. Hirsch, *Proc. Roy. Soc.*, 267, 11-30 (1962).
58. C.M. Sellars and J.A. Whiteman, *The Met. & Mat. Tech.*, 6, 441-448 (1974).
59. W.A. Anderson and R.F. Mehl, *Trans. AIME*, 161, 140-166 (1945).
60. T.L. Capeletti, L.A. Jackman and W.J. Childs, *Met. Trans.*, 3, 789-796 (1972).
61. R.A.P. Djaic and J.J. Jonas, *Met. Trans.*, 4, 621-624 (1973).
62. J.N. Cordeau and R.E. Hook, *Met. Trans.*, 1, 111-118 (1970).
63. G.R. Dunstan and R.W. Evans, *Metallurgia*, 79, 96-99 (1969).
64. R.W. Evans and G.R. Dunstan, *J. Inst. Metals*, 99, 4-14 (1971).
65. R.A. Petkovic, M.J. Luton and J.J. Jonas, *Can. Met. Quart.*, 14, 137-145 (1975).
66. M.M. Farag, C.M. Sellars and W.J. McG. Tegart, "Deformation Under Hot Working Conditions", P.100, *Iron Steel Inst.*, London (1968).
67. K.J. Irvine, T. Gladman, J. Orr and F.B. Pickering, *J. Iron Steel Inst.*, 208, 717-726 (1970).
68. J.D. Baird and R.R. Preston, "Processing and Properties of Low Carbon Steel", *AIME Symposium*, Cleveland, 1-46 (1972).
69. T. George, Strong, Tough Structural Steel, Publ. No. 104, *Iron and Steel Inst.*, London, 123-134 (1967).
70. J.D. Jones and A.B. Rothwell, "Deformation Under Hot Working Conditions", *Iron Steel Inst.*, London, 78-82 (1968).

71. J.L. Robbins, O.C. Shepard and O.D. Sherby, Trans. ASM, 60, 205-216 (1967).
72. H.W. Wagenaar "Deformation Under Hot Working Conditions", Iron Steel Inst., London, 38-41 (1968).
73. C.M. Sellars and J.A. Whiteman, Controlled Processing of HSLA Steels, Paper 5, York Conference, England (1976).
74. A. Le Bon, J. Rofes-Vernis and C. Rossard, "Controlled Processing of HSLA Steels", Paper 6, York Conference, England (1976).
75. A. Le Bon, J. Rofes-Vernis and C. Rossard, Metal Science, 9, 36-40 (1975).
76. I. Weiss and J.J. Jonas, "Recrystallization and Grain Growth in Materials", AIME Symposium, Chicago (1977).
77. D.E.R. Hughes, J. Iron Steel Inst., 170, 214-220 (1952).
78. D. Hardwick and W.J. McG. Tegart, J. Inst. Metals, 90, 17-20 (1961).
79. M.M. Farag, C.M. Sellars and W.J. McG. Tegart, "Deformation Under Hot Working Conditions", Iron Steel Inst., London, 60-67 (1968).
80. T.B. Vaughan, "Deformation Under Hot Working Conditions", Iron Steel Inst., London, 68-78 (1968).
81. D.C. Lemmon and O.D. Sherby, J. of Mat., 4, 444-456 (1969).
82. D.S. Fields and W.A. Backofen, ASTM Proceedings, 57, 1263-1275 (1957).
83. W.J. McG. Tegart, "Element of Mechanical Metallurgy", MacMillan, N.Y. and London, p. 76 (1966).
84. R. Von Mises, Reports of the Royal Scientific Society of Gottingen, Berlin, p. 582 (1913).